



Inorganic membranes for hydrogen separation

Simão P. Cardoso, Ivo S. Azenha, Zhi Lin, Inês Portugal, Alírio E. Rodrigues & Carlos M. Silva

To cite this article: Simão P. Cardoso, Ivo S. Azenha, Zhi Lin, Inês Portugal, Alírio E. Rodrigues & Carlos M. Silva (2017): Inorganic membranes for hydrogen separation, *Separation & Purification Reviews*, DOI: [10.1080/15422119.2017.1383917](https://doi.org/10.1080/15422119.2017.1383917)

To link to this article: <http://dx.doi.org/10.1080/15422119.2017.1383917>



Accepted author version posted online: 19 Oct 2017.



Submit your article to this journal



View related articles



View Crossmark data

Inorganic membranes for hydrogen separation

Simão P. Cardoso[§], Ivo S. Azenha[§], Zhi Lin[§], Inês Portugal[§], Alírio E. Rodrigues[¶], Carlos M. Silva^{§*}

[§] CICECO – Aveiro Institute of Materials, Department of Chemistry,
University of Aveiro, 3810-193, Aveiro, Portugal

[¶] Associate Laboratory LSRE - Laboratory of Separation and Reaction Engineering, Department of Chemical Engineering, Faculty of Engineering, University of Porto, 4200-465 Porto, Portugal

* Corresponding author: Tel.: + 351 234 401549; Fax: + 351 234 370084;
E-mail address: carlos.manuel@ua.pt

Received on February 27, 2017, accepted on September 4, 2017

Short running title: Inorganic membranes for hydrogen separation

Abstract

Hydrogen, one of the most promising energy carriers for the future, is currently produced mainly by natural gas reforming or coal gasification, where mixtures containing H₂, CO₂ and contaminants like CO, H₂S and CH₄ are obtained. Among other purification methods, membrane technology has received special attention due to its potential efficiency for hydrogen separation, simplicity of operation, low energy consumption, and because it is environmentally friendly. For this application, the inorganic membranes can be essentially divided into five main families: metallic and proton conducting (dense phases), and silica, zeolite and carbon molecular sieve (porous solids). Over the past twenty years, palladium-based membranes have been the most studied and implemented at industrial level, however recent advances in other membrane types are receiving great attention. This article critically reviews more than 520 recent publications, highlighting the latest research developments on inorganic membranes for the recovery and purification of hydrogen, with emphasis on their structural characteristics, synthesis, commercial application, drawbacks and challenges. Furthermore, a large compilation of data is provided in Supplemental Material divided according to membrane type.

Keywords: Inorganic membrane, hydrogen purification, molecular sieve, commercial applications

1 Introduction

The increasing global energy demand, which the International Energy Agency (IEA) expects to rise by 50 % until 2040, allied to the prevalence of fossil-fuels (oil, coal and gas) as the world's primary energy source (around 81 %), and the consensus about its negative environmental effects due to greenhouse gas emissions, make the development of sustainable and clean forms of energy a major priority (1, 2).

Hydrogen is one of the most promising alternative energy sources due to its high energetic efficiency and zero carbon emission, yielding only water when burned. Presently, the global production of hydrogen is around 700 billion m³ at normal pressure and temperature (\approx 60,000 kton) (2). Nevertheless, hydrogen is not a primary fuel being produced predominantly (over 90 %) from fossil fuels (*ca.* 50 % by natural gas reforming, *ca.* 18 % by coal gasification, and *ca.* 30% in petroleum refineries) with water electrolysis responsible for *ca.* 4 %. The fossil fuels based processes are equilibrium limited, and so the final product is composed by a mixture of H₂ and CO₂ with some other contaminants, such as CO, H₂S, and CH₄, arising from the water gas shift reaction (3–5).

To satisfy the high purity requirements of various potential applications, like fuel cell technology, and/or to provide an efficient hydrogen supply, downstream separation processes are necessary. Membrane technology stands out among various methods due to simplicity of operation and low energy consumption, cost effectiveness, environmental friendly features, and because it can be easily coupled with other processes (6).

A membrane is a selective physical barrier between two phases where mass transfer takes place under the action of a driving force. This allows for the preferential permeation of one or more components of a feed stream while impeding the passage of the remaining ones. The part of the feed that passes through the membrane is named permeate and the retained fraction is called retentate. Two major concepts are directly linked to membrane separation: permeance and selectivity. In the case of gas permeation, permeance is defined as the flow rate of compound *i* going through the membrane per unit area of membrane and per unit of transmembrane driving force. The selectivity or separation factor quantifies the membrane ability to separate a desired component from the feed mixture, and corresponds to the ratio of the distributions of two components between permeate and retentate. The ideal selectivity is expressed by the ratio of pure gas permeabilities (7, 8).

Membranes can be natural or synthetic, with the latter being divided into organic (polymeric), inorganic, and mixed-matrix (hybrid) (Figure 1b). Presently, industrial processes are performed mainly with synthetic or natural polymer membranes due to their ability to cope with high pressure drops, low cost, and good scalability. However, organic membranes are generally limited to operations in the temperature range 263–373 K (-10° – 100°C). Inorganic membranes provide several advantages, such as high thermal, chemical, and mechanical stabilities, minor plasticization, and controllable pore size distribution (thus better control of selectivity and permeability) (9). To take advantage of the good capabilities of inorganic membranes and of the low manufacturing costs of organic membranes, mixed-matrix membranes have emerged in recent years (10).

Inorganic membranes can be classified according to their characteristics, generally in two classes (Figure 1b): porous and dense (non-porous) membranes. The latter are subdivided into metallic and ceramic proton conducting membranes, and they are capable of separating molecules due to differences in both solubility and diffusivity. On the other hand, in porous membranes (silica, zeolites and carbon) fractionation relies on differences in size, shape, and/or affinity between the permeating molecules and the membrane (7, 11). Following the IUPAC classification of pores sizes, porous membranes can be microporous ($d_p < 2$ nm), mesoporous ($2 < d_p < 50$ nm) or macroporous ($d_p > 50$ nm), where d_p is the average pore diameter. Research on inorganic membranes for hydrogen separation/production has experienced a considerable growth in recent decades, as emphasized in

Figure 1a, being responsible for almost half of the total number of studies related with hydrogen separation (grey area of the plot).

The scope of this article is to provide an overview on hydrogen separation for each inorganic membrane type, pointing out their recent developments, most relevant benefits and drawbacks, synthesis features, hydrogen transport phenomena, and industrial applications. Dense membranes are discussed in Sections 2 and 3, while porous membranes are analyzed in detail in Sections 4, 5 and 6. Additionally, a large compilation of information for each membrane type is reported in Tables SM1-SM5 (Supplemental Material), namely, synthesis and membrane features, dynamic characterization and experimental conditions of assays, and available or calculated permeabilities/permeances and selectivities.

Dense metallic membranes (Section 2), specifically palladium-based and multi-component palladium alloys, are the most studied and commercialized (12). They are highly desirable for the production of pure hydrogen due to their extreme selectivity (since only hydrogen can permeate). Recent challenges for metallic membranes involve combining good sulfur tolerance with superior hydrogen permeability and reduced costs. Ceramic proton conducting materials (Section 3), such as perovskites and pyrochlores, have emerged as timid candidates for hydrogen separation due to lower costs than Pd-based membranes, and higher durability and stability in streams containing CO, CO₂ and H₂S. However, enhanced proton and electron conductivities are necessary, besides the usual chemical, mechanical, and thermal stability requirements (13).

Porous silica membranes (Section 4) are relatively easy to fabricate, production costs are low, and they exhibit high hydrogen permeances and moderate to high selectivities. Nonetheless, their instability in the presence of steam and at high temperatures is the limiting feature being investigated by researchers (14). Zeolites (Section 5) offer uniform pores with molecular dimensions and unique properties for catalytic, ion exchange, adsorption and membrane applications (15). Accordingly, zeolite membranes have emerged naturally as a potential alternative for hydrogen separation, since they frequently exceed the well-known Robeson upper boundary. Recent advances to improve hydrogen selectivity are discussed, namely various pre-treatment and post-synthesis methods that reduce or eliminate the presence of defects and/or reduce the crystal pore size. Finally, carbon molecular sieve membranes (Section 6), although seldom investigated for hydrogen separation, have great potential and exhibit better performance than polymer membranes (they also exceed the Robeson upper limit) (16). Different approaches to overcome the main limitations of carbon molecular sieve membranes, *e.g.* brittleness and low mechanical stability, are discussed along with the main parameters influencing their final structure.

2 Metallic membranes

Dense phase metallic and metallic alloy membranes are very attractive to obtain high purity hydrogen in a single step. In particular, palladium-based membranes are preferred due to the selective permeability of palladium to hydrogen, the catalytic activity of the surface, and their thermal and mechanical stability (3). Although experiments with palladium membranes date back to the 19th century and the first patent claiming their use for hydrogen purification was issued in 1916 (17), commercialization started much later only in 1964 by Johnson Matthey (12). Presently, there are several metal membrane systems commercially available (12) including palladium-based membrane reactors which embody alternative routes for pure hydrogen production via steam methane reforming (SMR) (18) and water gas shift (WGS) reactions (19).

2.1 Hydrogen diffusivity in metals

The transport of hydrogen in metallic membranes occurs by a solution–diffusion mechanism involving the dissociation of molecular hydrogen and the diffusion of atomic hydrogen within the

metal lattice (20, 21). The permeation mechanism described by the Ward and Dao model (21) comprises the following steps: (i) molecular transport of H₂ from the bulk gas to the surface (feed side); (ii) dissociative adsorption of H₂ onto the surface; (iii) transition of atomic hydrogen (H) from the surface into the bulk metal; (iv) diffusion of H through the bulk metal; (v) transition of H from the bulk to the surface (permeate side); (vi) recombinative molecular desorption of H₂ from the surface (permeate side); and, (vii) transport of H₂ from the surface (permeate side) to the bulk gas.

Hydrogen permeation through metals is generally described by the semi-empirical expression:

$$J_{H_2} = \frac{P_{m,H_2} (P_{H_2,ret}^n - P_{H_2,perm}^n)}{\delta} \quad (1)$$

where J_{H_2} (mol m⁻¹s⁻¹) is the hydrogen flux through the membrane, P_{m,H_2} (mol m⁻¹ s⁻¹ Paⁿ) is the permeability of hydrogen, δ (m) is the membrane's thickness, P_{H_2} (Pa) is the partial pressure of hydrogen with the subscripts _{ret} and _{perm} standing for retentate and permeate sides, respectively. The pressure exponent (n) generally ranges from 0.5 to 1, depending on the limiting step of the hydrogen permeation mechanism. Commonly, when the pressure is relatively low and the controlling step is the diffusion of atomic hydrogen through the bulk metal (step iv of the Ward and Dao model (21)) the value of n is 0.5 and Eq. (1) becomes the Sievert's law (22). Higher values of n are expected when mass transport to/from the surface (steps i and vii, respectively (21)) or dissociative/associative adsorption steps (steps ii and vi, respectively (21)) become rate determining. Similarly, n is higher than 0.5 for defective membranes (e.g. presence of pinholes) or when the rate is influenced by the membrane porous support, in both cases due to the relevance of transport mechanisms such as Knudsen and Poiseuille flow (22, 23).

Hydrogen permeation in metallic membranes involves the dissociative adsorption of H₂ and the diffusion of atomic hydrogen within the lattice (20, 21). Since dissociated hydrogen occupies tetrahedral interstitial sites and hops from site to site inside the lattice, hydrogen diffusivity is related to the distance between such sites. Consequently, diffusivity is usually greater in metals with body-centered cubic (bcc) lattice than in those with face-centered cubic (fcc) arrangement (24). In fact, hydrogen permeability in vanadium, niobium, and tantalum (group 5 elements with bcc structure) is up to several orders of magnitude higher than in palladium (group 10 element with fcc structure) especially at lower temperatures (Figure 2a) (12). However, the former metals are readily oxidized hindering the transport properties (4) and, in addition, their ability to dissociate hydrogen prior to permeation is low and thus a catalytic layer of a suitable material is required (25). In contrast, palladium can dissociate hydrogen without such layer and being a noble metal it is exceptionally resistant to oxidation. Moreover, at room temperature palladium can absorb about 600 times its own volume of hydrogen (26). For these reasons palladium-based membranes exhibit high selectivity, permeability, and stability (27), being very attractive for H₂ separation applications. Hydrogen selectivity is typically > 1000 for these membranes, as shown by the works of Zhang *et al.* (28), Mardilovich *et al.* (29), Gade *et al.* (30), and Braun *et al.* (31), with $\alpha_{H_2/N_2} > 3000, 5000, 40000$ and 10000, respectively (see Table SM1 in Supplemental Material).

Noteworthy, the use of pure palladium membranes is limited due to structural deformations induced by hydrogen. For instance, absorption of H₂ below its critical point (571 K or 298°C and 2 MPa) causes α -to- β phase transitions in palladium-hydrogen (Pd-H) systems. The nucleation of the β phase (rich in H) in the α phase (lean in H) causes shrink of the lattice and leads to the so-called hydrogen embrittlement and to grain boundary defects (12, 23). On the other hand, impurities typically present in the gas streams undergoing purification (e.g. hydrogen sulfide, ammonia, mercury, carbon dioxide, carbon monoxide, etc.) lead to poisoning of the palladium membrane surface (32). In fact, apart from inhibiting the H₂ flux (possibly due to blocking of H₂ dissociation sites) the corrosive H₂S gas can form a low permeable Pd₄S film on the palladium surface (33, 34).

The H₂ permeation rate is also reduced in the presence of CO and CO₂, mainly at low temperatures or high CO or CO₂ concentrations, due to the blocking of H₂ adsorption sites and to displacement of adsorbed hydrogen (35, 36). Palladium can be alloyed with other metals to enhance chemical stability and to maximize H₂ permeability. Moreover, because of the high and increasing price of palladium (6.5 USD per gram in 2005 and 25.9 USD per gram in 2017 (37)) the use of alloys can reduce the cost of Pd-based membranes.

2.2 Palladium-based membranes and fabrication methods

Palladium alloys membranes

Metallic elements such as cerium (Ce), copper (Cu), iron (Fe), nickel (Ni), platinum (Pt), ruthenium (Ru), silver (Ag), and yttrium (Y) can be alloyed with palladium (Pd) to obtain membrane materials with improved thermal and mechanical properties, good chemical compatibility with many hydrocarbon-containing gas streams, and higher hydrogen permeability. In fact, Pd alloys exhibit lower critical temperatures for the $\alpha \rightarrow \beta$ phase transition thus alleviating hydrogen embrittlement (23, 38). For instance, alloying Pd with Ag (Pd₇₇Ag₂₃, 23 wt.% of Ag) and Pt (Pd₈₁Pt₁₉, 19 wt.% of Pt) reduced the $\alpha \rightarrow \beta$ phase transition temperature from 573 K (298°C for pure Pd) to around room temperature (38). Moreover, many Pd alloys are more permeable to hydrogen than pure Pd as illustrated by the H₂ flux measurements presented in Figure 2b (39). These results evidence excellent hydrogen permeability of the rare-earth alloys Y-Pd and Ce-Pd (even for metal contents below 10 wt.%) because they can achieve higher hydrogen solubility due to the large atomic size of Ce and Y, and thus the hydrogen flux increases (40).

For Cu-Pd alloys, slightly better results were obtained just with 42 % of Cu (5 % more permeable than pure palladium, as shown in Figure 2b) (39). Even though alloying of Pd with Cu is complex, due to the various phases that may be formed, the use of Cu-Pd alloys has benefits such as lower costs, enhanced thermal properties, and good sulfur tolerance without loss of hydrogen permeability (38). In contrast, binary alloys of Pd with Fe, Ni, Ru, and Au displayed lower hydrogen permeability than pure Pd (39). Finally, Pd-Ag alloy membranes with 23 wt.% of Ag present a maximum for hydrogen permeability, *ca.* 1.7 times higher than pure Pd one at 623 K (350°C, Figure 2b) (39), related to the opposing effect of silver content on the solubility and the diffusivity of hydrogen. In fact, while solubility increases with silver content (reaching a maximum at 20–40 % Ag) the diffusion coefficient decreases (41). The selectivity values of these alloys can be similar to pure palladium membranes, as shown in Table SM1 in Supplemental Material, *i.e.* with orders of magnitude above 1000.

Ternary and higher Pd alloys have been studied to improve their operating performance at high temperature and pressure. In fact, the addition of small amounts of rare-earth elements is known to increase both solubility and mobility of hydrogen, while preserving the plasticity and texture of the metal, increasing the hardness and promoting the recrystallization temperature of the alloy (38). For instance, Rodina *et al.* (42) have shown that the permeability of hydrogen in Pd-Ag alloys can be significantly improved by the addition of a small amount of gold (*ca.* 3 wt.%). Recently, Didenko *et al.* (43) revealed that the permeability of Pd-Ru alloys containing 0.5 wt.% of indium (Pd₆In_{0.5}Ru_{3.5}) is 3 times higher than for the traditional Pd-Ag alloys (Pd₇₇Ag₂₃) at 823 K (550°C).

Another compelling reason to investigate multi-component Pd alloys is the need to overcome the limitations caused by H₂S poisoning (31, 34, 44, 45). For example, the good resistance of Pd-Au fcc alloys to bulk sulfidization, combined with the hydrogen permeability of Pd-Ag alloys, provided a Pd₇₈Ag₉Au₁₃ membrane with excellent resistance to H₂S (34). This is evident in Figure 3 that presents H₂ permeability data for Pd-based membranes before and after exposure to 100 ppm H₂S, at 673 K (400°C) (34).

Supported palladium-based membranes

Thin membranes are usually required for gas separations since the flux is inversely proportional to the film thickness (Eq. 1). Furthermore, thinner films incorporate lower amounts of the active phase and thus material costs are reduced. Hence, many efforts have been dedicated to the preparation of thin palladium films on low cost porous supports (38) to provide membranes with high hydrogen permeation rates, without loss of integrity (46, 47). Among the others, the most studied porous supports are ceramics, glass and stainless-steel (12, 48), although recently porous nickel support (PNS) (49, 50) and the superalloys Hastelloy (51, 52) and Inconel (53, 54) have drawn the attention of researchers.

One of the first substrates used for supported palladium membranes is porous Vycor glass characterized by its high content of silica (SiO_2 , 75–80 %), boron trioxide (B_2O_3 , 10–12 %) and alumina (Al_2O_3 , 4–6 %) (55), and by its resistance to high temperatures and thermal shock, excellent features for the adhesion of Pd films, and inherent mechanical fragility (12, 23). Ceramic materials, such as alumina (Al_2O_3), present better physical stability at high pressures and temperatures, good chemical inertia, high permeability and uniform nanosized pores (0.005–0.2 μm) (56). Porous metallic supports have larger non-uniform pore sizes (average size 0.2–100 μm), they are easily shaped into various forms (such as disks or tubes), easier to seal than the ceramic supports, and have a thermal expansion coefficient similar to that of palladium which ensures good mechanical stability if temperature varies (23). Porous stainless-steel (PSS) is the most frequently selected metal support due to its high mechanical strength and thermal stability, corrosion resistance, small pore size (0.2 μm), low cost and also because it is relatively easy to process (23).

In general, one of the drawbacks of membrane supports is that surface roughness is required to promote good adhesion of the Pd films but surface heterogeneity may cause undesirable defects or pinholes in the membrane. Furthermore, to ensure reliable membranes, the support should have a narrow pore size distribution and a particle size range smaller than the thickness of the top layer (23, 57). In the particular case of ceramic membranes, to prevent the occurrence of defects, Oyama *et al.* (58) suggested the use of multiple graded layers of alumina deposited on another porous substrate, with smaller particle sizes from bottom to top. This arrangement confers mechanical support at the bottom and a smooth top surface while maintaining the permeation rate. Since porous metal supports are more prone to surface defects, due to larger pore sizes and non-uniform pore size distribution, a thicker Pd film is required in comparison to ceramic supported membranes. Moreover, an additional non-metallic layer between the support and the Pd film is required to avoid the high temperature intermetallic diffusion of Pd into the support and of the support metals (such as Fe, Cr, and Ni) into the Pd film (59, 60).

Intermetallic diffusion in PSS supports reduces the long term stability and the permeability of Pd-based membranes due to the formation of low hydrogen permeable alloys at the interface (59, 60). To avoid these problems, Shu *et al.* (61) deposited a thin (*ca.* 0.1 μm) titanium nitride (TiN) intermediate layer between the Pd/Ag alloy membrane and the PSS support, which improved the thermal stability of the ensuing membranes at temperatures as high as 973 K (700°C). Similarly, Zhang *et al.* (60) tested a thin oxide intermediate layer formed by *in situ* oxidation of PSS and a mesoporous yttrium stabilized zirconia (YSZ) layer deposited on the PSS support by a sol-gel coating method. Although simpler to prepare, the *in situ* oxidized PSS support requires a thick Pd film (due to high surface roughness) and, as a result, the membranes have lower hydrogen permeability and lower thermal stability than the thinner Pd membranes prepared on the PSS support with YSZ interlayer (the former are stable up to 873 K (600°C) whereas the later are stable above 873 K). Wang *et al.* (62) studied the modification of PSS with zirconium oxide (ZrO_2) particles in order to reduce its average pore size and facilitate the preparation of defect-free Pd membranes.

The synthesis of defect-free membranes is easier with nonporous or semi-porous supports, such as metals, ion-conducting solids, and polymers. However, there are drawbacks associated to these supports, namely, the interdiffusion of Pd in metallic supports at high temperature (above 673 K or

400°C), the low hydrogen permeability in ion-conducting materials, and the limited operating temperature range of polymers (38). Noteworthy, metal-containing polymeric materials can be used to achieve better hydrogen permeability. For instance, Yu *et al.* (63) revealed that the permeabilities of H₂ in phenolphthalein poly(ether sulfone) membranes containing palladium (Pd-PES-C) are much higher than those in the pure PES-C membranes.

Fabrication methods of palladium-based membranes

Palladium membranes can be prepared by a variety of methods, depending on the geometric form and nature of the support, the desired Pd-film thickness and purity, and also on the manufacturing facilities available (46). Currently, deposition processes can be subdivided into (i) chemical ones, *e.g.* chemical vapor deposition (CVD), electrochemical vapor deposition (EVD), electroplating (EP), electroless plating deposition (ELP), sol-gel technique, molecular layering (ML), and spray pyrolysis, solvated metal atom deposition; and (ii) physical ones, *e.g.* conventional cold rolling, physical vapor deposition (PVD), sputtering and magnetron sputtering (MS) (27, 64). In the literature, the two most common are CVD and ELP.

The CVD method involves chemical reactions of a metal precursor (usually an organometallic complex) both in the gas phase and at the surface, at controlled temperature, to produce a uniform metal film on a substrate. The thickness of the film can vary over a wide range, from a single atomic layer to hundreds of nanometers (65). This method is reproducible, easy to scale-up and flexible, enabling the coating of supports with large areas and different geometries (64). The downside is the possibility of film contamination with constituents of the metal precursor (38).

The ELP technique consists of the electroless reduction of metallic salt complexes in solution, in the presence of a chemical reducing agent, by reactions occurring both on the substrate surface and within the solution with the metal deposited acting as catalyst (23, 66). This simple and effective low-cost plating method provides metal coatings with high uniformity, hardness, and excellent adhesion even on curved and complex shaped solid surfaces (metallic or nonmetallic) (64). Good temperature control and high-purity chemicals are required to avoid the decomposition of the plating bath that causes surface defects and lack of purity. These features and the difficulty in thickness control are the main drawbacks of ELP (65).

In practice, palladium thin films contain some defects, such as cracks, pinholes or pores, due to the tendency to produce thin films (to reduce production costs) and to the effect of the environment to which the membrane is exposed. For these reasons, the theoretically infinite selectivity of Pd membranes for hydrogen is not attainable (64) and this has prompted the research for non-palladium membranes in the field of hydrogen energy technologies (67).

2.3 Alternatives to palladium-based membranes

The increasing demand of hydrogen and the need to lower production costs stimulated the research and development of non-palladium membranes (67). A compilation of the metal membranes (palladium-based, palladium alloys and non-palladium membranes) reported in the literature is presented in Table SM1 in Supplemental Material, together with the information concerning the preparation method, film thickness (*L*), permeation operating temperature (*T*), and transmembrane pressure drop (ΔP). Hydrogen permeability, permeance and selectivity (a_{H_2}/a_{N_2}) are also summarized.

Nickel (Ni), vanadium (V), and its alloys are among the most promising materials. Ernst *et al.* (68) prepared a nickel film on an asymmetric tubular alumina support by electroless plating technique using hydrazine as the reducing agent, obtaining a stable (up to 873 K or 600°C) microstructure with high hydrogen permeability (close to the values given by Pd-based membranes) but lower permselectivity, indicating the presence of defects in the membrane. Recently, Wang *et al.* (69) fabricated a metallic nickel dense hollow fiber membrane by a combined spinning and high-

temperature sintering technique, achieving a maximum hydrogen flux of $7.7 \text{ mmol m}^{-2} \text{ s}^{-1}$ at 1273 K (1000°C) and exhibiting high stability at this temperature in either CO₂, CO, or steam-containing atmosphere. Some other examples include Ti₂₆Ni₂₁V₅₃ (67), V₉₀Al₁₀ (70), V₈₅Al₁₀Co₅ (71), V_{89.8}Cr₁₀Y_{0.2} (72), Ni (73), and Ni-Co (74, 75), in some cases coated with palladium to facilitate the access of hydrogen and to prevent metal surfaces oxidation (76). Ni-Nb-Ti alloys have been reported to display high permeability and high resistance to hydrogen embrittlement (77, 78). Similar alloys, such as Ni₃₀Ti₃₅Co₃₅ (79), Ta₅₃Ti₂₈Ni₁₉ (80), and Nb₄₀Hf₃₀Ni₃₀ (81), displayed comparable or even higher hydrogen permeability than that of pure Pd membranes.

Another important type of non-palladium membranes are based on amorphous metals. They are generally more attractive than their crystalline equivalents, exhibiting increased strength, ductility, corrosion resistance and hydrogen solubility (4). Furthermore, amorphous alloys do not suffer $\alpha \rightarrow \beta$ phase transition during hydrogen absorption which frequently causes structural damages of the membrane (82). Although the variety of amorphous alloys available is immense, the most examined are V-, Nb-, Ta- or Zr-based alloys such as, Ni-Nb-Zr-Co (83), Zr_{36-x}Hf_xNi₆₄ (84), Ni₉₀Al₁₀ (85), Ni-B (86), Ni-Nb-Zr (87), and Ni-Ta-Zr (88) membranes. In particular, Hara *et al.* (82) verified that hydrogen permeation through Zr₃₆Ni₆₄ without a noble metal deposition layer was an order of magnitude inferior to Pd₇₇Ag₂₃, but its cost was two orders of magnitude lower.

3 Ceramic proton conducting membranes

Hydrogen-permeable dense ceramic materials are oxides with high proton and electronic conductivity (25). Proton conductivity is observed in a variety of materials, mostly perovskite type oxides although significant developments have been reported for pyrochlorates, niobates, tantalates, and tungstates. The electronic conductivity can be enhanced by dispersing a metallic phase in a ceramic matrix (*cermet*) or using a ceramic-ceramic composite (*cercer*). In recent decades, dense ceramic membranes have received considerable attention due to chemical and mechanical stability at high temperatures, low manufacturing cost, and suitability for the production of high purity hydrogen, since they may be 100 % selective for hydrogen (89, 90). Other potential applications include protonic ceramic fuel cells, hydrogen sensors, electrochemical hydrogen pumps, and catalytic membrane reactors (90, 91). However, several improvements are still necessary to move from lab-scale towards industrial implementation (13). An overview of ceramic membranes is compiled in Table SM2 in Supplemental Material.

3.1 Proton conducting principles

Hydrogen separation in proton-electron conducting oxides involves the so-called ambipolar diffusion mechanism of protons and electrons through the membrane, in the same direction, as depicted in Figure 4a. At the gas feed side, a surface reaction dissociates and ionizes molecular hydrogen (H₂) into protons (H⁺). Due to the H₂ partial pressure difference (driving force) across the membrane, the protons diffuse to the permeate side where they are reduced and recombined to form H₂ at the membrane surface (90).

The solid-state transport of protons through metal oxide membranes involves their interaction with neighboring electronegative oxygen ions to form hydroxide defects (92). Although the transport mechanism is still under investigation, two mechanisms have been proposed in the literature: the vehicle mechanism and the Grotthuss or proton-hopping mechanism (13). According to the vehicle mechanism, protons bind to oxygen (the vehicle) forming a hydroxide ion that diffuses through the lattice by vacancy or interstitial diffusion. Electroneutrality is kept by the counter-diffusion of unprotonated vehicles or oxygen vacancies. The Grotthuss mechanism assumes that protons jump between stationary oxygen ions and that the diffusion of protons and electrons occurs in the same direction, maintaining electroneutrality and zero net electric current (13, 93). For structural reasons proton transport in oxides is preferentially explained by the Grotthuss mechanism (94).

The hydrogen permeation flux is influenced by electronic conductivity, proton conductivity, hydrogen pressure gradient and thickness of the membrane. Accordingly, the proton flux, J_{H^+} (mol cm⁻² s⁻¹), for a membrane containing only protonic-electronic conductors can be described by the Wagner theory (95):

$$J_{H^+} = \frac{RT}{2F^2\delta} \int_I^H (\sigma_{H^+} \times t_e) d \ln p_{H_2} \quad (2)$$

where $R = 8.314 \text{ J mol}^{-1} \text{ K}^{-1}$ is the universal gas constant, T (K) is absolute temperature, $F = 96485.3 \text{ C mol}^{-1}$ is the Faraday constant, σ_{H^+} (S cm⁻¹) is proton conductivity, t_e is the electronic transport number, p_{H_2} (Pa) is hydrogen partial pressure, and δ (cm) is membrane thickness. In this equation the driving force is hydrogen pressure gradient and the flux is directed from side I to side II. Since the material properties, such as σ_{H^+} and t_e , can be pressure dependent, Norby and Haugsrud (93) integrated Eq. (2) for different limiting situations. For instance, when the material exhibits dominating electronic conduction $t_e \approx 1$ and σ_{H^+} is proportional to $p_{H_2}^n$ where: (i) $n = 0.5$ when protons are minority defects, (ii) $n = 0.25$ when protons are majority defects compensated by electrons, and (iii) $n = 0$ when protons are majority defects compensated by acceptor-dopants (93). In the first two cases J_{H^+} is proportional to $[(p_{H_2}^I)^n - (p_{H_2}^H)^n]$ and thus the partial pressure on the feed side ($p_{H_2}^I$) has a strong effect on proton flux, whereas in the third case J_{H^+} is proportional to $\ln(p_{H_2}^H(g)/p_{H_2}^I(g))$ and, consequently, the pressure on both sides becomes equally important (93-95). These few examples illustrate the importance of understanding the transport mechanism and defect structure in dense mixed conducting membranes. The positive effect of temperature on hydrogen permeation rate is straightforward from Eq. 2 and it was confirmed by studies of Cai *et al.* (96) and Song *et al.* (97).

3.2 Proton conducting materials and composites

Family of Perovskites

Proton conductivity in SrCeO₃ was reported by Iwahara *et al.* (98), for the first time, and since then dense mixed proton-electron conducting ceramic membranes have attracted increasing interest. The predominant type of dense conducting ceramic materials are perovskite-based oxides (99) with the general chemical formula ABO₃, where A is a divalent ion (A²⁺) such as calcium, strontium, or barium, and B is a tetravalent ion (B⁴⁺) like cerium or zirconium. The most extensively studied perovskites are SrCeO₃, BaCeO₃, and SrZrO₃.

Generally, perovskites exhibit proton conductivities between 10⁻² and 10⁻³ S cm⁻¹ in temperature range 673-1273 K or 400°-1000°C (100, 101) though it is possible to improve their protonic transport, and consequently permeation properties, by doping the B sites (89). The most investigated dopants are trivalent ions, such as Y³⁺ or Yb³⁺, which form a AB_xD_{1-x}O_{3-δ} structure (102, 103). Other cations, such as In³⁺ (104), Nd³⁺ (96), Sm³⁺ (105), Gd³⁺ (106) and Eu³⁺ (97) have also been tested to increase hydrogen conductivity. Typically, proton conductivities of perovskites increase steadily with temperature leveling off at high temperatures as can be seen in Figure 5 for various perovskite-type oxides. However, in some cases (e.g. BaCeO₃ and SrCeO₃) a clear maximum is observed meaning

that in the high temperature region conductivity decreases with increasing temperature, due to its opposing effect in the concentration and mobility of protons (100).

Doped barium-cerium perovskites such as $\text{BaCe}_{0.90}\text{Y}_{0.10}\text{O}_{3-\delta}$ (BCY) have the highest proton conductivities. However, since they are unstable in the presence of CO_2 and/or steam at high temperatures (101), they are unsuitable for hydrogen permeation membranes (107, 108). In fact, at high temperatures barium cerates have a high tendency to react with CO_2 , forming a carbonate on the surface. To avoid these undesired reactions, Yang *et al.* (109) studied the effect of replacing Ce by Ti in $\text{BaCe}_{0.8-x}\text{Ti}_x\text{Sm}_{0.2}\text{O}_{3-\delta}$ (BCST) materials and reported that Ti doping increases the material resistance to CO_2 and H_2O . On the other hand, zirconates like $\text{BaZr}_{0.8}\text{Y}_{0.2}\text{O}_{3-\delta}$ (BZY) have higher chemical stability but lower protonic conductivity due to their high grain boundary resistance, which reduces the electrical performance (110, 111). Moreover, for zirconates a high density structure is difficult to obtain and higher sintering temperatures are required (112).

A solid proton conductor combining the high conductivity of cerates and the good chemical stability of zirconates is highly desirable and motivated several researchers. For example, Katahira *et al.* (113) investigated Zr-substituted BaCeO_3 ($\text{BaCe}_{0.9-x}\text{Zr}_x\text{Y}_{0.1}\text{O}_{3-\delta}$) and reported that chemical stability increases with zirconium content but protonic conductivity decreases. Ryu and Haile (114) studied compounds with general formula $\text{BaCe}_{0.9-x}\text{Zr}_x\text{M}_{0.1}\text{O}_{3-\delta}$ (where M is Gd or Nd, and x is 0 to 0.4) prepared by solid state reactions between Ba-cerate and Ba-zirconate, and confirmed that the introduction of Zr into doped barium cerate enhances chemical stability and decreases conductivity. A good compromise between conductivity and stability was obtained for the composition $\text{BaCe}_{0.77}\text{Zr}_{0.2}\text{Nd}_{0.1}\text{O}_{3-\delta}$ (114). Azad and Irvine (115) showed that Sc doping has a similar effect, increasing the chemical stability of cerates and zirconates. A total conductivity of $1.06 \times 10^{-3} \text{ S cm}^{-1}$ was reported for $\text{Ba}(\text{Ce},\text{Zr})_{0.8}\text{Sc}_{0.2}\text{O}_{3-\delta}$ (115). The addition of ZnO to yttrium-doped barium zirconate has improved sintering conditions (time and temperatures) and provided a good combination of electrical and chemical properties (116) (see below *Composite materials: Cermets and Cercers*). Some examples of doped cerates and zirconates are summarized in Table SM2 (Supplemental Material).

Overall, these findings explain why perovskite membranes have been widely embraced for fuel cells, electrolyzers, and hydrogen permeation (13, 117). A very recent study by Kalyakin *et al.* (118) refers the use of $\text{La}_{0.9}\text{Sr}_{0.1}\text{YO}_{3-\delta}$ materials to develop a hydrogen sensor with good response and precision for the detection of trace contents of hydrogen (0.1–3.3 vol.%).

Family of Pyrochlores

Pyrochlores are thermally stable crystalline metal oxides with a cubic symmetry and general formula $\text{A}_2\text{B}_2\text{O}_7$, where the A-site is usually a large cation (typically a rare-earth element) and the B-site is a smaller radius cation (usually a transition metal) (119, 120). Due to their relatively high resistance to CO_2 and H_2O atmospheres they have been scrutinized for H_2 separation (90). Shimura *et al.* (121) reported proton conductivities in different rare earth lanthanide (Ln) pyrochlore-type oxides, namely $\text{Ln}_2\text{Zr}_{2-x}\text{Y}_x\text{O}_{7-\delta}$ and $\text{Y}_2\text{Ti}_{2-x}\text{M}_x\text{O}_{7-\delta}$, where M = In or Mg, and Ln = La, Nd, Sm, Gd, or Er. Omata and Otsuka-Yao-Matsuo (122) investigated Ca-doped $\text{La}_2\text{Zr}_2\text{O}_{7-\delta}$ and reported that $\text{La}_2(\text{Zr}_{1.985}\text{Ca}_{0.015})\text{O}_{7-\delta}$ has a conductivity of 0.01 S cm^{-1} , which is the same order of magnitude as the values reported for high conductivity perovskites membranes. On the other hand, Haugsrud and Norby (123) reported a low proton conductivity ($\sim 5 \times 10^{-5} \text{ S cm}^{-1}$) for $(\text{La}_{2-x}\text{Ca}_x)\text{Ti}_2\text{O}_7$ with 2 % of calcium.

The hydrogen flux across a $(\text{La}_{2-x}\text{Ca}_x)\text{Ti}_2\text{O}_7$ membrane with $10 \mu\text{m}$ was $0.1 \text{ mL}_{\text{NTP}} \text{ cm}^{-2} \text{ min}^{-1}$, at 1023 K (750°C), under a pressure difference of 10 atm (123). However, this H_2 flux is approximately five times lower than that obtained with a perovskite $\text{SrCe}_{0.95}\text{Yb}_{0.05}\text{O}_{3-\delta}$ membrane at the same conditions (102). Promising results for hydrogen production have been reported by Merka *et al.* (124, 125) who tested and confirmed the good photocatalytic properties of nonstoichiometric pyrochlores, like $(\text{Y}_{1.5}\text{Bi}_{0.5})_{1-x}\text{Ti}_2\text{O}_{7-3x}$, $(\text{YBi})_{1-x}\text{Ti}_2\text{O}_{7-3x}$ and $(\text{Bi}_{1-x}\text{Ti}_{0.75x})\text{Ti}_2\text{O}_7$.

Family of Niobates and Tantalates

Haugsrud and Norby (126) were the first to disclose the good stability and proton conductivity of acceptor-doped rare earth ortho-niobates (LnNbO_4) and ortho-tantalates (LnTaO_4), where Ln is a lanthanide element. At high temperatures and in aggressive atmospheres (for example, in CO_2) the proton conduction was reported to be approximately 0.001 S cm^{-1} . Since then, doping studies were done to improve the proton conductivity of this new class of materials despite the low solubility of dopants in these oxides (in the order of 1 mol.%) (126).

Several studies have been published for doped ortho-niobates with a formula $\text{La}_{1-x}\text{A}_x\text{Nb}_{1-y}\text{B}_y\text{O}_{4-\delta}$, *i.e.* with A- and B-sites co-doping. Calcium is the most utilized and successful dopant in the A-site (126–130), though Sr (130, 131), Ba (130, 131) and Mg (132) have also been used with fair results. Examples for B-site co-doping include Sn (133), Ti (127, 134), Si (134) and Zr (134). Cao *et al.* (135) reported enhanced electronic and ionic conductivity of LaNbO_4 doped with Ce and Yb.

Proton conductivity of tantalates is approximately one order of magnitude lower than that of corresponding niobates (101). Haugsrud and Norby (136) studied the electrical properties of Ca-doped tantalite with different rare-earth acceptors ($\text{M}_{1-x}\text{Ca}_x\text{TaO}_4$, where $x = 0.01$ and M = La, Nd, Gd, Er). These authors reported that the total conductivity decreases with the ionic radius of the acceptor (La > Nd > Gd > Er) with a proton conductivity of $3 \times 10^{-4} \text{ S cm}^{-1}$ (at *ca.* 1273 K or 1000°C) being attained for the composition $\text{La}_{0.99}\text{Ca}_{0.01}\text{TaO}_4$.

Niobates and tantalates undergo a temperature induced second-order phase transition from monoclinic symmetry at low temperature (fergusonite-type phase) to tetragonal symmetry at high temperature (scheelite-type phase), between 773–1073 K (500°–800°C) and 1573–1723 K (1300°–1500°C), respectively (137). This phase transformation influences strongly the thermal expansion coefficient of both materials thus causing serious problems during thermal cycling (129). In the case of niobates, Vullum *et al.* (138) and Santibáñez-Mendieta *et al.* (139) overcame this problem by the partial replacement of Nb by Ta. Moreover, Brandão *et al.* (140) showed that the high-temperature scheelite phase of $\text{Sr}_{0.02}\text{La}_{0.98}\text{NbO}_{4-\delta}$ can be retained at room temperature via partial substitution of Nb by V (*i.e.* vanadium doping on the B-site). Additional examples of materials with tetrahedral TO_4 and proton conductor ability include, among others, gallates ($\text{Ln}_{1-x}\text{Ba}_{1+x}\text{GaO}_{4-x/2}$ and $\text{Ln}_{1-x}\text{Sr}_{1+x}\text{GaO}_{5-x/2}$) (141) and rare-earth ortho-phosphates (142).

Family of Tungstates

Rare-earth tungstates are lanthanide tungsten oxides ($\text{La}_6\text{WO}_{12}$) described as an ordered defect fluorite-type structure with the ideal formula $\text{La}_{28-y}\text{W}_{4+y}\text{O}_{54+\delta}\text{V}_{2-\delta}$ (143, 144). Their mixed protonic and electronic conductivity at high temperatures is a promising feature for hydrogen separation, as stated by Shimura *et al.* (143). These authors measured proton conductivity of $\text{La}_{5.8}\text{WO}_{11.7}$ in wet H_2 , at 1173 K, and reported the value of $5 \times 10^{-3} \text{ S cm}^{-1}$ (143). Haugsrud (145) published similar results for $\text{La}_6\text{WO}_{12}$ in his study on the conductivity of Ca-doped and undoped $\text{Ln}_6\text{WO}_{12}$ (Ln = La, Nd, Gd, and Er). The maximum proton conductivity was obtained for undoped $\text{La}_6\text{WO}_{12}$ (145).

Escolástico and co-workers (146–148) studied hydrogen flux through different lanthanide tungsten oxide-based membranes. In their later work, they compared $\text{Nd}_{5.5}\text{WO}_{11.25-\delta}$ with $(\text{Nd}_{5/6}\text{Ln}_{1/6})_{5.5}\text{WO}_{11.25-\delta}$ (Ln = La, Ce, Pr, Eu, and Tb) and concluded that the hydrogen flux was higher in Ln-doped tungstates, attaining values up to $0.12 \text{ mL min}^{-1} \text{ cm}^{-2}$, at 1273 K (1000°C), depending on the feed composition (*i.e.*, H_2 and H_2O content) (148). At temperatures below 1073 K (800°C), the hydrogen permeation in tungstate membranes is limited, due to loss of electronic conductivity. However, it has been reported that partial substitution of W^{6+} by Mo^{6+} increases the n-type conductivity and thus enhances the hydrogen flux (149, 150). An overview of these and other tungstate-based materials is presented in Table SM2 (Supplemental Material).

Despite their promising features, rare-earth tungstates exhibit some drawbacks linked to their chemical stability, namely (93, 111, 136): they may react with carbon-containing gases forming very stable WC_x compounds; at high temperatures and for long-term operation regimes WO_x species may evaporate from the lanthanide tungsten oxides, shifting phase equilibrium towards the Ln-oxide rich regions; the high activity of Ln-oxides originates material instability in the presence of H_2O and CO_2 ; and equilibrium shifts may cause the appearance of a secondary phase (for example, $La_6W_2O_{15}$ (111, 151)) in the bulk matrix, resulting in crack formation.

Composite materials: Cermets and Cercers

Although dopants can increase the electronic conductivity of dense ceramic materials, such improvement may be insufficient to allow the membrane to function effectively. Alternative approaches consist in composite materials combining: (i) a ceramic and a metallic phase (named *cermet*) with proton and electron conductivity, as illustrated in Figure 4(b) (93), or (ii) two ceramic phases (named *cercer*) ensuring both conductivities (152–154).

The preparation of a *cermet* involves the synthesis of the proton conducting powder which is subsequently mixed with a metal (such as Pt, Pd, Pd/Ag, Ni, Nb, Ta, or V) to form a continuous metallic phase within a dense matrix. The metal can be added in powder form or as a mixture of metal oxide precursors for later calcination (91). For example, Okada *et al.* (155) prepared a $Pd/BaZr_{0.8}Y_{0.2}O_{3-\delta}$ layer on an alumina porous support with the proton-conductor being introduced by impregnation and the palladium particles by chemical vapor deposition (CVD). A similar approach was followed to prepare membranes with Pd/YSZ ($YSZ = Y_2O_3$ -stabilized ZrO_2) (156), $Ni/BZPY$ ($BZPY = Ba(Zr_{0.7}Pr_{0.1}Y_{0.2})O_{3-\delta}$) (157), Pd/CZY ($CZY = Ca_{0.9}Y_{0.1}O_{3-\delta}$) (158), Ni/BCY ($BCY = Ba(Ce_{0.9}Y_{0.1})O_{3-\delta}$) (159), and Ta/YSZ (160) materials.

In general, *cermet* membranes provide good results in hydrogen separation. For instance, the $Pd/BZYO$ ($BZYO = BaZr_{0.8}Y_{0.2}O_{3-\delta}$) membrane prepared by Okada *et al.* (155) gave a hydrogen permeance of 1.2×10^{-9} mol $m^{-2} s^{-1} Pa^{-1}$ and H_2/N_2 selectivity of 5.7 at 873 K (600°C). Hydrogen permeation rates of some *cermet* materials are listed in Table SM2 (Supplemental Material).

Balachandran and co-authors (161, 162) studied the properties of several composite materials and their influence on hydrogen permeation. They concluded that H_2 can permeate through the metal, the oxide or both, depending on the proton conductivity in both phases though, in general, transport through the metallic phase is predominant (93). Compared to metal or alloy membranes, *cermets* are less susceptible to crack formation since the ceramic matrix allows the metal phase to expand and contract when temperature and hydrogen concentration change (163). However, *cermets* are unstable in carbonaceous gas environments because the catalytic activity of the metallic phase promotes the formation of carbon deposits (152).

Wang *et al.* (164) studied hydrogen permeation in dual-phase ($SrCe_{0.95}Y_{0.05}O_{3-\delta}/ZnO$) membranes and concluded that addition of ZnO has a double advantage: it increased hydrogen permeation and the sinterability of the membrane. The latter is an import aspect because densification of proton conducting materials requires high sintering temperatures and long annealing times (due to their refractory nature). For example, sintering parameters for BZY (temperature > 1873 K or 1600°C and time > 24 h) cause the evaporation of barium and the segregation of Y_2O_3 and, as a result, proton conductivity decreases (165). In view of this, sintering aids such as Li_2O , Al_2O_3 , LiF , $LiNO_3$, and transition metal oxides, like NiO , CuO , and ZnO , have been successfully used to lower the sintering temperature of ceramic materials (166–168).

In recent years ceramic-ceramic (*cercers*) composites have been successfully applied to enhance electronic transport in membranes, as an alternative strategy to *cermets* (152–154). *Cercers* present some advantages, namely: i) higher stability, lower catalytic activity, and lower costs than *cermets*; and ii) the possibility to obtain uniform thermal expansion of proton- and electron-conducting phases by tuning their composition (152). However, the degradation behavior over time is a disadvantage of

cercers (169). Interestingly, Rosensteel *et al.* (152) prepared a $\text{BaCe}_{0.8}\text{Y}_{0.2}\text{O}_{3-\delta}$ - $\text{Ce}_{0.8}\text{Y}_{0.2}\text{O}_{2-\delta}$ (proton conductor-electron conductor) composite membrane with the highest hydrogen permeability reported to date ($5.54 \times 10^{-8} \text{ mol cm}^{-2} \text{ s}^{-1}$, at 1123 K or 850°C), for which the permeability is $1.57 \times 10^{-13} \text{ mol cm}^{-1} \text{ s}^{-1} \text{ Pa}^{-1}$. Another example is provided by Lacz *et al.* (170) who modified the structure of $\text{BaCe}_{0.9}\text{Y}_{0.1}\text{O}_3$ by adding $\text{Ba}_3(\text{PO}_4)_2$ phase, thus improving the chemical stability of the composite material. Table SM2 lists some other examples from literature.

3.3 Thin proton conducting membrane fabrication

From the hydrogen permeation mechanism through proton conducting membranes discussed above (see Section 3.1), one may say that H_2 permeation flux is limited by surface reaction and bulk diffusion resistances. When the rate-determinant step is bulk transport, an effective way to improve hydrogen transmembrane flux is to reduce its thickness (7, 13). Consequently, asymmetric membranes composed by thin layers of an active phase on a porous ceramic support and the deposition of thin films of proton conducting materials on metal or metal alloys porous supports are being increasingly investigated. Film deposition techniques used for the preparation of dense ceramic membranes are similar to those previously presented for metal deposition (see Section 2). The most adopted include physical and chemical vapor deposition, sol-gel process, electrochemical vapor deposition, co-pressing, spin-coating, and dip-coating (13, 171).

Hamakawa *et al.* (102) deposited thin layers of $\text{SrZr}_{0.95}\text{Y}_{0.05}\text{O}_{3-\alpha}$ or $\text{SrCe}_{0.95}\text{Yb}_{0.05}\text{O}_{3-\alpha}$ on a porous $\text{SrZr}_{0.95}\text{Y}_{0.05}\text{O}_{3-\alpha}$ substrate by spin-coating colloidal suspensions of the powders, and studied the effect of layer thickness on H_2 permeation rates. For asymmetric membranes with identical compositions, H_2 permeation rates were inversely proportional to thickness, being 500 times greater for membranes with 2–140 μm layers than for 1000 μm layers. For a 2 μm thick membrane, hydrogen flux reached the value $6 \times 10^{-4} \text{ mol cm}^{-2} \text{ min}^{-1}$ (102).

Cheng *et al.* (172) fabricated cost-effective $\text{SrCe}_{0.95}\text{Tm}_{0.05}\text{O}_{3-\alpha}$ asymmetric proton conducting membranes for hydrogen separation. The thin film and the thick porous support were prepared from the same material, using small particles (fine powder) for the dense top layer and larger particles for the support. They verified that the porosity and shrinkage of the sintered materials are strongly influenced by the particle size of the powder. Since shrinkage control is important in the fabrication of thinner membranes, additional materials (such as NiO and soluble starch) can be used in their preparation. The advantages of adding NiO include its good chemisorption properties and the ability to form pores by H_2 exposure at high temperatures (under these conditions NiO is reduced to Ni). Soluble starch is normally used as extra pore former, to control the shrinkage of the support and match that of the toplayer (173). Similar thin-film/substrate membranes reported in the literature are: $\text{SrCeEuO}_{3-\delta}/\text{NiO-SrCeO}_3$ (174), $\text{SrZr}_{0.2}\text{Ce}_{0.8-x}\text{Eu}_x\text{O}_{3-\delta}/\text{NiO-SrZr}_{0.2}\text{Ce}_{0.8}\text{O}_{3-\delta}$ (175) and $\text{SrCe}_{0.95}\text{Y}_{0.05}\text{O}_{3-\delta}/\text{NiO-SrCe}_{0.05}\text{Y}_{0.95}\text{O}_{3-\delta}$ (173).

Ceramic membranes of hollow fibers, instead of the classical tubular or disk-shape, present many benefits such as: facile high temperature sealing, effective thin membrane because of its asymmetric structure, and larger membrane area per unit packing volume (176). For example, $\text{Ni-BaZr}_{0.1}\text{Ce}_{0.7}\text{Y}_{0.2}\text{O}_{3-\delta}$ cermet hollow fibers with metal–proton dual phases were prepared by Yang *et al.* (177) using modified oxides. A hydrogen permeation flux of $5.3 \times 10^{-7} \text{ mol cm}^{-2} \text{ min}^{-1}$ was obtained at 1173 K or 900°C.

With decreasing membrane thickness, surface activation gains importance and it can become the overall rate-limiting step. Therefore, to improve permeation flux one should increase the surface activation rate, for instance, increasing the surface area or coating the surface with a porous catalytic layer of a metal like Pd or Ni (178). Song *et al.* (179) reported that Pd-coating a $\text{BaCe}_{0.95}\text{Tb}_{0.05}\text{O}_{3-\delta}$ proton conducting hollow fiber membrane increased the hydrogen flux by a factor of 5.92, compared to the parent membrane, reaching $2 \times 10^{-7} \text{ mol cm}^{-2} \text{ min}^{-1}$ at 1273 K (1000°C). A similar modification for a $\text{BaCe}_{0.85}\text{Tb}_{0.05}\text{Co}_{0.10}\text{O}_{3-\delta}$ membrane increased hydrogen flux by 155 %, at the same 1273 K (178).

4 Silica Porous membranes

Microporous amorphous silica membranes are inorganic membranes with corner-sharing tetrahedral SiO_4 linked via covalent bonding to form a continuous infinite three-dimensional network with controllable pore sizes of approximately 0.5 nm. They can separate small gas molecules such as H_2 , He or O_2 , based on their adsorption behavior and kinetic diameters. Moreover, they are thermally, mechanically, and chemically stable over a wide range of operating conditions. For these reasons, and due to well established, easy and scalable synthesis methods allied to low cost of fabrication, silica membranes are successively attracting the interest particularly for the production and separation of hydrogen (4, 180). The first report about the synthesis and gas permeation properties of microporous silica membranes with good quality and high flux was published by Burggraaf and co-workers in 1989 (181).

Since optimum performance can be achieved with thin membranes that maximize the permeation flow rate and diminish the presence of cracks and pinholes, generally a thin defect-free silica film is deposited on a thick porous support, such as Vycor glass or α -alumina (182, 183). Vycor glass has a small pore size (2–4 nm) that limits the permeance – usually in the order of $10^{-8} \text{ mol m}^{-2} \text{ s}^{-1} \text{ Pa}^{-1}$ – thus decreasing its interest as membrane support for industrial applications. Conversely, symmetrical alumina supports are more attractive due to higher permeances associated to their large pores (>110 nm), and also because they are more economical, stronger, and resistant to high temperature than Vycor glass (184). However, due to their larger pores, intermediate layers (2–10 nm) are commonly used between the active silica layer and the alumina support tube, as shown in Figure 6, to improve permeance and selectivity (184). For example, asymmetrical structures are generally composed by a microporous silica toplayer, a γ -alumina-based intermediate layer, and the α -alumina support. The use of metal supports has been reported in the literature – see for example the works of Lee *et al.* (185), Park *et al.* (186) and more recently Gestel *et al.* (187). However, despite its high mechanical stability and the possibility of embedding the membrane in a module by welding, this type of support has not been widely used (187).

Taking into account the experimental values reported in literature and compiled in Table SM3 in Supplemental Material, silica membranes can attain great selectivities for hydrogen, since values as high as 500 are reported for H_2/N_2 , H_2/CO_2 , H_2/CH_4 and H_2/SF_6 .

4.1 Transport mechanism through microporous silica membranes

The transport mechanisms involved in inorganic microporous membranes (silica, zeolite and carbon molecular sieve membranes) are predominantly associated to pore radius, size of the permeating species, molecule-pore walls interaction potential, and transmembrane pressure difference (57, 188, 189). Practically, viscous flows dominates in macropores ($d_p > 50$ nm), Knudsen regime prevails in mesopores ($2 < d_p < 50$ nm), and surface and/or activated gaseous diffusions are the essential contributions through micropores ($d_p < 2$ nm). The last activated mechanisms are frequently assumed as the unique terms in microporous membranes flux but two or more contributions may be competing in parallel. For instance, due to the presence of defects (such as cracks, pinholes or gaps) in the micropore toplayer, membrane permeation can be represented by micropore diffusion through the crystal combined with intercrystalline transport (188, 190). Recently, Lito *et al.* (188) published a thorough review of the various transport mechanisms governing gas permeation in microporous membranes, which are schematically depicted in Figure 7. In particular the Maxwell-Steffan approach has been successfully applied to unary and multicomponent porous membrane permeation (188–196), for which an increased number of thermodynamic factors is being derived and published (188, 192, 193). The intraparticle diffusivities in micropores may depend on the solid loading, and a wide diversity of trends may be found between the extreme and paradigmatic cases of the weak

confinement scenario (constant diffusivity) and *strong confinement scenario* (linearly occupancy-dependent diffusivity) (188, 196–198). Concerning silica membranes modeling, the research works of Moon *et al.* (199, 200), Aghaeinejad-Meybodi *et al.* (201) and da Costa *et al.* (202) can be mentioned.

4.2 Synthesis of layered silica membranes

The two most used techniques for deposition of silica materials on porous substrates are sol-gel routes and chemical vapor deposition (CVD), which are briefly described in the following.

4.2.1 Sol-gel routes

Among the three different sol-gel routes, namely colloidal, inorganic, and polymeric, the latter is the most used. In this method, silica polymers are formed by a series of hydrolysis and condensation reactions of an alkoxysilane precursor, such as tetraethyloxosilane (TEOS), in the presence of a solvent, usually a water and ethanol mixture, and under controlled conditions. In the hydrolysis step alkoxide groups are replaced by hydroxyl groups and then condensation reactions among silanol groups produce siloxane bonds.

Silica membranes are made by dip-coating the sol-gel silica polymer solution on a mesoporous support, followed by drying and calcination between 673 and 1073 K or 400°–800°C (14, 203). Membranes with pore sizes in the range of 0.5–0.8 nm can be obtained by controlling the various synthesis parameters. The microporous silica layer should be as thin as possible, in the range 50–100 nm, in order to increase membrane permeance since the toplayer naturally presents low permeabilities due to its small pore size (184). The sol-gel route is the easiest and most cost-effective method to produce high quality membranes but it lacks reproducibility (4, 180).

4.2.2 Chemical vapor deposition

Chemical vapor deposition (CVD) is a technique that modifies the pores of the support membrane by depositing a thin layer of a solid product on a substrate through chemical reactions of one or several gases, at elevated temperature. TEOS (tetraethyloxosilane) and TMOS (tetramethoxysilane) are typical gaseous precursors used for preparing silica membranes by CVD, while argon or nitrogen are utilized as carrier gases (14, 184, 204). In general, CVD-derived silica membranes show high hydrogen permselectivity but low hydrogen permeance (one order of magnitude lower compared to sol-gel derived silica membranes) caused by its dense silica layer on a porous substrate (205).

There are two different approaches for CVD deposition of silica layers, differing essentially in the contact mode of reactants with the support surface and pores. In the first method, precursors are provided from one side of the support while the other side is usually vacuumed. In the second method, the two reactants are introduced from opposing sides of the support, they diffuse through the membrane and react when they come in contact with each other, forming a thin SiO₂ film (204). Successful reports on pore-size control of silica membranes prepared by CVD methods are seldom because of the difficulty of characterization in the subnanometer scale (206). Nonetheless, Sea *et al.* (207) and Otha *et al.* (208) succeeded in controlling pore size using the CVD method.

Otha *et al.* (208) used different types of precursors and found that membrane performance was related to the number of its phenyl groups. In fact, silica membranes prepared with TMOS, PTMS (phenyltrimethoxysilane), and DMPS (dimethoxydiphenylsilane) exhibited increased gas permeance and pore size (in the same order). Recently, Zhang *et al.* (209, 210) synthesized a new silica precursor with three phenyl groups - TPMS (triphenylmethoxysilane) - and revealed that the ensuing membrane has a better performance.

4.3 Hydrothermal Stability of Silica Membranes

The major problem of microporous silica membranes is their chemical and structural instability when exposed to humidity, causing loss of permeability (as much as 50 % or more in the first 12 h after exposure to steam) (211). For example, Tsapatsis and Gavalas (212) reported that hydrogen permeance of a silica membrane decreased from 1.1×10^{-8} to 5×10^{-9} mol_{NTP}m⁻² s⁻¹ Pa⁻¹ after 7 days exposure to water vapor at 773 K or 500°C.

A loss of permeability occurs by a degradation process, called densification, that can be divided in four successive stages: (i) sorption of water on the pore surface via silanol groups ($\equiv\text{Si}-\text{OH}$); (ii) breaking of available siloxane bonds ($\equiv\text{Si}-\text{O}-\text{Si}\equiv$) that form more silanol groups; (iii) migration of mobile silica oligomers inside the pore to thermodynamically favorable sites; and, (iv) condensation of silanol groups forming a dense silica structure ($\equiv\text{Si}-\text{OH}+\equiv\text{Si}-\text{OH}\rightarrow\equiv\text{Si}-\text{O}-\text{Si}\equiv$).

Densification phenomena are responsible for the collapse of small pores and the expansion of larger pores, which result in loss of selectivity, lower permeability, and embrittlement of the silica film. Since steam is a common component in hydrogen producing reactions this problem represents a large drawback for industrial applications of silica membranes (14, 180, 213).

Different strategies have been developed to improve the hydrothermal stability of silica membranes, especially sol-gel-derived ones which are generally more unstable than CVD silica membranes (14). One approach is to increase the hydrophobicity of the membranes via replacement of -OH groups by -CH₃ on the pore surface, using a hydrophobic methyl template covalently bonded to silica in the sol-gel route (203). For instance, Vos *et al.* (203) added methyltriethoxysilane (MTES) to TEOS in the sol-gel synthesis and reported ten times more hydrophobic silica membranes. Promising results have also been reported when TEOS is used with other precursors such as ethylenetriethoxysilane (TEVS) (214) and 1,2-bis(triethoxysilyl)ethane (BTESE) (215). Recently, Wei *et al.* (216) used the same procedure to incorporate a perfluorodecyl group in silica membranes which imparted a significant reduction of water wettability. However, since the organic group can be converted to -OH groups in oxygen containing atmospheres at high temperatures, the use of this method is limited to low temperature and nonoxidative environments (217). On the other hand, the hybrid organic-inorganic structures exhibit larger pore sizes and thus lower selectivity towards H₂ (203). Asaeda and Kashimoto (211) proposed an alternative technique that involves keeping coated membranes in moist for a few days and then calcinating them in steam.

Hydrophobicity of silica membranes can also be enhanced by incorporating transition metals in the silica network. Since oxygen forms more polar and stable bonds with transition metals (M-O-Si) than with silicon, the access of water molecules to silanol groups and the mobility of the silica phase are both reduced, thereby improving the hydrothermal stability of the membrane (218). Additionally, the affinity of the dopants to H₂ may increase the flux and selectivity of doped membranes compared to the undoped counterparts (219). For example, Yoshida *et al.* (220) evaluated the performance of silica-zirconia membranes after 20 h of exposure to steam (13-33 mol.%) at high temperature (773 K), and verified that H₂ permeance of a 10 mol.% ZrO₂-SiO₂ membrane decreased 70 % to 8.9×10^{-8} mol m⁻² s⁻¹ Pa⁻¹ whereas it did not change for a 50 mol.% ZrO₂-SiO₂ membrane. Kanezashi and Asaeda (221) disclosed Ni-SiO₂ composite membranes with superior performance and stability, with 20.5×10^{-8} mol m⁻² s⁻¹ Pa⁻¹ and $\text{H}_2/\text{N}_2 = 100$. Igi *et al.* (222) studied the performance and

hydrothermal stability of undoped and Co-doped silica membranes and revealed significant improvements in gas permeance (see Figures 8(a) and (b)). For example, H₂ permeance increased from 8.9×10^{-8} to 1.8×10^{-7} mol m⁻² s⁻¹ Pa⁻¹ and H₂/N₂ permeation ratio increased from 70 to 730, when comparing a silica membrane with a 33 mol.% Co-doped silica membrane (222).

Many more oxides and metal ions have been investigated as membrane dopants, namely TiO₂ (223, 224), ZrO₂ (220, 225), Al₂O₃ (226, 227), NiO (221), Nb₂O₅ (228, 229), Co₃O₄ (222, 230), Y₂O₃

(231). Recently, binary metal doped membranes, such as Pd-Co/Si (232) and Fe-Co/Si (233), have been reported. These and other systems are presented in Table SM3 in Supplemental Material which summarizes the main results of the literature with respect to hydrogen permeation in silica membranes, emphasizing the type of membrane, support, and intermediate layer, the deposition method and precursor, and the pore size.

5 Zeolite membranes

Zeolites are three-dimensional, crystalline, hydrated microporous aluminosilicate materials composed by Al^{IV} and SiO_4^{IV} tetrahedra building blocks connected to each other by oxygen atoms. They have well-defined channels and cavities occupied with mobile alkali or alkali-earth cations (to compensate the negative charge of the framework) and water molecules. The size of these channels is in the range of molecular dimensions (typically 0.3–1.0 nm (234)), conferring unique catalytic, adsorption and ion exchange properties to zeolites, which can be changed by modifying the Si/Al ratio during the synthesis and/or changing the mobile counter ion. Furthermore, the outstanding thermal, mechanical and chemical stabilities of zeolites make them more desirable than other microporous materials (15).

Zeolites can be natural minerals or synthetically produced, with the latter being preferred for commercial use due to higher purity and consistency (235). Although natural zeolites were discovered in 1756 and the first synthetic zeolite was obtained in 1862, commercialization started much later in 1954 (236). Nowadays, the zeolite family includes 231 framework types, mainly synthetic and without natural counterpart (237), but only a small part (about 5 %) is industrially relevant. The most used zeolite structures are FAU, MOR, MFI, FER, LTA, and BEA (235, 238). Figures 9(a) and (b) show the topology of the FAU (faujasite, Y-type and X-type) and MFI (silicalite and ZSM-5) zeolites, respectively.

Over time, the term “zeolite” has become broader in order to include non-aluminosilicate compositions and structures, giving rise to the terms “zeolite-like materials” or “zeotypes”. Presently, a zeotype is defined as a crystalline material with a three-dimensional framework in which the tetrahedral sites can be occupied by Al, B, P, Sn, Ti, Fe, Ge, Ta, and V elements, among others (235). The scientific community has paid considerable attention to aluminophosphate (AlPO), silicoaluminophosphate (SAPO), metalloaluminophosphate (MeAPO), and lanthanide silicate (heteropolyedra materials with transition metals and rare earth elements) zeotypes (239, 240). Figure 9(c) presents the CHA topology of SAPO-34. It is worth noting that AlPO frameworks possess no net charge and thus exhibit no cation exchange ability.

Zeolites and zeotypes can be classified according to the size of their pores or channels, as: small (8-ring), medium (10-ring), large (12-ring), and extra-large pore zeolites, if they are limited to 8, 10, 12, and >12 atoms in polyhedral coordination, respectively. The structures can also be classified as one-dimensional (1D), two-dimensional (2D) and three-dimensional (3D) according to the number of directions with channels (241).

Due to its exceptional attributes, zeolites are considered effective materials in three distinct areas: i) catalysis, being used in several organic reactions; ii) gas separation, in purification processes and bulk separation of gases by adsorption membranes; and iii) ion exchange, for example for drinking water purification and environmental decontamination of heavy and radioactive metals (234, 242–245). In the context of zeolite membranes, hydrogen is highly referenced in the literature in studies aiming hydrogen separation and purification, or as a single gas used to assess specific properties in order to characterize the membrane.

Since almost 80 % of hydrogen is produced by steam reforming of natural gas, in the hydrogen economy context zeolites are considered promising candidates for H₂ separation from impurities, such as CO₂, CH₄, CO, and H₂O, being the H₂/CO₂ mixture one of the most studied in the literature (246).

Data from a substantial number of publications concerning zeolite membranes for H₂/CO₂ separation are summarized in Table SM4 (Supplemental Material) and the selectivity *versus* permeability plot shown in Figure 10. The revised works cover membranes of FAU, MFI, LTA, MEL, CHA and DDR framework types, and focus on specific materials such as AlPO-18, titanosilicates (AM-3 and AM-2), ZSM-5, SSZ-13, SAPO-34, silicalite-1 and silicalite-2, zeolites P, L, X, Y and β , and clinoptilolite. The data reveal very good performance of zeotypes, since most of the results are above the revised Robeson's upper bound (red line in Figure 10) for H₂/CO₂ separation in polymeric membranes (247). Comparatively to dense membranes (metallic and ceramic) and silica porous membranes, zeolitic membranes exhibit moderate selectivities (frequently inferior to 50), as can be seen in Table SM4 (Supplemental Material).

Gas separation using zeolite membranes is many times achieved by the interplay of adsorption and diffusion phenomena, with the following five steps: i) adsorption of the gas molecules onto the zeolite pore surface; ii) diffusion from the surface to the interior zeolite channels; iii) diffusion inside the zeolite channels; iv) diffusion from the channel back to the external surface; and v) desorption from the surface to the bulk phase. Adsorption affinity is an important factor for separation performance and it depends on gas and zeolite characteristics. The most important parameters of the gas are polarizability and dipole or quadrupole moments, which are responsible for the strength of the interactions between molecule and zeolite surface. On the other hand, the most important parameters for the adsorbent are the polarity, the framework's topology, the type of counter ion, and the pore size. The polarity is directly related to the amount of Al present in the framework. In other words, aluminum rich zeolites (ratio Si/Al \approx 1) are highly selective for polar molecules while silica rich zeolites (ratio Si/Al \geq 10) show stronger adsorption towards non-polar molecules (248, 249).

With respect to the prevailing transport mechanisms in zeolite membranes, they are the same already presented above for the silica ones (see Section 4.1 and Figure 7). Several articles focus in detail the kinetics of gas permeation in zeotype membranes (188–198, 250). Despite the success in the development of zeolite membranes for gas separation, so far only one application appeared at industrial scale, namely the dewatering of bioethanol by steam permeation using LTA membrane (234).

5.1 Supports for zeolite membranes

Thin and self-standing zeolite layers are typically brittle and difficult to produce, thus zeolite membranes are usually synthesized on disk-shaped or tubular porous supports that convey mechanical resistance without penalizing mass transfer (251). The most common supports are α -Al₂O₃, TiO₂, ZrO₂ and stainless-steel, with α -Al₂O₃ being the most cited in the literature review summarized in Table SM4 (Supplemental Material), probably due to its smooth top surface (252). The interest in stainless-steel supports has been declining because of their higher thermal expansion coefficient and rougher surfaces which make them more susceptible to crack and adhesion problems (234). Recently, hollow fibers have been successfully applied as membrane supports due to their high effective area per unit volume, self-supporting capacity and ease of handling (253, 254). Despite these advantages, the high cost of this type of supports limits their use for zeolite membranes at industrial level. Since the ceramic support is responsible for, at least, 70 % of the zeolite membrane cost (255) the quest for cheaper materials has motivated some authors to investigate alternative materials such as clay-alumina and Mullite (256–258).

5.2 Zeolite membrane synthesis

Several strategies have been developed to synthesize supported zeolite membranes, the most important being hydrothermal synthesis without seeding (*in situ* crystallization method) (242, 259, 260), pore-plugging (254, 261), secondary growth methods (190, 191, 239, 246, 256, 262–268), dry

gel conversion methods (vapor-phase transport method and steam-assisted crystallization method) (269), and hydrothermal methods assisted with microwave heating (235, 270).

The *in situ* crystallization method is simple and easy to implement. It consists in the immersion of the support into the synthesis solution/gel, followed by direct crystallization of the zeolite membrane on the support surface, at high temperatures (>373 K or 100°C), without seeding. In order to obtain high quality and pinhole-free membranes, the surface of the support should be smooth and hydrophilic with good wettability, and the crystal size in the zeolite layer should be lower than $1\ \mu\text{m}$ (242). Vroon *et al.* (259) and Kong *et al.* (260) proposed a two-step growth of MFI membranes by varying the temperature at each step. In this way, a large number of nuclei is formed at low temperature (first step) and crystallization occurs at high temperature (second step), forming a good-quality continuous zeolite layer (260).

In the secondary growth method, nucleation sites are created and applied on the surface of a support separately. Seed crystals facilitate the formation of a pure zeolite layer and provide better control of microstructure (crystal size, coverage, orientation, and thickness), which affect the separation performance of the zeolite membranes (239, 246). Several methods have been used to attach zeolite seeds on a support surface, with rubbing (190, 191, 262, 263, 268), dip-coating (256, 264, 265), and cationic polymer addition (266, 267) being the most common, as can be seen in Table SM4 (Supplemental Material).

Microwave assisted hydrothermal methods have been successfully used in zeolite synthesis since 1990 (271). Crystallization is promoted by microwave heating instead of conventional oven-heating, advantageously creating small particles with narrow particle size distribution, and providing high purity materials in very short times (235). The improved permeance and selectivity reported in the literature for zeolite membranes prepared by this method makes it a promising route for industrial implementation (272, 273). For example, an LTA zeolite membrane synthesized without seeding by the two-step “*in situ* aging-microwave heating” method proposed by Li *et al.* (272) displayed high H_2 permeation ($1.7 \times 10^{-7}\ \text{mol m}^{-2}\ \text{s}^{-1}\ \text{Pa}^{-1}$) and H_2/N_2 ideal selectivity (5.6) values.

The ionothermal synthesis is an alternative method that uses ionic liquids as reaction media (instead of water or organic solvents) and occurs under atmospheric pressure. This method has been receiving attention and is considered very promising for the preparation of AlPO membranes (274, 275). Notwithstanding, the process presents some drawbacks namely the high cost of ionic liquids, the low yield of zeolites, and the low solubility of silica precursors in ionic liquids (274).

5.3 Zeolite membranes: seeding methods

Rubbing, dip-coating, and cationic polymer addition are the most common seeding methods used in the preparation of supported zeolite membranes (see Table SM4 in Supplemental Material).

Rubbing is a simple procedure in which small brushes are used to implant the crystal seeds on the outer or inner surface of tubular supports. It is generally challenging to get a continuous and regular seed layer (252), crucial to obtain good quality membranes.

Dip-coating is a seeding procedure wherein the support is immersed in the colloidal suspension of zeolite particles for a precise time, followed by drying, and sometimes by calcination, to promote the attachment of the crystals to the support surface. Due to the difficulty in obtaining a uniform and continuous seeding layer, usually the coating step is repeated several times (252, 276).

Seeding by the cationic polymer addition method involves the adsorption of positively charged cationic polymers, such as poly-DADMAC (258, 266) or Redifloc (266), on the support. The subsequent movement of the ammonium polymer anion (usually chlorides) to the solution attracts the negatively charged silicate nanoparticles to the positively charged surface (277).

Jabbari *et al.* (276) recently compared three different seeding methods (dip-coating, rubbing, and electrophoretic deposition) used for SAPO-34 thin film fabrication. Seed rubbing resulted in a defect-free and uniform layer evaluated for H₂ separation. Hydrogen purity of 84.2 mol.% was obtained for equimolar H₂/CH₄ mixture separation, with a permeance of 6×10^{-8} mol m⁻² s⁻¹ Pa⁻¹ and selectivity $\sigma_{H_2/CH_4} = 28.4$, at a pressure drop of 1 bar and room temperature (293 K).

Several attempts to improve the seeding step have been reported in the literature, such as: (i) the hot dip-coating method proposed by Chen *et al.* (278), (ii) the seeding procedure of Algieri *et al.* (252) which involves cross-flow filtration, support tilting, and support rotation, (iii) the sequential "dip-coating rubbing dip-coating" method from Xiao *et al.* (279), (iv) the rubbing-seed-paste seeding proposed by Wang *et al.* (280) to achieve high pervaporation performance of NaA membranes, (v) the wetting assisted rub-coating seed deposition technique which consists of dip-coating the support with a wetting agent and then rubbing with dry seeds (281), and (vi) the steam-assisted conversion seeding proposed by Zhou *et al.* (246) in the synthesis of SAPO-34 membranes.

5.4 Post-treatment methods of zeolite membranes

A large number of zeolites have a relatively large pore size (*e.g.* MFI zeolites \approx 0.55 nm) compared to H₂ which has a kinetic diameter of 0.289 nm. Therefore, it is difficult to use them directly in the separation of hydrogen from other light gas molecules by molecular sieve mechanism. On the other hand, boundary defects in polycrystalline membranes are normally formed during hydrothermal growth and calcination steps. Membrane performance can be improved by reducing these defects or diminishing the crystal pore size, using post-synthesis techniques (282). For an extensive review about several post-synthesis modifications see the publication of Valtchev *et al.* (238).

In the case of membranes for hydrogen separation, chemical vapor deposition (CVD) and catalytic cracking deposition (CCD) are the most common post-synthesis methods. CVD of amorphous silica is usually utilized to eliminate the intercrystalline defects of zeolite membranes, using either one-sided or counter-diffusion CVD methods (see Section 4 for a detailed description). Furthermore, CVD deposition of amorphous silica in the pores provides a uniform and narrow pore size distribution (283, 284). For instance, Kanezashi and Lin (285) studied MFI membranes post-treated by CVD methods, using tetraethoxysilane (TEOS) as reactant. They reported H₂/CO ideal selectivities 16 and 12 times higher after membrane treatment with one-sided CVD and with on-stream counter-diffusion CVD, respectively. Zheng *et al.* (286) showed that CVD applied on a DDR (Deca-Dodecasil 3 Rhombohedral) membrane improved H₂/CO₂ selectivity (from 2.6 to 32.7) and reduced H₂ permeance (from 23×10^{-7} to 0.3×10^{-7} mol m⁻² s⁻¹ Pa⁻¹) at 823 K (550°C). Zhu *et al.* (283) studied the influence of on-stream CVD modification on H₂ and CO₂ single gas permeances at 723 K (450°C), in MFI-type zeolite membranes. The results, presented in Figure 11, show a decrease in permanence of both gases (faster at the beginning, then slower) and an increase of the ideal selectivity (from 3.6 to 16) (283).

Catalytic cracking deposition (CCD) of silane compounds, which causes coke deposition in the pores of the zeolites, has been used to increase the selectivity of H₂ from mixtures containing other light gases despite the sharp drop in permeance (287, 288). The method exploits the chemisorption of coke (containing Si atoms) on the active sites of the zeolite and its subsequent calcination, forming an amorphous silica network (287). For instance, Masuda *et al.* (287) modified the effective pore of ZSM-5 membrane by CCD, using MDMS (methyldiethoxysilane) and MDMS (methyldimethoxysilane) as silane compounds, which are adsorbed on active sites within the zeolite. The catalytic cracking and calcination steps produce a reduction in pore size, which increase the H₂/N₂ selectivity from 1.4–4.5 to 90–140. Gu *et al.* (289) modified MFI membranes by on-stream CCD of MDMS reporting improved H₂/CO₂ ideal selectivity (from 2.78 to 17.5) and diminished unary H₂ gas permeance (from 2.75×10^{-7} to 1.86×10^{-7} mol m⁻² s⁻¹ Pa⁻¹) at 723 K (450°C). Hong *et al.* (288)

investigated on-stream CCD of MDES over MFI zeolites, with and without a previous H⁺ ion exchange (to increase acid sites in the membrane layer) aiming the improvement of the H₂/CO₂ separation. The results displayed in Figures 12(a) and (b) show that CO₂ permeance decreased significantly after 1 h modification, from 10⁻⁷ to 0.18x10⁻⁷ mol m⁻² s⁻¹ Pa⁻¹, and from 10⁻⁷ to 0.07x10⁻⁷ mol m⁻² s⁻¹ Pa⁻¹, for the membrane with (HMFI) and without (MFI) acid treatment, respectively. In both cases the H₂ permeance decreased slightly during the modification leading to a remarkable increase of the H₂/CO₂ separation factor, from 2.6 to 12.0 (MFI) and from 3.0 to 42.6 (HMFI) (288). Typically, the H₂ permeance in HMFI membrane after CCD modification was around 2.85x10⁻⁷ mol m⁻² s⁻¹ Pa⁻¹ at 773 K or 500°C (288).

Other post-treatment methods are being developed to overcome some of the drawbacks of the CVD and CCD methods, namely the expensive equipment required and the difficulties in scaling-up (277). Chemical liquid deposition (CLD) (282) and dip-coating (290) have been researched due the moderate operation conditions and simple scale-up, despite being less efficient than the previous mentioned methods.

Ion exchange is a unique characteristic of zeolites that can be exploited to improve its adsorption and diffusion properties without degrading the zeolite crystals or membranes (291, 292). In fact, ion exchange can be used to tune the pore size of zeolites through the accurate choice of the counter ion. For example, when Na⁺ is exchanged with Ca²⁺ the pore size of NaA zeolite is enlarged (from 0.4 nm to 0.5 nm) thus allowing the adsorption of linear hydrocarbons while still blocking the branched ones. On the other hand, exchanging Na⁺ with K⁺ reduces the pore size (from 0.4 nm to 0.3 nm), hence only small molecules, such as H₂O, He, and H₂, can penetrate the pores (293). Aoki *et al.* (293) studied ZSM-5 zeolite membranes (Si/Al = 25) ion exchanged with different cations from groups 1 and 2 of periodic table and concluded that single gas (He, H₂, CO₂, N₂, and others) permeance followed the order K⁺< Ba²⁺ ≈ Ca²⁺ < Cs⁺ < Na⁺ ≈ H⁺, increasing inversely to the ion size except for Cs⁺ ion. An *et al.* (291) investigated the performance of clinoptilolite membranes modified by cation exchange with different metal ions (Li⁺, Na⁺, K⁺, Ca²⁺, Sr²⁺, and Ba²⁺) at two temperatures. The results presented in Figure 13a show that the H₂/CO₂ selectivity is enhanced for the Li⁺ and Ca²⁺ exchanged forms (increasing around six and three times, respectively, at 573 K or 300°C) and practically unchanged for the other forms. Recalling once again the case of MFI and HMFI membranes introduced above and illustrated in Figure 12a and 12b, it is clear the influence of ion exchanging the parent MFI membrane with H⁺, taking into account the hydrogen permeance increased 20 % with this treatment (compare the initial 30 min of both figures). Nevertheless, few studies have been carried out on ion exchanged zeolite membranes for hydrogen separation.

5.5 Pre-treatment methods of zeolite membranes

One of the challenges in supported membrane synthesis is to guarantee a high density of nucleation sites on the support, and consequently improve crystal growth on its surface and avoid the formation of defects. In addition, under synthesis conditions ceramic supports and aluminosilicates exhibit the same negative zeta potential, which results in electrostatic repulsion and therefore unsuitable membranes (15). Different pre-treatment approaches have been described in the literature in order to increase van der Waals interactions, covalent bonding, and hydrogen bonding between the “anchoring” groups on the support and the zeolite crystals (294).

Huang and co-authors are pioneers in the preparation of zeolite LTA and FAU membranes without seeding, using 3-aminopropyltriethoxysilane (APTES) (295–297), 1,4-diisocyanate (DIC-4) (298), and 3-chloropropyltrimethoxysilane (CPTMS) (299) as covalent linker between the zeolite layer and a porous α-Al₂O₃ support. These molecular linkers attach and anchor the zeolite precursors onto the support surface by covalent bonds, promoting the nucleation and growth of the zeolite layers. For example, with CPTMS a 3.0 μm zeolite LTA layer on porous Al₂O₃ was obtained without cracks, pinholes or other defects, and exhibited H₂/CO₂, H₂/N₂, H₂/CH₄ real selectivities of 7.4, 6.8 and 5.2,

respectively (299). These values are higher than the corresponding Knudsen coefficients (4.7, 3.7 and 2.8) (299) at 293 K and 1 bar, which implies the membrane contains no macro- nor meso-defects (188). Similarly, a LTA/Al₂O₃ membrane prepared with APTES linker presented remarkably high selectivities for H₂/CH₄, H₂/N₂, H₂/O₂, and H₂/CO₂ systems (see Figure 13b), in comparison to the parent membrane without APTES treatment (296).

Polydopamine (PDA) (300, 301) is a bio-inspired adhesive recently disclosed as a versatile and environmentally friendly covalent linker, which allows the large-scale production of supported zeolite membranes and manufacturing at lower costs. The effect of the polymer pre-coating linker (buffer layer) was studied by Naskar and co-workers using polyethyleneimine (PEI) on NaA zeolite membranes (302), APTES on Silicalite-1 membranes (303), and polyvinylpyrrolidone (PVP) on NaA membranes (304). Permeation studies for PEI on NaA membranes gave ideal selectivities of 92 (H₂/CO₂) and 20.5 (H₂/N₂) at 338 K (65°C) and 1 bar (302). Other important studies related to covalent linkers are present by Zhou *et al.* (305) and Lee *et al.* (306). Recently, Xu *et al.* (307) combined the advantages of this polymer pre-treatment and the ion exchange post-treatment methods, and synthesized a supported LTA membrane on APTES-modified α -Al₂O₃ tube, followed by a silver-exchange treatment. The resulting Ag-LTA membrane exhibited high hydrogen selectivity, with the H₂/C₃H₈ separation factor increasing from *ca.* 19.4 (for the starting Na-LTA membrane) to *ca.* 120.8 (307).

Another approach to obtain uniform and dense membrane layers consists in the surface modification of the support with a cationic polymer, to promote the adsorption of negatively charged zeolite crystals on a positively charged polymer by van der Walls interactions, during the hydrothermal synthesis (294, 308).

The chemical nature of the support and its structural characteristics can affect the type of zeolite formed, which means that the precursor materials (such as Si or Al) or ionic impurities contained in the support can significantly alter the local synthesis on the support surface (309). On the other hand, zeolite membranes formed on a porous α -alumina support contain more aluminum than those formed on stainless-steel or zirconia supports, which can deteriorate the quality of the membrane, mainly at high temperature operating conditions (310). In fact, Dong and co-workers (284) verified that a zeolite membrane prepared from an aluminum free solution and synthesized *in situ* over a alumina porous support, incorporated Al³⁺ which migrated from the alumina porous support during the synthesis.

Intermediate layers can be coated on a porous substrate, as a buffer layer, to improve surface adhesion and the structural stability of the membrane. Chau *et al.* (309) studied the influence of metal and metal oxides ultrathin layer deposition on stainless-steel supports and concluded that this is a simple technique to control the number and type of nucleation sites available on the surface of the support. Yttria stabilized zirconia (YSZ) is an example of a barrier buffer used sometimes to prevent the diffusion of Al³⁺ from the porous support into the zeolite layer (310, 311). Wang *et al.* (311) used YSZ deposition to develop a bilayer MFI zeolite membrane (ZSM-5/silicalite/ α -alumina with YSZ as intermediate barrier) which was stable at 773 K, for at least 24 days. This membrane exhibited hydrogen permeance of about 1.2×10^{-7} mol m⁻² s⁻¹ Pa⁻¹ and selectivities of 23, 28 and 180 for H₂/CO₂, H₂/CO, and H₂/H₂O vapor, respectively (311).

Rapid thermal processing (RTP) is another pre-synthesis method where a pre-calcination treatment is adopted in order to eliminate or minimize possible grain boundary defects and crack formations occurring during zeolite synthesis (312). The condensation of Si-OH groups occurs between adjacent crystal grains, forming Si-O-Si bonds which improve the mechanical integrity. However, no experimental results for hydrogen separation have been reported yet.

6 Carbon molecular sieve membranes

Carbon molecular sieve membranes (CMSMs) result from pyrolysis or carbonization reactions of a polymeric precursor during a heat treatment under controlled atmosphere or in vacuum. The decomposition of the polymeric chains originates an amorphous carbon skeleton with interconnected pores, whose pore size distribution can be fine-tuned by controlling the synthesis conditions. These materials exhibit significant advantages for the separation of gas mixtures mainly due to their high thermal and chemical resistance, controllable pore size distribution, and high permeabilities and selectivities towards several permanent gases (*e.g.*, H₂, O₂, N₂). For instance, selectivities are well above the present Robeson upper bound (313), as shown in Figure 14, where literature data for the H₂/CO₂ and H₂/N₂ selectivities *versus* H₂ permeability are plotted for several CMSMs listed in Table SM5 in Supplemental Material. The experimental results show that the selectivities of these membranes towards H₂ are relatively higher when compared to zeolite membranes, but significantly lower than dense membranes.

The concept of carbon membrane has been used since 1973, when Ash *et al.* (314) compressed non-porous graphite into a plug and named it “carbon membrane”. However, its usefulness for gas separation emerged later, in 1983, when Koresh and Soffer (315) reported a CMSM with 0.3–0.5 nm micropores showing high selectivities in gas separations. In 1993, Rao and Sircar (316, 317) introduced surface flow membranes (SSF) a new type of carbon membranes with larger micropores (0.5–0.7 nm) than CMSM.

Since the internal constrictions of carbon membranes exhibit dimensions similar to those of adsorbing/permeating species, molecular sieving becomes the main separation mechanism. When micropores are slightly larger than the diffusion molecules (*e.g.*, in the range of 0.5–0.7 nm) adsorption takes place and the separation of nonadsorbable and/or weakly adsorbable components (such as O₂, N₂ and CH₄) from adsorbable molecules (such as NH₃, SO₂, H₂S) may be successfully accomplished (318). Others mechanisms responsible for mass transfer in microporous materials are briefly discussed in Section 4.1 and illustrated in Figure 7. The essays of Rao and Sircar (319), Ramirez (320) and Gilron and Soffer (321) may be pointed as examples of phenomenological and/or molecular dynamics modelling of CMSMs.

6.1 Configurations of carbon molecular sieve membranes

Carbon membranes can be unsupported or supported (self-supported), and prepared in different forms depending on the envisioned final application (313). Unsupported membranes are usually presented in the form of flat films, hollow fibers, and capillary tubes, while supported membranes can be flat or tubular, depending of the shape of the support. Several different supports can be used, such as α -alumina, γ -alumina, macroporous carbon supports, and porous metal supports (322). The supports are typically coated with a thin and uniform layer of the polymeric precursor for subsequent carbonization or pyrolysis. The coating is once again prepared using various known techniques such as ultrasonic deposition, dip-coating, vapor deposition, spin-coating, and spray coating (16).

Brittleness can be a problem for unsupported membranes. On the other hand, the multiple polymer deposition and carbonization cycles used in order to obtain crack-free supported membranes present an impediment to practical applications (4). In order to strengthen the interfacial adhesion between carbon molecular sieve (CMS) layers and the support, intermediate layers can be added to reduce pore sizes and improve the support chemical characteristics and therefore facilitate the formation of CMS layers. Mordenite framework inverted (MFI)-type on α -Al₂O₃ (323) and silica phase on stainless-steel supports (322) are some examples. Another approach involves the incorporation of nanofillers to change the support porous structure, namely, to reduce its average pore size and porosity (324). Table SM5 in Supplemental Material reviews different studies of hydrogen

separation using CMSMs, where the membrane configuration and the type of support, if present, are listed along with available or calculated permeabilities and selectivities.

6.2 Carbon-based membrane fabrication

The preparation of carbon-based membranes for gas separation involves the optimization of six sequential steps, identified by Saufi and Ismail (325) as follows: 1. Precursor selection; 2. Precursor preparation; 3. Pre-treatment; 4. Pyrolysis; 5. Post-treatment; and 6. Module construction. The first and fourth are the crucial steps, *i.e.* the ones which influence the most the final success of the membrane by determining the pore dimensions of the carbon network (4).

Precursors. Several carbon-containing compounds such as, for example, resins, pitch, coal, graphite, plants, and synthetic polymers can be used to obtain carbon membranes through pyrolysis or carbonization processes (326). Polymeric materials are usually preferred due to higher yields of fixed carbon, thermosetting properties, homogeneous texture, and good processability (327). In particular, the most used for hydrogen permeation are polyimides (328–330), polyetherimides (PEI) (323, 331, 332), and poly(furfuryl alcohol) (PFA) (333–335). The polymeric precursor should not melt or soften during pyrolysis, in order to prevent the presence of cracks and pinholes on the carbon structure (327, 336). Also important is the choice of support, which must consider factors like durability, carbon compatibility, chemical reactivity, heat transfer characteristics, and economics (*i.e.* cost, availability, *etc.*) (325). Table SM5 (Supplemental Material) identifies the main precursors cited in the literature for the preparation of CMSM used for H₂ separation.

Pre-treatment. Physical and chemical treatments may be applied before the pyrolysis step to ensure that the structure of the precursor is preserved and to provide additional dimensional stability to the polymeric matrix. For example, oxidation pre-treatments have been reported to stabilize certain polymer precursors thus preventing the melting or fusion of the film (membrane), and an excessive release of volatiles during the pyrolysis step (325). Furthermore, stretching of the polymer matrix is reduced and attenuates non uniformities in the pore size distribution, thus affecting the selectivity of the resulting CMSM (325).

Pyrolysis/carbonization. This is one of the main steps of the whole process, together with precursor selection. In this step the precursor is submitted to a specific heating protocol, under a controlled inert or vacuum atmosphere, generating an amorphous carbon membrane with a porous structure (pore size, shape, and their interconnectivity) characteristic of the polymer precursor used. The pyrolysis parameters, such as heating rate, soaking conditions, end temperature, and gas atmosphere, also intervene in the pore network structure and thus on the performance of CMSMs (327). The porous structure is associated to formation and release of volatile matter, typically H₂, H₂O, CO, CO₂, and residual HCN, CH₄ and NH₃, depending on precursor's nature (337). Representative pyrolysis conditions of CMSM used in the literature for H₂ separation are presented in Table SM5 (Supplemental Material).

Post-treatment. There are several post-treatment alternatives, for instance, another polymer or a second carbonization with other polymers is often used in order to repair eventual defects. Additionally, for a more precise pore tuning, post-oxidation or chemical vapor deposition methods can be used to reopen/enlarge or to close/reduce the pores, respectively (50, 335). Passivation treatments with hydrogen at high temperatures (873 K, 600°C) have also been used for the partial removal of oxygen functional groups from the surface of CMSMs (338).

Module construction. The geometry and the mode of packing membranes inside membrane modules are important features for their separation performance and industrial implementation. Modules of hollow fibers with asymmetric structure improve selectivity and permeability, and reduce the limitations due to membrane brittleness (339). Large-scale CMSM modules have been reported by Lagorsse *et al.*, namely, a module containing CMS hollow fiber membranes (340) and CMS flat

membrane with a honeycomb configuration (341). The cost of the module, the type of application, and the functionality of the module, all influence the selection of its final configuration.

6.3 Limitations of carbon molecular sieve membranes

Carbon membranes offer great advantages but a few drawbacks have been identified, such as brittleness, fragility, reproducibility, and production costs. For instance, the cost of a CMSM per unit of active area is one to three orders of magnitude higher when compared to polymeric membranes (342). Moreover, CMSMs exhibit complications related to their performance stability towards O₂ but especially towards humidity. In fact, quite often CMSMs suffer fast oxidation in contact with ambient air and permeability drops (it may decrease orders of magnitude) due to adsorption of water or other vapors as molecular clusters. In the presence of ambient air, O₂ combines with the active sites of CMSM to form surface oxygen containing functional groups that reduce the open porosity. Then, in contact with humidity, water initially adsorbs onto these hydrophilic sites and then the adsorbate-adsorbate interactions promote the adsorption of other molecules through hydrogen bonds, thus forming clusters that may block the membrane (338).

Campo *et al.* (343) developed a new preparation approach to produce CMSM from cellophane paper in a single pyrolysis step. These CMSMs proved to be stable towards humidity (at least up to 80 % relative humidity) and in the presence of O₂, and they provide high permeabilities and selectivities well above the Robeson upper bound. Although based on single component permeation experiments, the selectivities for the pairs H₂/N₂, H₂/O₂, and H₂/CO₂ were considered relevant for hydrogen separation, taking into account they achieve values of 1310.0, 170.9, and 58.6, respectively (343).

6.4 Composite carbon molecular sieve membranes

To surpass the abovementioned CMSM limitations (brittleness, lower mechanical stability and low reproducibility) and in an attempt to improve permeability and/or selectivity, composite carbon/inorganic membranes have emerged (16). Composite CMS membranes are produced by pyrolysis of a mixed-matrix membrane containing a continuous polymer matrix and nanosized inorganic particles incorporated in the polymer. The particles are mostly metals, silica, zeolites, and carbons (339). The separation performance of different metal and zeolite CMS composite membranes (M-CMS and Zeolite-CMS, respectively) for H₂/CO₂ and H₂/N₂ separations is illustrated in Figure 14.

Lie *et al.* (344) observed that CMSMs containing Ag and Cu exhibited higher H₂ permeabilities than those doped with Ca and Mg, due to the facilitated transport effects of Ag and Cu. Yoshimune *et al.* (345) prepared hollow fiber carbon membranes derived from sulfonated poly(phenylene oxide) and doped with different metals ions (Na⁺, Mg²⁺, Al³⁺, Ag⁺, Cu²⁺, and Fe³⁺). Yoda *et al.* (346) investigated Pt- and Pd-doped carbon membranes of polyimide films prepared by supercritical impregnation, for hydrogen separation. Suda *et al.* (347) revealed that increasing the metal content in Pd-doped CMSM, from 0 to 3.8 wt.%, results in an increase of H₂/N₂ selectivity from 331.3 to 5579.8, as shown in Figure 15.

In the last decade, the use of silica and zeolite as additives for mixed-matrix carbon membranes has sparked considerable interest (322, 348, 349). According to Liu *et al.* (349), phase separation effect between the carbon matrix and the zeolite leads to the formation of interfacial gaps and subsequent improvement in the permeability.

Carbon membranes doped with carbon nanotubes are also successfully employed (350). These results are also summarized in Table SM5 in Supplemental Material together with the main characteristics of composite CMSMs reported in the literature for hydrogen separation.

6.5 Carbon nanotubes

Since their discovery in 1991, carbon nanotubes (CNTs) have attracted great interest due to remarkable properties such as high strength, large specific area, and good electrical conductivity (351). CNTs belong to the fullerene structural family and can be produced by arc discharge process, laser ablation, chemical vapor deposition of hydrocarbon gases, or pyrolysis of plastics (352, 353). Structurally, CNTs are divided into two distinct forms, namely single-walled (SWNT) and multi-walled (MWNT), depending if they consists of either one cylindrical graphene sheet or of several nested cylinders with an interlayer spacing, respectively (354). Due to the great smoothness of the nanotubes walls, these materials present exceptionally high transport rates (355).

Mi *et al.* (356) studied the permeances of different gases through vertically aligned MWNT membranes grown on a porous alumina support and concluded that the diffusivity measured is about four times larger than the Knudsen model prediction. Molecular dynamic calculations reported by Chen and Sholl (357) also indicate higher fluxes and preferential adsorption of CH₄ over H₂, when a mixture of these gases permeates through SWNT. On the other hand, Ge *et al.* (358) reported that hydrogen permeance is one to two orders of magnitudes higher than the Knudsen prediction, while the gas selectivities are still in the Knudsen range. Ge *et al.* (359) reported enhanced hydrogen separation (higher selectivity) achieved with CNT membranes containing a zeolite framework as a gas selective layer. These and other results are compiled in Table S5 (Supplemental Material).

6.6 Applications of carbon molecular sieve membranes

The production of low cost and pure nitrogen from air is by far the largest application of carbon membranes, yet hydrogen separation remains an active field of investigation (313, 342). The recovery of hydrogen from off-gas streams in refineries and other petrochemical-based complexes is gaining importance in order to achieve significant overall cost reductions (360, 361). CMSMs are a promising type of membranes for this purpose, for it has been demonstrated that they are able to achieve excellent performance in the separation of light hydrocarbons from hydrogen, *e.g.* methane (362). Moreover, Grainger and Hägg (363) reported the recovery of hydrogen from hydrogen-natural gas mixtures in a distribution network using CMSMs.

CMSMs can be considered as a possible alternative to Pd-based membranes currently used in membrane reactors for hydrogen production (339). Many more examples can be found in the literature for the use of CMSM in membrane reactors for hydrogen production and/or to increase product yield, such as, for example: dehydrogenation of cyclohexane (364), hydrogenation of olefins (365), hydrogenation of propylene (366), dehydrogenation of isobutene (367), methanol steam reforming (368), and water gas shift reaction (369, 370). Recently, Parsley *et al.* (371) reported the preparation and testing of full-scale CMSM modules (containing 86 tubes) used as membrane reactor to produce high-purity H₂ from biomass and/or coal derived syngas *via* water gas shift reaction.

7 Conclusions

Over the past 20 years inorganic membranes experienced great progress becoming a real alternative for separation/purification of hydrogen from gas mixtures. In this review, the main inorganic material types were addressed being possible to divide them into dense phase (metallic and proton conducting) and porous (silica, zeolites and carbon molecular sieve) membranes, which can be further classified as unsupported and supported. The latter are more attractive because a supported thin top layer of a specific inorganic material guarantees inferior mass transfer resistance, and thus higher gas permeance, and frequently lower costs. The most important deposition methods for each membrane type were reviewed, with emphasis on the well-known chemical vapor deposition, electroless plating deposition for metallic membranes, sol-gel for proton conducting and silica membranes, and dip-

coating, rubbing and in situ hydrothermal synthesis for zeolitic membranes. Although different supports can be used, the most employed are symmetrical and asymmetrical alumina supports. Notwithstanding recent improvements addressed in this review, the most challenging task for porous membranes is their scale up for hydrogen producing technologies. In Table 1 it is presented a comparison between the various inorganic membrane types for hydrogen separation, where their main features, strengths and weaknesses are emphasized.

Palladium membranes are the most studied and implemented at industrial level despite their high price, due to high permeance (in the order of $\mu\text{mol m}^{-2} \text{s}^{-1} \text{Pa}^{-1}$) and huge selectivity towards H₂. Nevertheless the quest for cheaper membranes with high permeability and good chemical/thermal stability still goes on, steering the research on composite Pd/alloy membranes, non-palladium metallic/alloy membranes, and ceramic proton conducting membranes for hydrogen separation. The latter are selective towards hydrogen and intrinsically stable at high temperatures, leading to the development of alternative *cermet* and *cercer* composite materials (*i.e.* ceramics containing a metal or a ceramic dopant, respectively).

Concerning porous membranes, amorphous silica membranes emerge as the simplest and cheapest to produce, but being susceptible to the presence of moisture, which is unavoidable in hydrogen separations, they need to be functionalized using precursors or doping with transition metals to overcome hydro-instability. Zeolite, zeotype and carbon molecular sieve membranes, with permeances generally found in the range 10^{-7} to $10^{-8} \text{ mol m}^{-2} \text{s}^{-1} \text{Pa}^{-1}$ and permeability-selectivity plots frequently exceeding the well-known Robeson upper boundary, are promising candidates for hydrogen separation, since their pore size distribution and gas-solid interactions can be fine-tuned by controlling the synthesis conditions and functionalization. Recent advances for improving adsorption and diffusion properties, reducing defects and/or the pore size of zeolitic membranes, have been made through chemical vapor deposition, catalytic cracking deposition, and ion exchange post-synthesis methods. Covalent linkers between support and zeolite crystals have also been applied to avoid the appearance of defects. Composite carbon molecular sieve membranes (composite CMSMs), particularly metal-CMSM, have been developed to eliminate or control some drawbacks such as brittleness, fragility and synthesis reproducibility, and improve selectivity. Nonetheless, there are no industrial scale applications yet.

Funding

S. P. Cardoso acknowledges a Ph.D. grant from Fundação para a Ciência e a Tecnologia (Portugal) (SFRH/BD/75164/2010). This work was developed within the scope of the project: CICECO-Aveiro Institute of Materials, POCI-01-0145-FEDER-007679 (FCT Ref. UID/CTM/50011/2013), financed by national funds through the FCT/MEC and when appropriate co-financed by FEDER under the PT2020 Partnership Agreement; and Project POCI-01-0145-FEDER-006984 – Associate Laboratory LSRE-LCM funded by FEDER funds through COMPETE2020 – Programa Operacional Competitividade e Internacionalização (POCI).

References

1. (IEA), I.E.A. (2015) World Energy Outlook 2015. Tech. rep., Paris.
2. Ball, M. and Weeda, M. (2015) The hydrogen economy—Vision or reality? *Int. J. Hydrogen Energy*, 40(25): 7903–7919.
3. Zornoza, B., Casado, C., and Navajas, A. (2013) Advances in Hydrogen Separation and Purification with Membrane Technology. Gandia, L.M., Arzamendi, G., and Dieguez, P.M. (eds.), *Renewable Hydrogen Technologies*, pp. 245–268, Elsevier.

4. Ockwig, N.W. and Nenoff, T.M. (2007) Membranes for hydrogen separation. *Chem. Rev.*, 107(10): 4078–4110.
5. Michalkiewicz, B. and Koren, Z.C. (2015) Zeolite membranes for hydrogen production from natural gas: state of the art. *J. Porous Mater.*, 22(3): 635–646.
6. Li, P., Wang, Z., Qiao, Z., Liu, Y., Cao, X., Li, W., Wang, J., and Wang, S. (2015) Recent developments in membranes for efficient hydrogen purification. *J. Membr. Sci.*, 495: 130–168.
7. Mulder, M. (1997) *Basic principles of membrane technology*. Kluwer Academic Publishers, second edition: Dordrecht, Netherlands.
8. Tavolaro, A. and Drioli, E. (1999) Zeolite membranes. *Adv. Mater.*, 11(12): 975–996.
9. Ismail, A.F., Khulbe, K.C., and Matsuura, T. (2015) *Gas Separation Membranes*. Springer: Switzerland.
10. Chung, T.S., Jiang, L.Y., Li, Y., and Kulprathipanja, S. (2007) Mixed matrix membranes (MMMs) comprising organic polymers with dispersed inorganic fillers for gas separation. *Prog. Polym. Sci.*, 32(4): 483–507.
11. Burggraaf, A.J. and Cot, L. (1996) *Fundamentals of inorganic membranes science and technology*. Elsevier: Amsterdam, Netherlands.
12. Basile, A., Gallucci, F., and Tosti, S. (2008) Synthesis, Characterization, and Applications of Palladium Membranes. Mallada, R. and Menéndez, M. (eds.), *Inorganic Membranes: Synthesis, Characterization and Applications*, pp. 255–323, Elsevier: Oxford.
13. Tao, Z., Yan, L., Qiao, J., Wang, B., Zhang, L., and Zhang, J. (2015) A review of advanced proton-conducting materials for hydrogen separation. *Prog. Mater. Sci.*, 74:1–50.
14. Ayral, A., Julbe, A., Rouessac, V., Roualdes, S., and Durand, J. (2008) Microporous Silica Membrane: Basic Principles and Recent Advances. Mallada, R. and Menéndez, M. (eds.), *Inorganic Membranes: Synthesis, Characterization and Applications*, vol. 13 of *Membrane Science and Technology*, chap. 2, pp. 33–79, Elsevier: Oxford.
15. Gascon, J., Kapteijn, F., Zornoza, B., Sebastián, V., Casado, C., and Coronas, J. (2012) Practical Approach to Zeolitic Membranes and Coatings: State of the Art, Opportunities, Barriers, and Future Perspectives. *Chem. Mater.*, 24(15): 2829–2844.
16. Hägg, M.B. and He, X. (2011) Carbon Molecular Sieve Membranes for Gas Separation. Drioli, E. and Barbieri, G. (eds.), *Membrane Engineering for the Treatment of Gases, Volume 2: Gas-separation Problems Combined with Membrane Reactors*, chap. 15, pp. 162–191, Royal Society of Chemistry.
17. Snelling, W.O., Apparatus for separating gases. US patent 1174631, 7 march 1916.
18. El Hawa, H.W.A., Lundin, S.T.B., Patki, N.S., and Way, J.D. (2016) Steam methane reforming in a Pd-Au membrane reactor: Long-term assessment. *Int. J. Hydrogen Energy*, 41(24): 10193–10201.
19. Brunetti, A., Caravella, A., Fernandez, E., Tanaka, D. A. P. Gallucci, F., Drioli, E., Curcio, E., Viviente, J.L., and Barbieri, G. (2015) Syngas upgrading in a membrane reactor with thin Pd-alloy supported membrane. *Int. J. Hydrogen Energy*, 40(34): 10883–10893.
20. Barrer, R.M. (1951) *Diffusion in and Through Solids*. Cambridge University Press: Cambridge.
21. Ward, T.L. and Dao, T. (1999) Model of hydrogen permeation behavior in palladium membranes. *J. Memb. Sci.*, 153(2): 211–231.
22. Caravella, A., Barbieri, G., and Drioli, E. (2008) Modelling and simulation of hydrogen permeation through supported Pd-alloy membranes with a multicomponent approach. *Chem. Eng. Sci.*, 63(8): 2149–2160.
23. Yun, S. and Oyama, S.T. (2011) Correlations in palladium membranes for hydrogen separation: A review. *J. Memb. Sci.*, 375(1–2): 28–45.
24. Mundschauf, M.V. (2009) Hydrogen Separation Using Dense Composite Membranes: Part 1 Fundamentals. Bose, A.C. (ed.), *Inorganic Membranes for Energy and Environmental Applications*, pp. 125–153, Elsevier.
25. Damle, A. (2008) Hydrogen Separation and Purification. Gupta, R.B. (ed.), *Hydrogen Fuel: Production, Transport, and Storage*, pp. 283–324, CRC Press: Boca Raton, FL.

26. Hughes, R. (2001) Composite palladium membranes for catalytic membrane reactors. *Membr. Technol.*, 2001(131): 9–13.
27. Basile, A., Iulianelli, A., Longo, T., Liguori, S., and de Falco, M. (2011) Pd-based Selective Membrane State-of-the-Art. de Falco, M., Marrelli, L., and Iaquaniello, G. (eds.), *Membrane Reactors for Hydrogen Production Processes*, pp. 21–55, Springer Verlag: London.
28. Zhang, X., Xiong, G., and Yang, W. (2008) A modified electroless plating technique for thin dense palladium composite membranes with enhanced stability. *J. Memb. Sci.*, 314 (1–2): 226–237.
29. Mardilovich, P.P., She, Y., Ma, Y.H., and Rei, M.H. (1998) Defect-free palladium membranes on porous stainless-steel support. *AiChE J.*, 44(1–2): 310–322.
30. Gade, S.K., Thoen, P.M., and Way, J.D. (2008) Unsupported palladium alloy foil membranes fabricated by electroless plating. *J. Memb. Sci.*, 316(1–2): 112–118.
31. Braun, F., Miller, J.B., Gellman, A.J., Tarditi, A.M., Fleutot, B., Kondratyuk, P., and Cornaglia, L.M. (2012) PdAgAu alloy with high resistance to corrosion by H₂S. *Int. J. Hydrogen Energy*, 37(23): 18547–18555.
32. Morreale, B., Ciferno, J., Howard, B., Ciocco, M., Marano, J., Iyoha, O., and Enick, R. (2009) Gasification and Associated Degradation Mechanisms Applicable to Dense Metal Hydrogen Membranes. Bose, A.C. (ed.), *Inorganic Membranes for Energy and Environmental Applications*, pp. 173–201, Springer: New York.
33. Morreale, B.D., Howard, B.H., Iyoha, O., Enick, R.M., Ling, C., and Sholl, D.S. (2007) Experimental and Computational Prediction of the Hydrogen Transport Properties of Pd₄S. *Ind. Eng. Chem. Res.*, 46(19): 6313–6319.
34. Braun, F., Tarditi, A.M., Miller, J.B., and Cornaglia, L.M. (2014) Pd-based binary and ternary alloy membranes: Morphological and perm-selective characterization in the presence of H₂S. *Ind. Eng. Chem. Res.*, 450: 299–307.
35. Chabot, J., Lecomte, J., Grumet, C., and Sannier, J. (1988) Fuel Clean-Up System: Poisoning of Palladium-Silver Membranes by Gaseous Impurities. *Fusion Sci. Technol.*, 14: 614–618.
36. Boon, J., Pieterse, J.A.Z., van Berkel, F.P.F., van Delft, Y.C., and Annaland, van S.M. (2015) Hydrogen permeation through palladium membranes and inhibition by carbon monoxide, carbon dioxide, and steam. *J. Memb. Sci.*, 496: 344–358.
37. Platinum Matthey, Johnson Matthey, <http://www.platinum.matthey.com/prices/pricetables>. Accessed in 2017-08-17.
38. Paglieri, S.N. and Way, J.D. (2002) Innovations in Palladium Membrane Research. *Sep. Purif. Rev.*, 31(1): 1–169.
39. Knapton, A.G. (1977) Palladium Alloys for Hydrogen Diffusion Membranes. *Membranes. Platin. Met. Rev.*, 21(2): 44–50.
40. Doyle, M.L. and Harris, I.R. (1988) Palladium-rare earth alloys: Their order-disorder transformations and behavior with hydrogen. *Membranes. Platin. Met. Rev.*, 32(3): 130–140.
41. Vicinanza, N., Svenum, I.H., Naess, L.N., Peters, T.A., Bredesen, R., Borg, A., and Venvik, H.J. (2015) Thickness dependent effects of solubility and surface phenomena on the hydrogen transport properties of sputtered Pd77%Ag23% thin film membranes. *J. Memb. Sci.*, 476: 602–608.
42. Rodina, A.A., Gurevich, M.A., and Doronicheva, N.I. (1971) The Interaction of Hydrogen with Certain Palladium-Gold and Palladium-Silver-Gold Alloys. *Russ. J. Phys. Chem.*, 45(5): 621–623.
43. Didenko, L.P., Savchenko, V.I., Sementsova, L.A., and Bikov, L.A. (2016) Hydrogen flux through the membrane based on the Pd–In–Ru foil. *Int. J. Hydrogen Energy*, 41(1): 307–315.
44. Peters, T.A., Kaleta, T., Stange, M., and Bredesen, R. (2012) Hydrogen transport through a selection of thin Pd-alloy membranes: Membrane stability, H₂S inhibition, and flux recovery in hydrogen and simulated WGS mixtures. *Catal. Today*, 193(1): 8–19.
45. Zhao, L., Goldbach, A., and Xu, H. (2016) Tailoring palladium alloy membranes for hydrogen separation from sulfur contaminated gas streams. *J. Memb. Sci.*, 507: 55–62.
46. Shu, J., Grandjean, B.P.A., Ghali, E., and Kaliagaine, S. (1993) Simultaneous deposition of Pd and Ag on porous stainless steel by electroless plating. *J. Memb. Sci.*, 77(2–3): 181–195.

47. Yan, S., Maeda, H., Kusakabe, K., and Morooka, S. (1994) Thin Palladium Membrane Formed in Support Pores by Metal-Organic Chemical Vapor Deposition Method and Application to Hydrogen Separation. *Ind. Eng. Chem. Res.*, 33(3): 616–622.
48. Ryi, S.K., Lee, S.W., Oh, D.K., Seo, B.S., Park, J.W., Park, J.S., and Lee, D.-W. Kim, S.S. (2014) Electroless plating of Pd after shielding the bottom of planar porous stainless steel for a highly stable hydrogen selective membrane. *J. Memb. Sci.*, 467: 93–99.
49. Xiong, L., Liu, S., and Rong, L. (2010) Fabrication and characterization of Pd/ Nb₄₀Ti₃₀Ni₃₀/ Pd/ porous nickel support composite membrane for hydrogen separation and purification. *Int. J. Hydrogen Energy*, 35(4): 1643–1649.
50. Lee, C.B., Lee, S.W., Park, J.S., Ryi, S.K., Lee, D.W., Hwang, K.R., and Kim, S.H. (2013) Ceramics used as intermetallic diffusion barriers in Pd-based composite membranes sputtered on porous nickel supports. *J. Alloys Compd.*, 578: 425–430.
51. Ryi, S.K., Xu, N., Li, A., Lim, C.J., and Grace, J.R. (2010) Electroless Pd membrane deposition on alumina modified porous Hastelloy substrate with EDTA-free bath. *Int. J. Hydrogen Energy*, 35(6): 2328–2335.
52. Fernandez, E., Medrano, J.A., Melendez, J., Parco, M., Viviente, J.L., Annaland, S.M., Gallucci, F., and Tanaka, P.D. (2016) Preparation and characterization of metallic supported thin Pd–Ag membranes for hydrogen separation. *Chem. Eng. J.*, 305: 182–190.
53. Shi, Z., Wu, S., and Szpunar, J.A. (2006) Microstructure transformation of Pd membrane deposited on a porous Inconel substrate in hydrogen permeation at elevated temperature. *J. Memb. Sci.*, 284(1–2): 424–430.
54. Jarosch, K. and de Lasa, H.I. (1999) Novel Riser Simulator for methane reforming using high temperature membranes. *Chem. Eng. Sci.*, 54(10): 1455–1460.
55. Uemiya, S., Sato, N., Ando, H., Kude, Y., Matsuda, T., and Kikuchi, E. (1991) Separation of hydrogen through palladium thin film supported on a porous glass tube. *J. Memb. Sci.*, 56(3): 303–313.
56. Zaman, J. and Chakma, A. (1994) Inorganic membrane reactors. *J. Memb. Sci.*, 92(1): 1–28.
57. Burggraaf, A.J. (1996) Important characteristics of inorganic membranes. Burggraaf, A.J. and Cot, L. (eds.), *Fundamentals of Inorganic Membrane Science and Technology*, pp. 22–28, Elsevier: Amsterdam, Netherlands.
58. Oyama, S.T., Gu, Y., and Lee, D., Hydrogen-selective silica-based membrane. US patent 7179325, 20 february 2007.
59. Chotirach, M., Tantayanon, S., Tungasmita, S., and Kriausakul, K. (2012) Zr-based intermetallic diffusion barriers for stainless steel supported palladium membranes. *J. Memb. Sci.*, 405: 92–103.
60. Zhang, K., Gao, H., Rui, Z., Liu, P., Li, Y., and Lin, Y.S. (2009) High-Temperature Stability of Palladium Membranes on Porous Metal Supports with Different Intermediate Layers. *Ind. Eng. Chem. Res.*, 48(4): 1880–1886.
61. Shu, J., Adnot, A., Grandjean, B.P.A., and Kaliaguine, S. (1996) Structurally stable composite Pd–Ag alloy membranes: Introduction of a diffusion barrier. *Thin Solid Films*, 286(1–2): 72–79.
62. Wang, D., Tong, J., Xu, H., and Matsumura, Y. (2004) Preparation of palladium membrane over porous stainless steel tube modified with zirconium oxide. *Catal. Today*, 93–95: 689–693.
63. Yu, Z., Xu, Y., Liao, S., and Liu, R. (1996) Catalytic behaviors and gas permeation properties of palladium-containing phenophthalein poly(ether sulfone). *J. Appl. Polym. Sci.*, 61(4): 599–605.
64. Lu, G.Q., da Costa, J.C.D., Duke, M., Giessler, S., Socolow, R., Williams, R.H., and Kreutz, T. (2007) Inorganic membranes for hydrogen production and purification: a critical review and perspective. *J. Colloid Interface Sci.*, 314(2): 589–603.
65. Shu, J., Grandjean, B.P.A., Neste, A.V., and Kaliaguine, S. (1991) Catalytic palladium based membrane reactors: A review. *Can. J. Chem. Eng.*, 69(5): 1036–1060.
66. Ayturk, M.E. and Ma, Y.H. (2009) Electroless Pd and Ag deposition kinetics of the composite Pd and Pd/Ag membranes synthesized from agitated plating baths. *J. Memb. Sci.*, 330(1–2): 233–245.

67. Jeon, S.I., Magnone, E., Park, J.H., and Lee, Y. (2011) The effect of temperature and pressure on the hydrogen permeation through Pd-coated $Ti_{26}Ni_{21}V_{53}$ alloy membrane under different atmospheres. *Mater. Lett.*, 65(15–16): 2495–2497.
68. Ernst, B., Haag, S., and Burgard, M. (2007) Permselectivity of a nickel/ceramic composite membrane at elevated temperatures: A new prospect in hydrogen separation? *J. Membr. Sci.*, 288(1–2): 208–217.
69. Wang, M., Song, J., Wu, X., Tan, X., Meng, B., and Liu, S. (2016) Metallic nickel hollow fiber membranes for hydrogen separation at high temperatures. *J. Membr. Sci.*, 509: 156–163.
70. Jeon, S.I., Park, J.H., Magnone, E., Lee, Y.T., and Fleury, E. (2012) Hydrogen permeation of Pd-coated $V_{90}Al_{10}$ alloy membranes at different pressures in the presence and absence of carbon dioxide. *Curr. Appl. Phys.*, 12(2): 394–400.
71. Fleury, E., Suh, J.Y., Kim, D.i., Jeong, C.H., and Park, J.H. (2012) Hydrogen permeation characteristics of rolled $V_{85}Al_{10}Co_5$ alloys. *Curr. Appl. Phys.*, 12(4): 1131–1138.
72. Jeon, S.I. and Park, J.H. (2013) Hydrogen permeation properties of Pd-coated $V_{89.8}Cr_{10}Y_{0.2}$ alloy membrane using WGS reaction gases. *Int. J. Hydrogen Energy*, 38(14): 6085–6091.
73. Meng, B., Tan, X., Meng, X., Qiao, S., and Liu, S. (2009) Porous and dense Ni hollow fibre membranes. *J. Alloys Compd.*, 470(1): 461–464.
74. Park, J., Hong, T.W., and Jung, M. (2010) Hydrogen permeation on Al_2O_3 -based nickel/cobalt composite membranes. *Int. J. Hydrogen Energy*, 35(23): 12976–12980.
75. Lupi, C., Dell'Era, A., and Pasquali, M. (2009) Nickel–cobalt electrodeposited alloys for hydrogen evolution in alkaline media. *Int. J. Hydrogen Energy*, 5(34): 2101–2106.
76. Buxbaum, R.E. and Kinney, A.B. (1996) Hydrogen Transport through Tubular Membranes of Palladium-Coated Tantalum and Niobium. *Ind. Eng. Chem. Res.*, 35(2):530–537.
77. Luo, W., Ishikawa, K., and Aoki, K. (2006) High hydrogen permeability in the Nb-rich Nb–Ti–Ni alloy. *J. Alloys Compd.*, 407(1–2): 115–117.
78. Hashi, K., Ishikawa, K., Matsuda, T., and Aoki, K. (2004) Hydrogen permeation characteristics of multi-phase Ni–Ti–Nb alloys. *J. Alloys Compd.*, 368(1–2): 215–220.
79. Hashi, K., Ishikawa, K., Matsuda, T., and Aoki, K. (2006) Microstructure and hydrogen permeability in Nb–Ti–Co multiphase alloys. *J. Alloys Compd.*, 425(1–2): 284–290.
80. Hashi, K., Ishikawa, K., Matsuda, T., and Aoki, K. (2005) Hydrogen permeation characteristics of (V, Ta)–Ti–Ni alloys. *J. Alloys Compd.*, 404–406: 273–278.
81. Shi, F. (2010) Microstructure and hydrogen permeability of $Nb_{40}Hf_{30}Ni_{30}$ ternary alloy. *Int. J. Hydrogen Energy*, 35(19): 10556–10559.
82. Hara, S., Sakaki, K., Itoh, N., Kimura, H.M., Asami, K., and Inoue, A. (2000) An amorphous alloy membrane without noble metals for gaseous hydrogen separation. *J. Memb. Sci.*, 164(1–2): 289–294.
83. Shimpo, Y., Yamaura, S.I., Nishida, M., Kimura, H., and Inoue, A. (2006) Development of melt-spun Ni–Nb–Zr–Co amorphous alloy for high-performance hydrogen separating membrane. *J. Memb. Sci.*, 286(1–2): 170–173.
84. Hara, S., Sakaki, K., Itoh, N., Kimura, H.M., Asami, K., and Inoue, A. (2003) Hydrogen permeation through amorphous - $Zr_{36-x}Hf_xNi_{64}$ - alloy membranes. *J. Memb. Sci.*, 211(1): 149–156.
85. Park, K.W. and Shibusaki, Y. (2011) Effect of hydrogenation on the mechanical property of amorphous $Ni_{90}Al_{10}$ membranes. *Int. J. Hydrogen Energy*, 36(15): 9324–9334.
86. Xue, D., Chen, H., Wu, G.H., and Deng, J.F. (2001) Amorphous Ni–B alloy membrane: preparation and application in ethanol dehydrogenation. *Appl. Catal. B*, 214(1): 87–94.
87. Lai, T., Singh, S.S., Singaravelu, A.S.S., Vadari, K.S., Khosravi, A., Chawla, N., and Lind, M.L. (2016) Hydrogen permeability and mechanical properties of NiNb-M (M = Sn, Ti and Zr) amorphous metallic membranes. *J. Alloys Compd.*, 684: 359–365.
88. Paglieri, S.N., Pal, N.K., Dolan, M.D., Kim, S.M., Chien, W.M., Lamb, J., Chandra, S., Hubbard, K.M., and Moore, D.P. (2011) Hydrogen permeability, thermal stability and hydrogen embrittlement of Ni–Nb–Zr and Ni–Nb–Ta–Zr amorphous alloy membranes. *J. Memb. Sci.*, 378(1–2): 42–50.

89. Elangovan, S., Nair, B., Small, T., Heck, B., Bay, I., Timper, M., Hartvigsen, J., and Wilson, M. (2009) Ceramic Membrane Devices for Ultra-High Purity Hydrogen Production: Mixed Conducting Membrane Development. Bose, A.C. (ed.), *Inorganic Membranes for Energy and Environmental Applications*, pp. 67–81, Springer: New York.
90. Phair, J.W. and Badwal, S.P.S. (2006) Review of proton conductors for hydrogen separation. *Ionics*, 12(2): 103–115.
91. Reijers, R. and Haije, W.G. (2008) *Literature Review on High Temperature Proton Conducting Materials: Electrolyte for Fuel Cell Or Mixed Conducting Membrane for H₂ Separation*. ECN.
92. Fabbri, E., Pergolesi, D., and Traversa, E. (2010) Materials challenges toward proton conducting oxide fuel cells: a critical review. *Chem. Soc. Rev.*, 39(11): 4355–4369.
93. Norby, T. and Haugsrød, R. (2006) Dense Ceramic Membranes for Hydrogen Separation. Sammells, A.F. and Mundschau, M.V. (eds.), *Nonporous Inorganic Membranes: For Chemical Processing*, pp. 1–48, Wiley-VCH Verlag.
94. Kreuer, K.D. (2000) On the complexity of proton conduction phenomena. *Solid State Ionics*, 136: 149–160.
95. Fontaine, M., Norby, T., Larring, Y., Grande, T., and Bredesen, R. (2008) Oxygen and Hydrogen Separation Membranes Based on Dense Ceramic Conductors. Mallada, R. and Menéndez, M. (eds.), *Inorganic Membranes: Synthesis, Characterization and Applications*, pp. 401–458, Elsevier: Oxford.
96. Cai, M., Liu, S., Efimov, K., Caro, J., Feldhoff, A., and Wang, H. (2009) Preparation and hydrogen permeation of BaCe_{0.95}Nd_{0.05}O_{3-δ} membranes. *J. Membr. Sci.*, 343(1–2): 90–96.
97. Song, S. (2004) Hydrogen permeability of SrCe_{1-x}M_xO_{3-δ} ($x = 0.05$, M=Eu, Sm). *J. Membr. Sci.*, 167(1–2): 99–105.
98. Iwahara, H., Esaka, T., Uchida, H., and Maeda, N. (1981) Proton conduction in sintered oxides and its application to steam electrolysis for hydrogen production. *Solid State Ionics*, 3–4: 359–363.
99. Zhang, Q., Liu, T., Zhu, Z., Hao, L., and Liu, W. (2012) Modeling of hydrogen permeation for Ni-ceramic proton conductor composite membrane with symmetric structure. *J. Membr. Sci.*, 415–416: 328–335.
100. Norby, T. (2009) Proton Conductivity in Perovskite Oxides. Ishihara, T. (ed.), *Perovskite Oxide for Solid Oxide Fuel Cells*, pp. 217–241, Springer: Boston.
101. Meulenberg, W.A., Ivanova, M.E., Serra, J.M., and Roitsch, S. (2011) Proton-conducting ceramic membranes for solid oxide fuel cells and hydrogen (H₂) processing. Basile, A. and Nunes, S. (eds.), *Advanced Membrane Science and Technology for Sustainable Energy and Environmental Applications*, pp. 541–567, Elsevier: Cambridge.
102. Hamakawa, S. (2002) Synthesis and hydrogen permeation properties of membranes based on dense SrCe_{0.95}Yb_{0.05}O_{3-α} thin films. *Solid State Ionics*, 148(1–2): 71–81.
103. Guan, J., Dorris, S.E., Balachandran, U., and Liu, M. (1997) Transport properties of BaCe_{0.95}Y_{0.05}O_{3-α} mixed conductors for hydrogen separation. *Solid State Ionics*, 100(1–2): 45–52.
104. Zhao, F., Liu, Q., Wang, S., Brinkman, K., and Chen, F. (2010) Synthesis and characterization of BaIn_{3-x}Y_xCe_{0.7}O_{3-δ} ($x = 0, 0.1, 0.2, 0.3$) proton conductors. *Int. J. Hydrogen Energy*, 35(9): 4258–4263.
105. Zhang, C. and Zhao, H. (2012) Chemical and Structural Stability of Sm- and In- Co-Doped Proton Conductor BaCe_{0.80-x}Sm_{0.20}In_xO_{3-δ} in Various Atmospheres. *J. Electrochem. Soc.*, 159(7): 316–321.
106. Wu, Z. (1997) Stability of BaCe_{0.80}Gd_{0.20}O_{0.3} in a H₂O-Containing Atmosphere at Intermediate Temperatures. *J. Electrochem. Soc.*, 144(6): 2170–2175.
107. Fang, S., Bi, L., Yan, L., Sun, W., Chen, C., and Liu, W. (2010) CO₂-Resistant Hydrogen Permeation Membranes Based on Doped Ceria and Nickel. *J. Phys. Chem. C*, 114(24): 10986–10991.
108. Efimov, K., Czuprat, O., and Feldhoff, A. (2011) In-situ X-ray diffraction study of carbonate formation and decomposition in perovskite-type BCFZ. *J. Solid State Chem.*, 184(5): 1085–1089.
109. Yang, C., Zhao, H., Du, Z., Shen, Y., and Yan, C. (2016) Effect of titanium doping on chemical and structural stability and electrical properties of proton-conducting solid electrolyte BaCe_{0.80}Sm_{0.20}O_{3-δ}. *J. Membr. Sci.*, 508: 104–112.

110. Meulenberg, W.A., Ivanova, M.E., van Gestel, T., Bram, M., Buchkremer, H.P., Stover, D., and Serra, J.M. (2010) State of art of ceramic membranes for hydrogen separation. Stolten, D. (ed.), *Hydrogen and Fuel Cells*, pp. 321–350, Wiley - VCH Verlag: Weinheim.
111. Ivanova, M.E. and Seeger, J. (2012) Influence of the $\text{La}_6\text{W}_2\text{O}_{15}$ Phase on the Properties and Integrity of $\text{La}_{6-x}\text{WO}_{12-\delta}$ -Based Membranes. *Chem. Mater. Res.*, 2(2): 56–81.
112. Lin, B., Hu, M., Ma, J., Jiang, Y., Tao, S., and Meng, G. (2008) Stable, easily sintered $\text{BaCe}_{0.5}\text{Zr}_{0.3}\text{Y}_{0.16}\text{Zn}_{0.04}\text{O}_{3-\delta}$ electrolyte-based protonic ceramic membrane fuel cells with $\text{Ba}_{0.5}\text{Sr}_{0.5}\text{Zn}_{0.2}\text{Fe}_{0.8}\text{O}_{3-\delta}$ perovskite cathode. *J. Power Sources*, 183(2): 479–484.
113. Katahira, K., Kohchi, Y., Shimura, T., and Iwahara, H. (2000) Protonic conduction in Zr-substituted BaCeO_3 . *Solid State Ionics*, 138(1–2): 91–98.
114. Ryu, K.H. and Haile, S.M. (1999) Chemical stability and proton conductivity of doped BaCeO_3 – BaZrO_3 solid solutions. *Solid State Ionics*, 125(1–4): 355–367.
115. Azad, A. and Irvine, J. (2007) Synthesis, chemical stability and proton conductivity of the perovksites $\text{Ba}(\text{Ce}, \text{Zr})_{1-x}\text{Sc}_x\text{O}_{3-\delta}$. *Solid State Ionics*, 178(7–10): 635–640.
116. Tao, S.W. and Irvine, J.T.S. (2006) A Stable, Easily Sintered Proton-Conducting Oxide Electrolyte for Moderate-Temperature Fuel Cells and Electrolyzers. *Adv. Mater.*, 18(12): 1581–1584.
117. Medvedev, D., Murashkina, A., Pikalova, E., Demin, A., Podias, A., and Tsiaikaras, P. (2014) BaCeO_3 : Materials development, properties and application. *Prog. Mater. Sci.*, 60: 72–129.
118. Kalyakin, A., Lyagaeva, J., Medvedev, D., Volkov, A., Demin, A., and Tsiaikaras, P. (2016) Characterization of proton-conducting electrolyte based on $\text{La}_{0.9}\text{Sr}_{0.1}\text{YO}_{3-\delta}$ and its application in a hydrogen amperometric sensor. *Sensors Actuators B Chem.*, 225: 446–452.
119. Pakhare, D., Wu, H., Narendra, S., Abdelsayed, V., Haynes, D., Shekhawat, D., Berry, D., and Spivey, J. (2013) Characterization and activity study of the Rh-substituted pyrochlores for CO_2 (dry) reforming of CH_4 - Springer. *Appl. Petrochemical Res.*, 3: 446–452.
120. Pakhare, D. and Spivey, J. (2014) A review of dry (CO_2) reforming of methane over noble metal catalysts. *Chem. Soc. Rev.*, 43(22): 7813–7837.
121. Shimura, T., Komori, M., and Iwahara, H. (1996) Ionic conduction in pyrochlore-type oxides containing rare earth elements at high temperature. *Solid State Ionics*, 86–88: 685–689.
122. Omata, T. and Otsuka-Yao-Matsuo, S. (2001) Infrared Absorption Spectra of High Temperature Proton Conducting Ca^{2+} -Doped $\text{La}_2\text{Zr}_2\text{O}_7$. *Solid State Ionics*, 148(12): 475–482.
123. Haugsrud, R. and Norby, T. (2015) On the mixed ionic-electronic conductivity in Ca-doped $\text{La}_2\text{Ti}_2\text{O}_7$. Linderoth, S., Smith, A., Bonanos, N., Hagen, A., Mikkelsen, L., Kammer, K., Lybye, D., Hendriksen, P., Poulsen, F., Mogensen, M., and Wang, W.G. (eds.), *Proceedings of the 26th Risø International Symposium on Materials Science*, pp. 209–2015, Solid State Electrochemistry: Roskilde, Denmark.
124. Merka, O., Bahnemann, D.W., and Wark, M. (2014) Photocatalytic hydrogen production with non-stoichiometric pyrochlore bismuth titanate. *Catal. Today*, 225: 102–110.
125. Merka, O., Raisch, O., Steinbach, F., Bahnemann, D.W., and Wark, M. (2013) Effects of Nonstoichiometry and Cocatalyst Loading on the Photocatalytic Hydrogen Production with $(\text{Y}_{1.5}\text{Bi}_{0.5})_{1-x}\text{Ti}_2\text{O}_{7-3x}$ and $(\text{YBi})_{1-x}\text{Ti}_2\text{O}_{7-3x}$ Pyrochlores. *J. Am. Ceram. Soc.*, 96 (2): 634–642.
126. Haugsrud, R. and Norby, T. (2006) Proton conduction in rare-earth ortho-niobates and ortho-tantalates. *Nat. Mater.*, 5(3): 193–196.
127. Huse, M., Norby, T., and Haugsrud, R. (2012) Effects of A and B site acceptor doping on hydration and proton mobility of LaNbO_4 . *Int. J. Hydrogen Energy*, 37(9): 8004–8016.
128. Amsif, M., Marrero-López, D., Ruiz-Morales, J.C., Savvin, S., and Núñez, P. (2012) Low temperature sintering of LaNbO_4 proton conductors from freeze-dried precursors. *J. Eur. Ceram. Soc.*, 32(6): 1235–1244.
129. Bi, Z., Peña-Martínez, J., Kim, J.H., Bridges, C.A., Huq, A., Hodges, J.P., and Paranthaman, M.P. (2012) Effect of Ca doping on the electrical conductivity of the high temperature proton conductor LaNbO_4 . *Int. J. Hydrogen Energy*, 37(17): 12751–12759.
130. Mokkelbost, T., Lein, H.L., Vullum, P.E., Holmestad, R., Grande, T., and Einarsrud, M.A. (2009) Thermal and mechanical properties of LaNbO_4 -based ceramics. *Ceram. Int.*, 35(7): 2877–2883.

131. Mokkelbost, T., Kaus, I., Haugsrud, R., Norby, T., Grande, T., and Einarsrud, M.A. (2008) High-Temperature Proton-Conducting Lanthanum Ortho-Niobate-Based Materials. Part II: Sintering Properties and Solubility of Alkaline Earth Oxides. *J. Am. Ceram. Soc.*, 91(3): 879–886.
132. Mielewczyk-Grym, A., Gdula-Kasica, K., Kusz, B., and Gazda, M. (2013) High temperature monoclinic-to-tetragonal phase transition in magnesium doped lanthanum ortho-niobate. *Ceram. Int.*, 39(4): 4239–4244.
133. Chi, X., Wen, Z., Zhang, J., and Liu, Y. (2014) Enhanced conductivity of lanthanum niobate proton conductor by A and B-site co-doping: Synthesis, phase, microstructure and transport properties. *Solid State Ionics*, 268: 326–329.
134. Brandão, A.D., Gracio, J., Mather, G.C., Kharton, V.V., and Fagg, D.P. (2011) B-site substitutions in $\text{LaNb}_{1-x}\text{M}_x\text{O}_{4-\delta}$ materials in the search for potential proton conductors ($\text{M}=\text{Ga, Ge, Si, B, Ti, Zr, P, Al}$). *J. Solid State Chem.*, 184(4): 863–870.
135. Cao, Y., Chi, B., Pu, J., and Jian, L. (2014) Effect of Ce and Yb co-doping on conductivity of LaNbO_4 . *J. Solid State Chem.*, 34(8): 1981–1988.
136. Haugsrud, R. and Norby, T. (2007) High-Temperature Proton Conductivity in Acceptor Substituted Rare-Earth Ortho-Tantalates, LnTaO_4 . *J. Am. Ceram. Soc.*, 90(4): 1116–1121.
137. Stubican, V.S. (1964) High-Temperature Transitions in Rare-Earth Niobates and Tantalates. *J. Am. Ceram. Soc.*, 47(2): 55–58.
138. Vullum, F., Nitsche, F., Selbach, S.M., and Grande, T. (2008) Solid solubility and phase transitions in the system $\text{LaNb}_{1-x}\text{Ta}_x\text{O}_4$. *J. Solid State Chem.*, 181(10): 2580–2585.
139. Santibáñez-Mendieta, A.B., Fabbri, E., Licoccia, S., and Traversa, E. (2012) Tailoring phase stability and electrical conductivity of $\text{Sr}_{0.02}\text{La}_{0.98}\text{Nb}_{1-x}\text{Ta}_x\text{O}_4$ for intermediate temperature fuel cell proton conducting electrolytes. *Solid State Ionics*, 216: 6–10.
140. Brandão, A.D., Antunes, I., Frade, J.R., Torre, J., Kharton, V.V., and Fagg, D.P. (2010) Enhanced Low-Temperature Proton Conduction in $\text{Sr}_{0.02}\text{La}_{0.98}\text{NbO}_{4-\delta}$ by Scheelite Phase Retention. *Chem. Mater.*, 22(24): 6673–6683.
141. Schonberger, F., Kendrick, E., Islam, M.S., and Slater, P. (2005) Investigation of proton conduction in $\text{Ln}_{1-x}\text{Ba}_{1+x}\text{GaO}_{4-x/2}$ and $\text{Ln}_{1-x}\text{Sr}_{1+x}\text{GaO}_{5-x/2}$. *Solid State Ionics*, 176 (39–40): 2951–2953.
142. Kitamura, N., Amezawa, K., Uchimoto, Y., Tomii, Y., Hanada, T., and Yamamoto, N. (2006) Electrical conduction properties of rare earth orthophosphates under reducing conditions. *Solid State Ionics*, 177(26–32): 2369–2373.
143. Shimura, T. (2001) Proton conduction in non-perovskite-type oxides at elevated temperatures. *Solid State Ionics*, 143(1): 117–123.
144. Magrasó, A., Polfus, J.M., Frontera, C., Canales-Vázquez, J., Kalland, L.E., Hervoches, C.H., Erdal, S., Hancke, R., Islam, M.S., Norby, T., and Haugsrud, R. (2012) Complete structural model for lanthanum tungstate: a chemically stable high temperature proton conductor by means of intrinsic defects. *J. Mater. Chem.*, 22(5): 1762–1764.
145. Haugsrud, R. (2007) Defects and transport properties in $\text{Ln}_6\text{WO}_{12}$ ($\text{Ln}=\text{La, Nd, Gd, Er}$). *Solid State Ionics*, 178(7–10): 555–560.
146. Escolástico, S., Solís, C., and Serra, J.M. (2007) Study of hydrogen permeation in $(\text{La}_{5/6}\text{Nd}_{1/6})_{5.5}\text{WO}_{12-\delta}$ membranes. *Solid State Ionics*, 216: 31–35.
147. Escolástico, S., Solís, C., Scherb, T., Schumacher, G., and Serra, J.M. (2013) Hydrogen separation in $\text{La}_{5.5}\text{WO}_{11.25-\delta}$ membranes. *J. Membr. Sci.*, 444: 276–284.
148. Escolástico, S., Schroeder, M., and Serra, J.M. (2014) Optimization of the mixed protonic–electronic conducting materials based on $(\text{Nd}_{5/6}\text{Ln}_{1/6})_{5.5}\text{WO}_{11.25-\delta}$. *J. Mater. Chem. A*, 2(18): 6616–6630.
149. Amsif, M., Magrasó, A., Marrero-López, D. and Ruiz-Morales, J.C., Canales-Vázquez, J., and Núñez, P. (2012) Mo-Substituted Lanthanum Tungstate $\text{La}_{28-y}\text{W}_{4+y}\text{O}_{54+\alpha}$: A Competitive Mixed Electron–Proton Conductor for Gas Separation Membrane Applications. *Chem. Mater.*, 24(20): 3868–3877.
150. Magrasó, A. (2013) Transport number measurements and fuel cell testing of undoped and Mo-substituted lanthanum tungstate. *J. Power Sources*, 240(20): 583–588.

151. Yoshimura, M. and Rouanet, A. (1976) High temperature phase relation in the system La_2O_3 - WO_3 . *Mater. Res. Bull.*, 11(2): 151–158.
152. Rosensteel, W.A., Ricote, S., and Sullivan, N.P. (2016) Hydrogen permeation through dense $\text{BaCe}_{0.8}\text{Y}_{0.3}\text{O}_{3-\delta}$ – $\text{Ce}_{0.8}\text{Y}_{0.2}\text{O}_{2-\delta}$ composite-ceramic hydrogen separation membranes. *Int. J. Hydrogen Energy*, 41(4): 2598–2606.
153. Polfus, J.M., Xing, W., Fontaine, M.L., Denonville, C., Henriksen, P.P., and Bredesen, R. (2015) Hydrogen separation membranes based on dense ceramic composites in the $\text{La}_{27}\text{W}_5\text{O}_{55.5}$ – LaCrO_3 system. *J. Membr. Sci.*, 479(10): 39–45.
154. Escolástico, S., Solís, C., Kjølseth, C., and Serra, J.M. (2014) Outstanding hydrogen permeation through CO_2 -stable dual-phase ceramic membranes. *Energy Environ. Sci.*, 7(11): 3736–3746.
155. Okada, S., Mineshige, A., Kikuchi, T., Kobune, M., and Yazawa, T. (2007) Cermettype hydrogen separation membrane obtained from fine particles of high temperature proton-conductive oxide and palladium. *Thin Solid Films*, 515(18): 7342–7346.
156. Balachandran, U., Lee, T.H., Park, C.Y., Emerson, J.E., Picciolo, J.J., and Dorris, S.E. (2014) Dense cermet membranes for hydrogen separation. *Sep. Purif. Technol.*, 121:54–59.
157. Zhu, Z., Sun, W., Dong, Y., Wang, Z., Shi, Z., Zhang, Q., and Liu, W. (2014) Evaluation of hydrogen permeation properties of Ni – $\text{Ba}(\text{Zr}_{0.7}\text{Pr}_{0.1}\text{Y}_{0.2})\text{O}_{3-\delta}$ cermet membranes. *Int. J. Hydrogen Energy*, 39(22): 11683–11689.
158. Jeon, S.Y., Lim, D.K., Choi, M.B., Wachsman, E.D., and Song, S.J. (2011) Hydrogen separation by Pd – $\text{CaZr}_{0.9}\text{Y}_{0.1}\text{O}_{3-\delta}$ cermet composite membranes. *Sep. Purif. Technol.*, 79(3): 337–341.
159. Kim, H., Kim, B., Lee, J., Ahn, K., Kim, H.R., Yoon, K.J., Kim, B.K., Cho, Y.W., Lee, H.W., and Lee, J.H. (2014) Microstructural adjustment of Ni – $\text{BaCe}_{0.9}\text{Y}_{0.1}\text{O}_{3-\delta}$ cermet membrane for improved hydrogen permeation. *Ceram. Int.*, 40(3): 4117–4126.
160. Park, J.H., Jeon, S.I., Sim, W.J., Baek, I.H., and Choi, S.H. (2011) Stability of Ta/YSZ cermet membrane for hydrogen separation. *Energy Procedia*, 4: 756–762.
161. Balachandra, U., Lee, T.H., Zhang, G., Dorris, S.E., Rothenberger, K.S., Howard, B.H., Morreale, B., Cugini, A.V., Siriwardane, R.V., Poston, J.A., and Fisher, E.P. (2001) *Proceedings of the 26th International Technical Conference on Coal Utilization and Fuel Systems*, pp. 751–761, Coal Technical Association: Clearwater, FL.
162. Balachandran, U. (2005) Development of Dense Ceramic Membranes for Hydrogen Separation. *Proceedings of 2005 U.S. DOE Hydrogen Annual Merit Review Meeting*: Arlington, VA.
163. Shane, E.R., Mackay, R., and Michael, V.M., Adense, layered membranes for hydrogen separation. US patent 7001446 B2, 21 february 2006.
164. Wang, T., Zhang, H., Meng, B., Wang, X., Sunarso, J., Tan, X., and Liu, S. (2016) $\text{SrCe}_{0.95}\text{Y}_{0.05}\text{O}_{3-\delta}$ – ZnO dual-phase membranes for hydrogen permeation. *RSC Adv.*, 43 (6): 36786–36793.
165. Yoo, C.Y., Yun, D.S., Joo, J.H., and Yu, J.H. (2015) The effects of NiO addition on the structure and transport properties of proton conducting $\text{BaZr}_{0.8}\text{Y}_{0.2}\text{O}_{3-\delta}$. *J. Alloys Compd.*, 621: 263–267.
166. Tong, J., Clark, D., Hoban, M., and O’Hayre, R. (2010) Cost-effective solid-state reactive sintering method for high conductivity proton conducting yttrium-doped barium zirconium ceramics. *Solid State Ionics*, 181(11): 496–503.
167. Fan, L., Xie, H., and Su, P.C. (2016) Spray coating of dense proton-conducting $\text{BaCe}_{0.7}\text{Zr}_{0.1}\text{Y}_{0.2}\text{O}_3$ electrolyte for low temperature solid oxide fuel cells. *Int. J. Hydrogen Energy*, 41(15): 6516–6525.
168. Fang, S., Wang, S., Brinkman, K.S., Su, Q., Wang, H., and Chen, F. (2015) Spray coating of dense proton-conducting $\text{BaCe}_{0.7}\text{Zr}_{0.1}\text{Y}_{0.2}\text{O}_3$ electrolyte for low temperature solid oxide fuel cells. *J. Power Sources*, 278: 614–622.
169. Polfus, J.M., Li, Z., Xing, W., Sunding, M.F., Walmsley, J.C., Fontaine, M.L., Henriksen, P.P., and Bredesen, R. (2016) Chemical stability and H_2 flux degradation of cercer membranes based on lanthanum tungstate and lanthanum chromite. *J. Membr. Sci.*, 503: 42–47.
170. Lacz, A., Silarska, K., Piecha, I., and Pasierb, P. (2016) Structure, chemical stability and electrical properties of $\text{BaCe}_{0.9}\text{Y}_{0.1}\text{O}_{3-\delta}$ proton conductors impregnated with $\text{Ba}_3(\text{PO}_4)_2$. *Int. J. Hydrogen Energy*, 41(31): 13726–13735.

171. Will, J. (2000) Fabrication of thin electrolytes for second-generation solid oxide fuel cells. *Solid State Ionics*, 131(1–2): 79–96.
172. Cheng, S., Gupta, V., and Lin, J. (2005) Synthesis and hydrogen permeation properties of asymmetric proton-conducting ceramic membranes. *Solid State Ionics*, 176(35–36): 2653–2662.
173. Zhan, S., Zhu, X., Ji, B., Wang, W., Zhang, X., Wang, J., Yang, W., and Lin, L. (2009) Preparation and hydrogen permeation of $\text{SrCe}_{0.95}\text{Y}_{0.05}\text{O}_{3-\delta}$ asymmetrical membranes. *J. Membr. Sci.*, 340(1–2): 241–248.
174. Yoon, H., Song, S.J., Oh, T., Li, J., Duncan, K.L., and Wachsman, E.D. (2009) Fabrication of Thin-Film $\text{SrCe}_{0.9}\text{Eu}_{0.1}\text{O}_{3-\delta}$ Hydrogen Separation Membranes on Ni-SrCeO₃ Porous Tubular Supports. *J. Am. Ceram. Soc.*, 92(8): 1849–1852.
175. Oh, T., Yoon, H., Li, J., and Wachsman, E. (2009) Hydrogen permeation through thin supported $\text{SrZr}_{0.2}\text{Ce}_{0.8-x}\text{Eu}_x\text{O}_{3-\delta}$ membranes. *J. Membr. Sci.*, 345(1): 1–4.
176. Tan, X., Song, J., Meng, X., and Meng, B. (2012) Preparation and characterization of $\text{BaCe}_{0.95}\text{Tb}_{0.05}\text{O}_{3-\alpha}$ hollow fibre membranes for hydrogen permeation. *J. Eur. Ceram. Soc.*, 32(10): 2351–2357.
177. Yang, C.L., Xu, Q.M., Zhu, Z.W., and Liu, W. (2012) Hydrogen Permeation Performance of Ni-BaZr_{0.1}Ce_{0.7}Y_{0.2}O_{3- δ} Metal-Ceramic Hollow Fiber Membrane. *Chinese J. Chem. Phys.*, 25(2): 125–128.
178. Song, J., Kang, J., Tan, X., Meng, B., and Liu, S. (2016) Proton conducting perovskite hollow fibre membranes with surface catalytic modification for enhanced hydrogen separation. *J. Eur. Ceram. Soc.*, 36(7): 1669–1677.
179. Song, J., Meng, B., Tan, X., and Liu, S. (2015) Surface-modified proton conducting perovskite hollow fibre membranes by Pd-coating for enhanced hydrogen permeation. *Int. J. Hydrogen Energy*, 40(18): 6118–6127.
180. Smart, S., Beltramini, J., da Costa, J.C.D., Katikaneni, S.P., and Pham, T. (2013) Microporous silica membranes: fundamentals and applications in membrane reactors for hydrogen separation. Basile, A. (ed.), *Handbook of Membrane Reactors*, chap. 9, pp. 337–369, Elsevier: Cambridge.
181. Uhlhorn, R.J.R., In't Veld, M.H.B.J.H., Keizer, K., and Burggraaf, A.J. (1989) High permselectivities of microporous silica-modified γ -alumina membranes. *J. Mater. Sci. Lett.*, 8(10): 1135–1138.
182. Yoshino, Y., Suzuki, T., Nair, B., Taguchi, H., and Itoh, N. (2005) Development of tubular substrates, silica based membranes and membrane modules for hydrogen separation at high temperature. *J. Membr. Sci.*, 267(1–2): 8–17.
183. Lee, D.W., Yu, C.Y., and Lee, K.H. (2008) Synthesis of Pd particle-deposited microporous silica membranes via a vacuum-impregnation method and their gas permeation behavior. *J. Colloid Interface Sci.*, 325(2): 447–452.
184. Khatib, S.J. and Oyama, S.T. (2013) Silica membranes for hydrogen separation prepared by chemical vapor deposition (CVD). *Sep. Purif. Technol.*, 111: 20–42.
185. Lee, D.W., Lee, Y.G., Nam, S.E., Ihm, S.K., and Lee, K.H. (2003) Study on the variation of morphology and separation behavior of the stainless steel supported membranes at high temperature. *J. Membr. Sci.*, 220(1–2): 137–153.
186. Park, S.J., Lee, D.W., Yu, C.Y., Lee, K.Y., and Lee, K.H. (2008) Effect of Silica Particle Size on Performance of Porous Stainless-Steel-Supported Silica Membranes Prepared by the DRFF and SRFF Method. *Ind. Eng. Chem. Res.*, 47(16): 6211–6215.
187. Van Gestel, T., Hauler, F., Bram, M., Meulenberg, W.A., and Buchkremer, H.P. (2014) Synthesis and characterization of hydrogen-selective sol–gel SiO₂ membranes supported on ceramic and stainless steel supports. *Sep. Purif. Technol.*, 121: 20–29.
188. Lito, P.F., Cardoso, S.P., Rodrigues, A.E., and Silva, C.M. (2015) Kinetic Modeling of Pure and Multicomponent Gas Permeation Through Microporous Membranes: Diffusion Mechanisms and Influence of Isotherm Type. *Sep. Purif. Rev.*, 44(4): 283–307.
189. Krishna, R. (1993) Problems and pitfalls in the use of the Fick formulation for intraparticle diffusion. *Chem. Eng. Sci.*, 48(5): 845–861.
190. Cardoso, S.P., Lin, Z., Portugal, I., Rodrigues, A.E., and Silva, C.M. (2017) Synthesis, dynamic characterization, and modeling studies of an AM-3 membrane for light gases separation. *Micropor. Mesopor. Mater.*, Under review.

191. Lito, P.F., Zhou, C.F., Santiago, A.S., Rodrigues, A.E., Rocha, J., Lin, Z., and Silva, C.M. (2010) Modelling gas permeation through new microporous titanosilicate AM-3 membranes. *Chem. Eng. J.*, 165(2): 395–404.
192. Lito, P.F., Santiago, A.S., Cardoso, S.P., Figueiredo, B.R., and Silva, C.M. (2011) New expressions for single and binary permeation through zeolite membranes for different isotherm models. *J. Membr. Sci.*, 367(1-2): 21–32.
193. Cardoso, S.P., Azenha, I.S., Lin, Z., Portugal, I., Rodrigues, A.E., and Silva, C.M. (2017) Single and binary surface diffusion permeation through zeolite membranes using new Maxwell-Stefan factors for Dubinin-type isotherms and occupancy-dependent kinetics. *Sep. Purif. Technol.*, 182(182): 207–218.
194. van de Graaf, J.M., Kapteijn, M.F., and Moulijn, J.A. (1999) Modeling permeation of binary mixtures through zeolite membranes. *Aiche J.*, 45(3): 497–511.
195. van den Broeke, L.J.P., Bakker, W.J.W., Kapteijn, F., and Moulijn, J.A. (1999) Binary permeation through a silicalite-1 membrane. *Aiche J.*, 45(5): 976–985.
196. Nicolas, C.H., Sublet, J., Schuurman, Y., and Pera-Titus, M. (2011) Role of adsorption and diffusion pathways on the CO₂/N₂ separation performance of nanocomposite (B)MFI-alumina membranes. *Chem. Eng. Sci.*, 66(23): 6057–6068.
197. Van De Graaf, J.M., Kapteijn, F., and Moulijn, J.A. (2000) Diffusivities of light alkanes in a silicalite-1 membrane layer. *Micropor. Mesopor. Mater.*, 35–36: 267–281.
198. Krishna, R., Paschek, D., and Baur, R. (2004) Modeling the occupancy dependence of diffusivities in zeolites. *Micropor. Mesopor. Mater.*, 76(1-3): 233–246.
199. Moon, J.H., Bae, J.H., Bae, Y.S., Chung, J.T., and Lee, C.H. (2008) Hydrogen separation from reforming gas using organic templating silica/alumina composite membrane. *J. Membr. Sci.*, 318(1-2): 45–55.
200. Moon, J.H. and Lee, C.H. (2007) Hydrogen separation of methyltriethoxysilane templating silica membrane. *J. Membr. Sci.*, 353(12): 3125–3136.
201. Aghaeinejad-Meybodi, A., Ghasemzadeh, K., Babaloo, A.A., Morrone, P., and Basile, A. (2015) Modeling study of silica membrane performance for hydrogen separation. *Asia Pac. J. Chem. Eng.*, 10(5): 781–790.
202. da Costa, J.C.D., Lu, G.Q., Rudolph, V., and Lin, Y.S. (2002) Novel molecular sieve silica (MSS) membranes: characterization and permeation of single-step and two-step sol–gel membranes. *J. Membr. Sci.*, 198(1): 9–21.
203. de Vos, R.M., Maier, W.F., and Verweij, H. (1999) Hydrophobic silica membranes for gas separation. *J. Membr. Sci.*, 158(1-2): 277–288.
204. Khatib, S.J., Oyama, S.T., de Souza, K.R., and Noronha, F.B. (2011) Review of Silica Membranes for Hydrogen Separation Prepared by Chemical Vapor Deposition. *Inorganic Polymeric and Composite Membranes - Structure, Function and Other Correlations*, vol. 14 of *Membrane Science and Technology*, chap. 2, pp. 25–60, Elsevier: Amsterdam.
205. Kanezashi, M., Yada, K., Yoshioka, T., and Tsuru, T. (2010) Organic–inorganic hybrid silica membranes with controlled silica network size: Preparation and gas permeation characteristics. *J. Membr. Sci.*, 348(1-2): 310–318.
206. Somiya, S., Akamatsu, K., and Nakao, S.i. (2013) Hydrogen-Production Technologies Using Amorphous Silica Membranes. Somiya, S. (ed.), *Handbook of Advanced Ceramics*, chap. 4.1, pp. 331–341, Elsevier, 2 edn: Amsterdam.
207. Sea, B.K., Kusakabe, K., and Morooka, S. (1997) Pore size control and gas permeation kinetics of silica membranes by pyrolysis of phenyl-substituted ethoxysilanes with crossflow through a porous support wall. *J. Membr. Sci.*, 130(1-2): 41–52.
208. Ohta, Y., Akamatsu, K., Sugawara, T., Nakao, A., Miyoshi, A., and Nakao, S.I. (2008) Development of pore size-controlled silica membranes for gas separation by chemical vapor deposition. *J. Membr. Sci.*, 315(1): 93–99.
209. Zhang, X.L., Yamada, H., Saito, T., Kai, T., Murakami, K., Nakashima, M., Ohshita, J., Akamatsu, K., and Nakao, S.i. (2016) Development of hydrogen-selective triphenylmethoxysilane-derived silica membranes with tailored pore size by chemical vapor deposition. *J. Membr. Sci.*, 499: 28–35.

210. Zhang, X.L., Akamatsu, K., and Nakao, S.i. (2016) Hydrogen Separation in Hydrogen–Methylcyclohexane–Toluene Gaseous Mixtures through Triphenylmethoxysilane-Derived Silica Membranes Prepared by Chemical Vapor Deposition. *Ind. Eng. Chem. Res.*, 55 (18): 5395–5402.
211. Asaeda, M. and Kashimoto, M. (1998) Sol-gel silica membranes for separation of hydrogen at high temperature - separation performance and stability against steam. Nakao, S.I., Asaeda, M., and Morooka, S. (eds.), *Proceedings of the 5th International Conference on Inorganic Membranes, ICIM5*, Nagoya, Japan, pp. 172–175.
212. Tsapatsis, M. and Gavalas, G. (1994) Structure and aging characteristics of H₂ permselective SiO₂-Vycor membranes. *J. Membr. Sci.*, 87(3): 281–296.
213. Duke, M., da Costa, J.C.D., Do, D., Gray, P., and Lu, G. (2006) Hydrothermally Robust Molecular Sieve Silica for Wet Gas Separation. *Adv. Funct. Mater.*, 16(9): 1215–1220.
214. Wei, Q., Wang, Y.L., Nie, Z.R., Yu, C.X., Li, Q.Y., Zou, J.X., and Li, C.J. (2008) Facile synthesis of hydrophobic microporous silica membranes and their resistance to humid atmosphere. *Micropor. Mesopor. Mater.*, 111(1-3): 97–103.
215. Qi, H. (2011) Preparation of Composite Microporous Silica Membranes Using TEOS and 1, 2-Bis(triethoxysilyl)ethane as Precursors for Gas Separation. *Chinese J. Chem. Eng.*, 19(3): 404–409.
216. Wei, Q., Ding, Y.L., Nie, Z.R., Liu, X.G., and Li, Q.Y. (2014) Wettability, pore structure and performance of perfluorodecyl-modified silica membranes. *J. Membr. Sci.*, 466:114–122.
217. Lin, Y. (2001) Microporous and dense inorganic membranes: current status and prospective. *Sep. Purif. Technol.*, 25(1-3): 39–55.
218. Sekulić, J., Luiten, M.W.J., ten Elshof, J.E., Benes, N.E., and Keizer, K. (2002) Microporous silica and doped silica membrane for alcohol dehydration by pervaporation. *Desalination*, 148(1-3): 19–23.
219. Ikuhara, Y.H., Mori, H., Saito, T., and Iwamoto, Y. (2007) High-Temperature Hydrogen Adsorption Properties of Precursor-Derived Nickel Nanoparticle-Dispersed Amorphous Silica. *J. Am. Ceram. Soc.*, 90(2): 546–552.
220. Yoshida, K., Hirano, Y., Fujii, H., Tsuru, T., and Asaeda, M. (2001) Hydrothermal Stability and Performance of Silica-Zirconia Membranes for Hydrogen Separation in Hydrothermal Conditions. *J. Chem. Eng. Japan*, 34(4): 523–530.
221. Kanezashi, M. and Asaeda, M. (2006) Hydrogen permeation characteristics and stability of Ni-doped silica membranes in steam at high temperature. *J. Membr. Sci.*, 271(1-2): 86–93.
222. Igi, R., Yoshioka, T., Ikuhara, Y.H., Iwamoto, Y., and Tsuru, T. (2008) Characterization of Co-Doped Silica for Improved Hydrothermal Stability and Application to Hydrogen Separation Membranes at High Temperatures. *J. Am. Ceram. Soc.*, 91(9): 2975–2981.
223. Gu, Y. and Oyama, S.T. (2009) Permeation properties and hydrothermal stability of silica–titania membranes supported on porous alumina substrates. *J. Membr. Sci.*, 345 (1-2): 267–275.
224. Lee, D.W., Ihm, S.K., and Lee, K.H. (2006) Synthesis of a mesoporous titania/silica and its application to a composite membrane with high hydrothermal stability. *Desalination*, 199(1-3): 363–364.
225. Choi, H.S., Ryu, C.H., and Hwang, G.J. (2013) Obtention of ZrO₂–SiO₂ hydrogen permselective membrane by chemical vapor deposition method. *Chem. Eng. J.*, 232: 302–309.
226. Gu, Y., Hacarlioglu, P., and Oyama, S.T. (2008) Hydrothermally stable silica–alumina composite membranes for hydrogen separation. *J. Membr. Sci.*, 310(1-2): 28–37.
227. Hekkink, J.H.A., de Lange, R.S.A., Ten Hoeve, A.A., Blankenvoorde, P.J.A.M., Keizer, K., and Burggraaf, A.J. (1992) Characterization and Permeation Properties of Binary SiO₂–TiO₂ and SiO₂–Al₂O₃ Modified Gamma-Alumina Membranes. *Key Eng. Mater.*, vol. 61-62, pp. 375– 378.
228. Boffa, V., ten Elshof, J.E., Garcia, R., and Blank, D.H.A. (2009) Microporous niobia–silica membranes: Influence of sol composition and structure on gas transport properties. *Micropor. Mesopor. Mater.*, 118(1-3): 202–209.
229. Qi, H., Chen, H., Li, L., Zhu, G., and Xu, N. (2012) Effect of Nb content on hydrothermal stability of a novel ethylene-bridged silsesquioxane molecular sieving membrane for H₂/CO₂ separation. *J. Membr. Sci.*, 421-422: 190–200.

230. Battersby, S., Tasaki, T., Smart, S., Ladewig, B., Liu, S., Duke, M.C., Rudolph, V., and da Costa, J.C.D. (2009) Performance of cobalt silica membranes in gas mixture separation. *J. Membr. Sci.*, 329(1-2): 91–98.
231. Khanmohammadi, S. and Taheri-Nassaj, E. (2014) Micro-porous silica–yttria membrane by sol–gel method: Preparation and characterization. *Ceram. Int.*, 40(7): 9403–9411.
232. Ballinger, B., Motuzas, J., Smart, S., and da Costa, J.C.D. (2014) Palladium cobalt binary doping of molecular sieving silica membranes. *J. Membr. Sci.*, 451: 185–191.
233. Darmawan, A., Motuzas, J., Smart, S., Julbe, A., and da Costa, J.C.D. (2015) Binary iron cobalt oxide silica membrane for gas separation. *J. Membr. Sci.*, 474: 32–38.
234. Algieri, C., Barbieri, G., and Drioli, E. (2011) Zeolite Membranes for Gas Separation. Drioli, E. and Barbieri, G. (eds.), *Membrane Engineering for the Treatment of Gases, Volume 2: Gas-separation Problems Combined with Membrane Reactors*, pp. 223–252, Royal Society of Chemistry: London.
235. Feng, C., Khulbe, K.C., Matsuura, T., Farnood, R., and Ismail, A. (2015) Recent Progress in Zeolite/Zeotype Membranes. *J. Membr. Sci. Res.*, 1(2): 49–72.
236. Szostak, R. (1989) *Molecular sieves principles of synthesis and identification*. Van Nostrand Reinhold: New York.
237. <http://www.iza-structure.org/>. (Accessed in 16 August 2017).
238. Valtchev, V., Majano, G., Mintova, S., and Pérez-Ramírez, J. (2013) Tailored crystalline microporous materials by post-synthesis modification. *Chem. Soc. Rev.*, 42(1).
239. Caro, J. and Noack, M. (2008) Zeolite membranes – Recent developments and progress. *Micropor. Mesopor. Mater.*, 115(3): 215–233.
240. Figueiredo, B.R., Valente, A.A., Lin, Z., and Silva, C.M. (2016) Photoluminescent porous and layered lanthanide silicates: A review. *Micropor. Mesopor. Mater.*, 234: 73–97.
241. Xu, R., Pang, W., Yu, J., Huo, Q., and Chen, J. (2007) *Chemistry of Zeolites and Related Porous Materials: Synthesis and Structure*. John Wiley & Sons: Singapore.
242. Caro, J. and Noack, M. (2009) Zeolite Membranes - Status and Prospective. Ernst, S. (ed.), *Advances in Nanoporous Materials - Volume 1*, chap. 1, pp. 1–96, Elsevier B.V., 1 edn: Oxford.
243. Lito, P.F., Aniceto, J.P.S., and Silva, C.M. (2012) Removal of Anionic Pollutants from Waters and Wastewaters and Materials Perspective for Their Selective Sorption. *Water Air Soil Pollut.*, 223(9): 6133–6155.
244. Lopes, C.B., Lito, P.F., Cardoso, S.P., Pereira, E., Duarte, A.C., and Silva, C.M. (2012) Metal Recovery, Separation and/or Pre-concentration. Inamuddin, D. and Luqman, M. (eds.), *Ion Exchange Technology II - Applications*, chap. 11, pp. 237–322, Springer: New York.
245. Popa, K. and Pavel, C. (2012) Radioactive wastewaters purification using titanosilicates materials: State of the art and perspectives. *Desalination*, 293: 78–86.
246. Zhou, L., Yang, J., Li, G., Wang, J., Zhang, Y., Lu, J., and Yin, D. (2014) Highly H₂ permeable SAPO-34 membranes by steam-assisted conversion seeding. *Int. J. Hydrogen Energy*, 39(27): 14949–14954.
247. Robeson, L.M. (2008) The upper bound revisited. *J. Membr. Sci.*, 320(1-2): 390–400.
248. Calleja, G., Pau, J., and Calles, J.A. (1998) Pure and Multicomponent Adsorption Equilibrium of Carbon Dioxide, Ethylene, and Propane on ZSM-5 Zeolites with Different Si/Al Ratios. *J. Chem. Eng. Data*, 43(6): 994–1003.
249. Coterillo, C.C., MENDIA, A.M.U., and Uribe, I.O. (2008) Pervaporation and Gas Separation Using Microporous Membranes. Mallada, R. and Menéndez, M. (eds.), *Inorganic Membranes: Synthesis, Characterization and Applications*, vol. 13 of *Membrane Science and Technology*, chap. 7, pp. 217–253, Elsevier: Oxford.
250. Zito, P.F., Caravella, A., Brunetti, A., Drioli, E., and Barbieri, G. (2017) Knudsen and surface diffusion competing for gas permeation inside silicalite membranes. *J. Membr. Sci.*, 523: 456–469.
251. Coronas, J. and Santamaría, J. (1999) Separations using zeolite membranes. *Sep. Purif. Methods*, 28(2): 127–177.

252. Algieri, C., Bernardo, P., Barbieri, G., and Drioli, E. (2009) A novel seeding procedure for preparing tubular NaY zeolite membranes. *Micropor. Mesopor. Mater.*, 119(1-3): 129–136.
253. Hong, Z., Sun, F., Chen, D., Zhang, C., Gu, Z., and Xu, N. (2013) Improvement of hydrogen-separating performance by on-stream catalytic cracking of silane over hollow fiber MFI zeolite membrane. *Int. J. Hydrogen Energy*, 38(20): 8409–8414.
254. Simplício, M., Afonso, M.D., Borisevich, O., Lefebvre, X., and Demange, D. (2014) Permeation of single gases and binary mixtures of hydrogen and helium through a MFI zeolite hollow fibres membrane for application in nuclear fusion. *Sep. Purif. Technol.*, 122: 199–205.
255. Caro, J., Noack, M., and Kolsch, P. (2005) Zeolite membranes: From the laboratory scale to technical applications. *Adsorpt. Int. Adsorpt. Soc.*, 11(3-4): 215–227.
256. Bose, A., Sen, M., Das, J.K., and Das, N. (2014) Sonication mediated hydrothermal process – an efficient method for the rapid synthesis of DDR zeolite membranes. *RSC Adv.*, 4(36): 19043.
257. Das, J.K., Das, N., and Bandyopadhyay, S. (2013) Highly oriented improved SAPO 34 membrane on low cost support for hydrogen gas separation. *J. Mater. Chem. A*, 1(16):4966.
258. Das, J.K. and Das, N. (2014) Mercaptoundecanoic acid capped palladium nanoparticles in a SAPO-34 membrane: a solution for enhancement of H₂/CO₂ separation efficiency. *ACS Appl. Mater. Interfaces*, 6(23): 20717–20728.
259. Vroon, Z.A.E.P., Keizer, K., Gilde, M.J., Verweij, H., and Burggraaf, A.J. (1996) Transport properties of alkanes through ceramic thin zeolite MFI membranes. *J. Membr. Sci.*, 113(2): 293–300.
260. Kong, C., Lu, J., Yang, J., and Wang, J. (2006) Preparation of silicalite-1 membranes on stainless steel supports by a two-stage varying-temperature in situ synthesis. *J. Membr. Sci.*, (1-2): 258–264.
261. Li, Y., Peratitus, M., Xiong, G., Yang, W., Landrivon, E., Miachon, S., and Dalmon, J. (2008) Nanocomposite MFI-alumina membranes via pore-plugging synthesis: Genesis of the zeolite material. *J. Membr. Sci.*, 325(2): 973–981.
262. Wu, T., Wang, B., Lu, Z., Zhou, R., and Chen, X. (2014) Alumina-supported AlPO-18 membranes for CO₂/CH₄ separation. *J. Membr. Sci.*, 471: 338–346.
263. Yu, M., Funke, H.H., Noble, R.D., and Falconer, J.L. (2011) H₂ separation using defect free, inorganic composite membranes. *J. Am. Chem. Soc.*, 133(6): 1748–1750.
264. Huang, A. and Caro, J. (2010) Steam-stable hydrophobic ITQ-29 molecular sieve membrane with H₂ selectivity prepared by secondary growth using Kryptofix 222 as SDA. *Chem. Commun.*, 46(41): 7748–50.
265. Xu, X., Yang, W., Liu, J., and Lin, L. (2001) Synthesis of NaA zeolite membranes from clear solution. *Micropor. and Mesopor. Mater.*, 43(3): 299–311.
266. Noack, M., Kölsch, P., Schäfer, R., Toussaint, P., Sieber, I., and Caro, J. (2001) Preparation of MFI membranes of enlarged area with high reproducibility. *Micropor. Mesopor. Mater.*, 49(1-3): 25–37.
267. Hedlund, J., Jareman, F., Bons, A.J., and Anthonis, M. (2003) A masking technique for high quality MFI membranes. *J. Membr. Sci.*, 222(1-2): 163–179.
268. Li, X.W., Zhou, C.F., Lin, Z., Rocha, J., Lito, P.F., Santiago, A.S., and Silva, C.M. (2011) Titanosilicate AM-3 membrane A new potential candidate for H₂ separation. *Micropor. Mesopor. Mater.*, 137(1-3): 43–48.
269. Julbe, A. (2007) *Introduction to Zeolite Science and Practice*, vol. 168 of *Studies in Surface Science and Catalysis*. Elsevier: Amsterdam.
270. Arruebo, M., Mallada, R., and M.P. Pina (2009) Zeolite Membranes: Synthesis, Characterization, Important Applications, and Recent Advances. Pabby, A.K., Rizvi, S.S.H., and Sastre, A.M. (eds.), *Handbook of Membrane Separations. Chemical, Pharmaceutical, Food, and Biotechnological Applications*, chap. 10, pp. 269–324, CRC Press: Boca Raton.
271. Xu, X., Yang, W., Liu, J., and Lin, L. (2001) Synthesis of NaA zeolite membrane by microwave heating. *Sep. Purif. Technol.*, 25(1-3): 241–249.
272. Li, Y., Chen, H., Liu, J., and Yang, W. (2006) Microwave synthesis of LTA zeolite membranes without seeding. *J. Membr. Sci.*, 277(1-2): 230–239.

273. Zhu, G., Li, Y., Zhou, H., Liu, J., and Yang, W. (2008) FAU-type zeolite membranes synthesized by microwave assisted in situ crystallization. *Mater. Lett.*, 62(28): 4357–4359.
274. Li, K., Tian, Z., Li, X., Xu, R., Xu, Y., Wang, L., Ma, H., Wang, B., and Lin, L. (2012) Ionothermal synthesis of aluminophosphate molecular sieve membranes through substrate surface conversion. *Angew. Chem. Int. Ed. Engl.*, 51(18): 4397–400.
275. Li, X., Li, K., Ma, H., Xu, R., Tao, S., and Tian, Z. (2015) Ionothermal synthesis of a CHA-type aluminophosphate molecular sieve membrane and its formation mechanism. *Micropor. Mesopor. Mater.*, 217: 54–62.
276. Jabbari, Z., Fatemi, S., and Davoodpour, M. (2014) Comparative study of seeding methods; dip-coating, rubbing and EPD, in SAPO-34 thin film fabrication. *Adv. Powder Technol.*, 25(1): 321–330.
277. Rangnekar, N., Mittal, N., Elyassi, B., Caro, J., and Tsapatsis, M. (2015) Zeolite membranes - a review and comparison with MOFs. *Chem. Soc. Rev.*, 44(20): 7128–7154.
278. Chen, X., Wang, J., Yin, D., Yang, J., Lu, J., Zhang, Y., and Chen, Z. (2013) High performance zeolite T membrane for dehydration of organics by a new varying temperature hot-dip coating method. *AICHE J.*, 59(3): 936–947.
279. Xiao, W., Chen, Z., Zhou, L., Yang, J., Lu, J., and Wang, J. (2011) A simple seeding method for MFI zeolite membrane synthesis on macroporous support by microwave heating. *Micropor. Mesopor. Mater.*, 142(1): 154–160.
280. Wang, Z., Ge, Q., Gao, J., Shao, J., Liu, C., and Yan, Y. (2011) High-Performance Zeolite Membranes on Inexpensive Large-Pore Supports: Highly Reproducible Synthesis using a Seed Paste. *ChemSusChem*, 4(11): 1570–1573.
281. Peng, Y., Zhan, Z., Shan, L., Li, X., Wang, Z., and Yan, Y. (2013) Preparation of zeolite MFI membranes on defective macroporous alumina supports by a novel wetting–rubbing seeding method: Role of wetting agent. *J. Memb. Sci.*, 444: 60–69.
282. Zhou, R., Wang, H., Wang, B., Chen, X., Li, S., and Yu, M. (2015) Defect-Patching of Zeolite Membranes by Surface Modification Using Siloxane Polymers for CO₂ Separation. *Ind. Eng. Chem. Res.*, 54(30): 7516–7523.
283. Zhu, X., Wang, H., and Lin, Y.S. (2010) Effect of the Membrane Quality on Gas Permeation and Chemical Vapor Deposition Modification of MFI-Type Zeolite Membranes. *Ind. Eng. Chem. Res.*, 49(20): 10026–10033.
284. Tang, Z., Dong, J., and Nenoff, T.M. (2009) Internal surface modification of MFI-type zeolite membranes for high selectivity and high flux for hydrogen. *Langmuir*, 25(9): 4848–4852.
285. Kanezashi, M. and Lin, Y.S. (2009) Gas Permeation and Diffusion Characteristics of MFI-Type Zeolite Membranes at High Temperatures. *J. Phys. Chem. C.*, 113(9): 3767–3774.
286. Zheng, Z., Hall, A.S., and Gulians, V.V. (2008) Synthesis, characterization and modification of DDR membranes grown on α -alumina supports. *J. Mater. Sci.*, 43(7): 2499–2502.
287. Masuda, T., Fukumoto, N., Kitamura, M., Mukai, S.R., Hashimoto, K., Tanaka, T., and Funabiki, T. (2001) Modification of pore size of MFI-type zeolite by catalytic cracking of silane and application to preparation of H₂-separating zeolite membrane. *Micropor. Mesopor. Mater.*, 48(1-3): 239–245.
288. Hong, Z., Wu, Z., Zhang, Y., and Gu, X. (2013) Catalytic Cracking Deposition of Methyldiethoxysilane for Modification of Zeolitic Pores in MFI/ α -Al₂O₃ Zeolite Membrane with H⁺ Ion Exchange Pretreatment. *Ind. Eng. Chem. Res.*, 52(36): 13113–13119.
289. Gu, X., Tang, Z., and Dong, J. (2008) On-stream modification of MFI zeolite membranes for enhancing hydrogen separation at high temperature. *Micropor. Mesopor. Mater.*, 111 (1-3): 441–448.
290. Matsuda, H., Yanagishita, H., Negishi, H., Kitamoto, D., Ikegami, T., Haraya, K., Nakane, T., Idemoto, Y., Koura, N., and Sano, T. (2002) Improvement of ethanol selectivity of silicalite membrane in pervaporation by silicone rubber coating. *J. Membr. Sci.*, 210(2): 433–437.
291. An, W., Swenson, P., Gupta, A., Wu, L., Kuznicki, T.M., and Kuznicki, S.M. (2013) Improvement of H₂/CO₂ selectivity of the natural clinoptilolite membranes by cation exchange modification. *J. Membr. Sci.*, 433: 25–31.
292. Hong, M., Li, S., Funke, H.F., Falconer, J.L., and Noble, R.D. (2007) Ion-exchanged SAPO-34 membranes for light gas separations. *Micropor. Mesopor. Mater.*, 106(1-3):140–146.

293. Aoki, K., Tuan, V.A., Falconer, J.L., and Noble, R.D. (2000) Gas permeation properties of ion-exchanged ZSM-5 zeolite membranes. *Micropor. Mesopor. Mater.*, 39(3): 485–492.
294. Aguado, S., Gascon, J., Farrusseng, D., Jansen, J.C., and Kapteijn, F. (2011) Simple modification of macroporous alumina supports for the fabrication of dense NaA zeolite coatings: Interplay of electrostatic and chemical interactions. *Micropor. Mesopor. Mater.*, 146(1-3): 69–75.
295. Huang, A., Wang, N., and Caro, J. (2012) Seeding-free synthesis of dense zeolite FAU membranes on 3-aminopropyltriethoxysilane-functionalized alumina supports. *J. Membr. Sci.*, 389: 272–279.
296. Huang, A., Liang, F., Steinbach, F., and Caro, J. (2010) Preparation and separation properties of LTA membranes by using 3-aminopropyltriethoxysilane as covalent linker. *J. Membr. Sci.*, 350(1-2): 5–9.
297. Huang, A., Wang, N., and Caro, J. (2012) Synthesis of multi-layer zeolite LTA membranes with enhanced gas separation performance by using 3-aminopropyltriethoxysilane as interlayer. *Micropor. Mesopor. Mater.*, 164: 294–301.
298. Huang, A. and Caro, J. (2011) Facile synthesis of LTA molecular sieve membranes on covalently functionalized supports by using diisocyanates as molecular linkers. *J. Mater. Chem.*, 21(30): 11424.
299. Huang, A., Liu, Q., Wang, N., Tong, X., Huang, B., Wang, M., and Caro, J. (2013) Covalent synthesis of dense zeolite LTA membranes on various 3-chloropropyltrimethoxysilane functionalized supports. *J. Membr. Sci.*, 437: 57–64.
300. Yuan, C., Liu, Q., Chen, H., and Huang, A. (2014) Mussel-inspired polydopamine modification of supports for the facile synthesis of zeolite LTA molecular sieve membranes. *RSC Adv.*, 4(79): 41982–41988.
301. Zhou, C., Yuan, C., Zhu, Y., Caro, J., and Huang, A. (2015) Facile synthesis of zeolite FAU molecular sieve membranes on bio-adhesive polydopamine modified Al₂O₃ tubes. *J. Membr. Sci.*, 494: 174–181.
302. Dey, K.P., Kundu, D., Chatterjee, M., and Naskar, M.K. (2013) Preparation of NaA Zeolite Membranes Using Poly(Ethylenimine) as Buffer Layer, and Study of Their Permeation Behavior. *J. Am. Ceram. Soc.*, 96(1): 68–72.
303. Naskar, M.K., Kundu, D., and Chatterjee, M. (2009) Silicalite-1 zeolite membranes on unmodified and modified surfaces of ceramic supports: A comparative study. *Bull. Mater. Sci.*, 32(5): 537–541.
304. Naskar, M.K., Kundu, D., and Chatterjee, M. (2010) Influence of PVP buffer layer on the formation of NaA zeolite membrane. *J. Porous Mater.*, 18(3): 319–327.
305. Zhou, M., Liu, X., Zhang, B., and Zhu, H. (2008) Assembly of oriented zeolite monolayers and thin films on polymeric surfaces via hydrogen bonding. *Langmuir*, 24(20): 11942–11946.
306. Lee, J.S., Kim, J.H., Lee, Y.J., Jeong, N.C., and Yoon, K.B. (2007) Manual assembly of microcrystal monolayers on substrates. *Angew. Chem. Int. Ed. Engl.*, 46(17): 3087–90.
307. Xu, K., Yuan, C., Caro, J., and Huang, A. (2016) Silver-exchanged zeolite LTA molecular sieving membranes with enhanced hydrogen selectivity. *J. Membr. Sci.*, 511: 1–8.
308. Huang, A. and Caro, J. (2010) Cationic Polymer Used to Capture Zeolite Precursor Particles for the Facile Synthesis of Oriented Zeolite LTA Molecular Sieve Membrane. *Chem. Mater.*, 22(15): 4353–4355.
309. Chau, J.L.H., Tellez, C., Yeung, K.L., and Ho, K. (2000) The role of surface chemistry in zeolite membrane formation. *J. Membr. Sci.*, 164(1-2): 257–275.
310. Kanezashi, M., O'Brien, J., and Lin, Y.S. (2007) Thermal stability improvement of MFI-type zeolite membranes with doped zirconia intermediate layer. *Micropor. Mesopor. Mater.*, 103(1-3): 302–308.
311. Wang, H., Dong, X., and Lin, Y. (2014) Highly stable bilayer MFI zeolite membranes for high temperature hydrogen separation. *J. Membr. Sci.*, 450: 425–432.
312. Navarro, M., Mateo, E., Diosdado, B., Tsapatsis, M., and Coronas, J. (2015) Activation of giant silicalite-1 monocrystals combining rapid thermal processing and ozone calcination. *RSC Adv.*, 5(23): 18035–18040.
313. Ismail, A.F. and David, L.I.B. (2001) A review on the latest development of carbon membranes for gas separation. *J. Membr. Sci.*, 193: 1–18.
314. Ash, R., Barrer, R.M., and Lawson, R.T. (1973) Transport of single gases and of binary gas mixtures in a microporous carbon membrane. *J. Chem. Soc. Faraday Trans. 1 Phys. Chem. Condens. Phases.*, 69: 2166–2178.

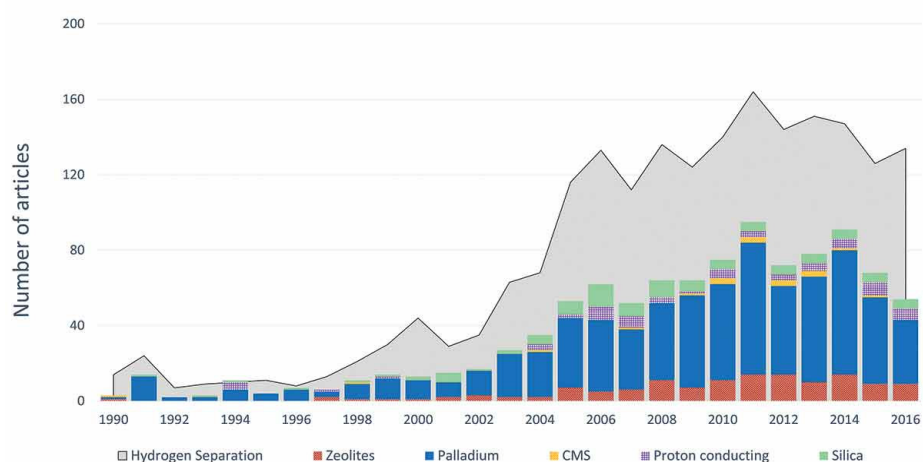
315. Koresh, J.E. and Sofer, A. (2006) Molecular Sieve Carbon Permselective Membrane. Part I. Presentation of a New Device for Gas Mixture Separation. *Sep. Sci. Technol.*, 18(8): 723–734.
316. Rao, M.B. and Sircar, S. (1993) Nanoporous carbon membranes for separation of gas mixtures by selective surface flow. *J. Membr. Sci.*, 85(3): 253–264.
317. Rao, M.B. and Sircar, S. (1993) Nanoporous carbon membrane for gas separation. *Gas Sep. Purif.*, 7(4): 279–284.
318. Ismail, A., Rana, D., Matsuura, T., and Foley, H. (2011) Transport Mechanism of Carbon Membranes. Ismail, A.F., Rana, D., Matsuura, T., and Foley, H. (eds.), *Carbon-based Membranes for Separation Processes*, chap. 2, pp. 5–16, Springer: New York.
319. Rao, M.B. and Sircar, S. (1996) Performance and pore characterization of nanoporous carbon membranes for gas separation. *J. Membr. Sci.*, 110(1): 109–118.
320. Ramirez, A. (2011) A kinetic Monte Carlo approach to diffusion in disordered nanoporous carbons. *Chem. Eng. Sci.*, 66(22): 5663–5671.
321. Gilron, J. and Soffer, A. (2002) Knudsen diffusion in microporous carbon membranes with molecular sieving character. *J. Membr. Sci.*, 209: 339–352.
322. Rajagopalan, R., Merritt, A., Tseytlin, A., and Foley, H.C. (2006) Modification of macroporous stainless steel supports with silica nanoparticles for size selective carbon membranes with improved flux. *Carbon*, 44(10): 2051–2058.
323. Wey, M.Y., Tseng, H.H., and Chiang, C.k. (2013) Effect of MFI zeolite intermediate layers on gas separation performance of carbon molecular sieve (CMS) membranes. *J. Membr. Sci.*, 446: 220–229.
324. Merritt, A., Rajagopalan, R., and Foley, H.C. (2007) High performance nanoporous carbon membranes for air separation. *Carbon*, 45(6): 1267–1278.
325. Saufi, S.M. and Ismail, A.F. (2004) Fabrication of carbon membranes for gas separation - A review. *Carbon*, 42: 241–259.
326. Liang, C., Sha, G., and Guo, S. (1999) Carbon membrane for gas separation derived from coal tar pitch. *Carbon*, 37(9): 1391–1397.
327. Ismail, A.F. and Li, K. (2008) From polymeric precursors to hollow fiber carbon and ceramic membranes. *Inorganic Membranes: Synthesis, Characterization and Applications*, chap. 3, pp. 81–119. Elsevier: Oxford.
328. Petersen, J., Matsuda, M., and Haraya, K. (1997) Capillary carbon molecular sieve membranes derived from Kapton for high temperature gas separation. *J. Membr. Sci.*, 131(1-2): 85–94.
329. Suda, H. and Haraya, K. (1997) Gas Permeation through Micropores of Carbon Molecular Sieve Membranes Derived from Kapton Polyimide. *J. Phys. Chem. B*, 5647(96): 3988–3994.
330. Favvas, E.P., Heliopoulos, N.S., Papageorgiou, S.K., Mitropoulos, A.C., Kapantaidakis, G.C., and Kanellopoulos, N.K. (2015) Helium and hydrogen selective carbon hollow fiber membranes: The effect of pyrolysis isothermal time. *Sep. Purif. Technol.*, 142: 176–181.
331. Tseng, H.H., Shiu, P.T., and Lin, Y.S. (2011) Effect of mesoporous silica modification on the structure of hybrid carbon membrane for hydrogen separation. *Int. J. Hydrogen Energy*, 36(23): 15352–15363.
332. Itta, A.K., Tseng, H.H., and Wey, M.Y. (2010) Effect of dry/wet-phase inversion method on fabricating polyetherimide-derived CMS membrane for H₂/N₂ separation. *Int. J. Hydrogen Energy*, 35(4): 1650–1658.
333. Wang, C., Yu, J., Hu, X., and Huang, Y. (2013) An improvement of the hydrogen permeability of C/Al₂O₃ membranes by palladium deposition into the pores. *Int. J. Hydrogen Energy*, 38(25): 10819–10825.
334. Song, C., Wang, T., Jiang, H., Wang, X., Cao, Y., and Qiu, J. (2010) Gas separation performance of C/CMS membranes derived from poly(furfuryl alcohol) (PFA) with different chemical structure. *J. Membr. Sci.*, 361(1-2): 22–27.
335. Hirota, Y., Ishikado, A., Uchida, Y., Egashira, Y., and Nishiyama, N. (2013) Pore size control of microporous carbon membranes by post-synthesis activation and their use in a membrane reactor for dehydrogenation of methylcyclohexane. *J. Membr. Sci.*, 440: 134–139.

336. Soffer, A., Rosen, D., Saguee, S., and Koresh, J.E., Carbon membranes. GB patent 2207666, 8 august 1989.
337. Geiszler, V.C. and Koros, W.J. (1996) Effects of Polyimide Pyrolysis Conditions on Carbon Molecular Sieve Membrane Properties. *Ind. Eng. Chem. Res.*, 35(9): 2999–3003.
338. Lagorsse, S., Campo, M.C., Magalhães, F.D., and Mendes, A. (2005) Water adsorption on carbon molecular sieve membranes: Experimental data and isotherm model. *Carbon*, 43(13): 2769–2779.
339. Yoshimune, M. and Haraya, K. (2011) Microporous Carbon Membranes. Basile, A. and Gallucci, F. (eds.), *Membranes for Membrane Reactors*, chap. 1, pp. 63–97, John Wiley & sons.
340. Lagorsse, S. (2004) Carbon molecular sieve membranes: Sorption, kinetic and structural characterization. *J. Memb. Sci.*, 241(2): 275–287.
341. Lagorsse, S., Leite, A., Magalhães, F.D., Bischofberger, N., Rathenow, J., and Mendes, A. (2005) Novel carbon molecular sieve honeycomb membrane module: Configuration and membrane characterization. *Carbon*, 43: 809–819.
342. Ismail, A.F., Rana, D., Matsuura, T., and Foley, H.C. (2011) *Carbon-based Membranes for Separation Processes*. Springer: New York.
343. Campo, M.C., Magalhães, F.D., and Mendes, A. (2010) Carbon molecular sieve membranes from cellophane paper. *J. Memb. Sci.*, 350: 180–188.
344. Lie, J.A. and Hägg, M.B. (2005) Carbon membranes from cellulose and metal loaded cellulose. *Carbon*, 43: 2600–2607.
345. Yoshimune, M., Fujiwara, I., Suda, H., and Haraya, K. (2006) Gas transport properties of carbon molecular sieve membranes derived from metal containing sulfonated poly(phenylene oxide). *Desalination*, 193(1-3): 66–72.
346. Yoda, S., Hasegawa, A., Suda, H., Uchimaru, Y., Haraya, K., Tsuji, T., and Otake, K. (2004) Preparation of a platinum and palladium/polyimide nanocomposite film as a precursor of metal-doped carbon molecular sieve membrane via supercritical impregnation. *Chem. Mater.*, 16(8): 2363–2368.
347. Suda, H., Yoda, S., Hasegawa, A., Tsuji, T., Otake, K., and Haraya, K. (2006) Gas permeation properties of carbon molecular sieve membranes dispersed with palladium nano particles via supercritical CO₂ impregnation. *Desalination*, 193(1-3): 211–214.
348. Park, H.B. and Lee, Y.M. (2005) Fabrication and Characterization of Nanoporous Carbon/Silica Membranes. *Adv. Mater.*, 17(4): 477–483.
349. Liu, Q., Wang, T., Liang, C., Zhang, B., Liu, S., Cao, Y., and Qiu, J. (2006) Zeolite Married to Carbon: A New Family of Membrane Materials with Excellent Gas Separation Performance. *Chem. Mater.*, 18(26): 6283–6288.
350. Zhang, X., Liu, H., Wang, T., Wang, A., and Yeung, K.L. (2006) Modification of carbon membranes and preparation of carbon–zeolite composite membranes with zeolite growth. *Carbon*, 44(3): 501–507.
351. Acomb, J.C., Wu, C., and Williams, P.T. (2015) Effect of growth temperature and feedstock:catalyst ratio on the production of carbon nanotubes and hydrogen from the pyrolysis of waste plastics. *J. Anal. Appl. Pyrolysis.*, 113: 231–238.
352. Acomb, J.C., Wu, C., and Williams, P.T. (2014) Control of steam input to the pyrolysisgasification of waste plastics for improved production of hydrogen or carbon nanotubes. *Appl. Catal. B Environ.*, 147: 571–584.
353. Liu, J., Jiang, Z., Yu, H., and Tang, T. (2011) Catalytic pyrolysis of polypropylene to synthesize carbon nanotubes and hydrogen through a two-stage process. *Polym. Degrad. Stab.*, 96(10): 1711–1719.
354. Ajayan, P.M. (1999) Nanotubes from Carbon. *Chem. Rev.*, 99(7): 1787–1800.
355. Skoulidas, A., Ackerman, D., Johnson, J., and Sholl, J. (2002) Rapid Transport of Gases in Carbon Nanotubes. *Phys. Rev. Lett.*, 89(18): 185901.
356. Mi, W., Lin, Y.S., and Li, Y. (2007) Vertically aligned carbon nanotube membranes on macroporous alumina supports. *J. Memb. Sci.*, 304(1-2): 1–7.
357. Chen, H. and Sholl, D.S. (2006) Predictions of selectivity and flux for CH₄/H₂ separations using single walled carbon nanotubes as membranes. *J. Memb. Sci.*, 269(1-2): 152–160.

358. Ge, L., Wang, L., Du, A., Hou, M., Rudolph, V., and Zhu, Z. (2012) Vertically-aligned carbon nanotube membranes for hydrogen separation. *RSC Adv.*, 2(12): 5329–5336.
359. Ge, L., Du, A., Hou, M., Rudolph, V., and Zhu, Z. (2012) Enhanced hydrogen separation by vertically-aligned carbon nanotube membranes with zeolite imidazolate frameworks as a selective layer. *RSC Adv.*, 2(31): 11793–11800.
360. Faraji, S., Sotudeh-Gharebagh, R., and Mostoufi, N. (2005) Hydrogen recovery from refinery off-gases. *J. Applied Sci.*, 5: 459–464.
361. Gorski, A., Okeowo, O., and Wang, M., Method and system for increasing hydrogen yield/production in a refinery. WO patent 2011082210 a2, 7 july 2011.
362. Grainger, D. and Hägg, M.B. (2007) Evaluation of cellulose-derived carbon molecular sieve membranes for hydrogen separation from light hydrocarbons. *J. Memb. Sci.*, 306 (1-2): 307–317.
363. Garinger, D. and Hägg, M.B. (2008) The recovery by carbon molecular sieve membranes of hydrogen transmitted in natural gas networks. *Int. J. Hydrogen Energy.*, 33(9): 2379–2388.
364. Itoh, N. and Haraya, K. (2000) A carbon membrane reactor. *Catal. Today*, 56(1-3): 103–111.
365. Strano, M.S. and Foley, H.C. (2001) Synthesis and characterization of catalytic nanoporous carbon membranes. *AICHE J.*, 47(1): 66–78.
366. Lapkin, A.A., Tennison, S.R., and Thomas, W.J. (2002) A porous carbon membrane reactor for the homogeneous catalytic hydration of propene. *Chem. Eng. Sci.*, 57(13): 2357–2369.
367. Sznejer, G. and Sheintuch, M. (2004) Application of a carbon membrane reactor for dehydrogenation reactions. *Chem. Eng. Sci.*, 59(10): 2013–2021.
368. Zhang, X., Hu, H., Zhu, Y., and Zhu, S. (2006) Methanol Steam Reforming to Hydrogen in a Carbon Membrane Reactor System. *Ind. Eng. Chem. Res.*, 45(24): 7997–8001.
369. Harale, A., Hwang, H.T., Liu, P.K.T., Sahimi, M., and Tsotsis, T.T. (2007) Experimental studies of a hybrid adsorbent-membrane reactor (HAMR) system for hydrogen production. *Chem. Eng. Sci.*, 62(15): 4126–4137.
370. Yu, J., Tan, M., Liu, P.K.T., Sahimi, M., and Tsotsis, T.T. (2014) Hydrogen Production from Biomass-Derived Syngas Using a Membrane Reactor Based Process. *Ind. Eng. Chem. Res.*, 53(2): 819–827.
371. Parsley, D., Ciora, R.J., Flowers, D.L., Laukaitaus, J., Chen, A., Liu, P.K.T., Yu, J., Sahimi, M., Bonsu, A., and Tsotsis, T.T. (2014) Field evaluation of carbon molecular sieve membranes for the separation and purification of hydrogen from coal- and biomass-derived syngas. *J. Memb. Sci.*, 450: 81–92.

Figure 1: (a) Evolution of the number of publications related with each inorganic membrane type and to hydrogen separation, since 1990 (Advanced search in Scopus database included “hydrogen separation” or “hydrogen purification” alone (Hydrogen separation) or together with the following keywords for each particular membrane group: “zeolit*” or “zeotype” (Zeolites); “palladium” or “Pd” (Palladium); “CMS” or “Carbon molecular sieve” (CMS); “proton conduct*” or “perovskites” or “pyrochlores” or “dense ceramic” (Proton conducting); “amorphous silica” or “silica membranes” (Silica). (b) Scheme of nature classification of membranes.

(a)



(b)

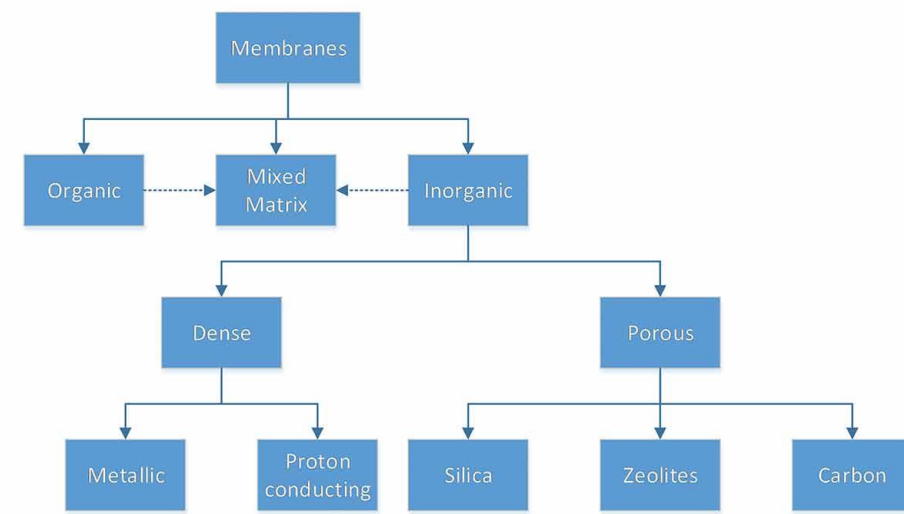


Figure 2: (a) Hydrogen permeability of various metallic elements as function of temperature. Data from (12). (b) Volumetric flux of hydrogen through Pd-metal based membranes with different metal content, at 623 K and 2.2 MPa. Data from (39).

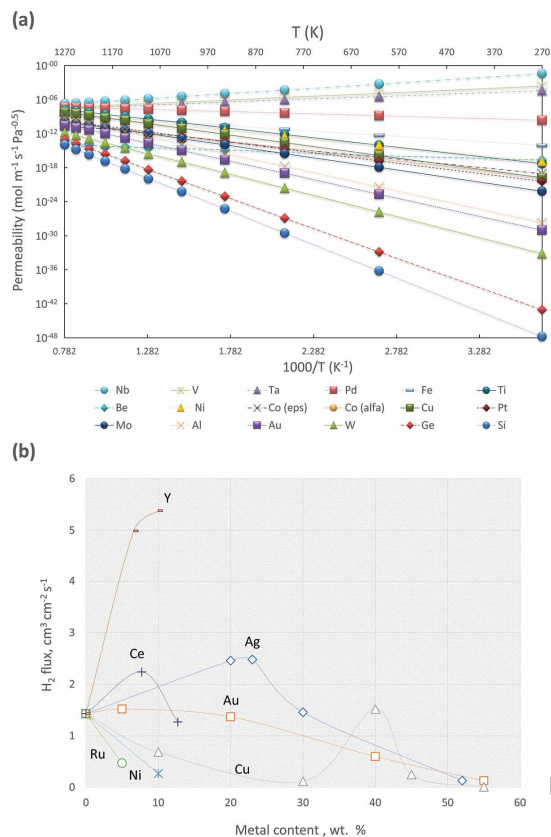


Figure 3: Hydrogen permeability through Pd-based membranes measured before exposure to H₂S, after 24h of exposure to H₂S, and after steady flux recovery in pure H₂. Exposure conditions: [H₂S]= 100 ppm, T = 673 K, time = 24 h, and ΔP = 50 kPa. Data from (34).

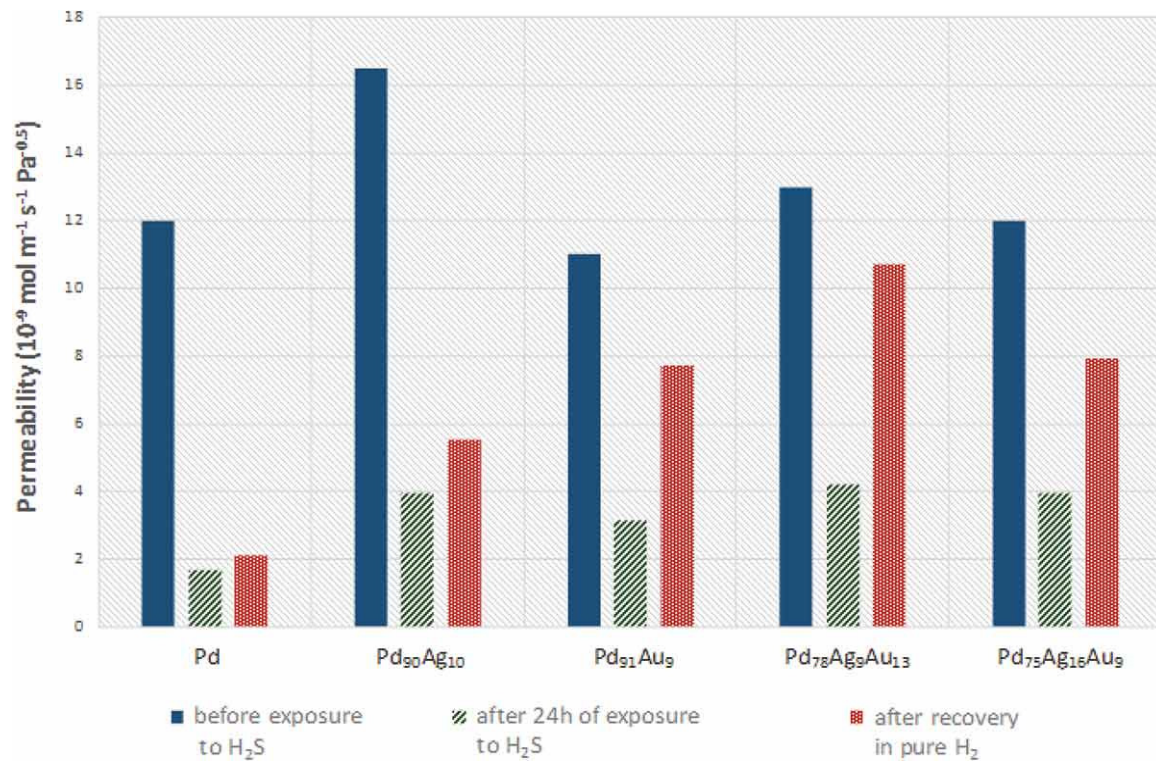


Figure 4: Illustration of hydrogen permeation through: (a) a mixed proton-electron conductor membrane, using a nitrogen/hydrogen feed mixture as example, and (b) a composite ceramic membrane.

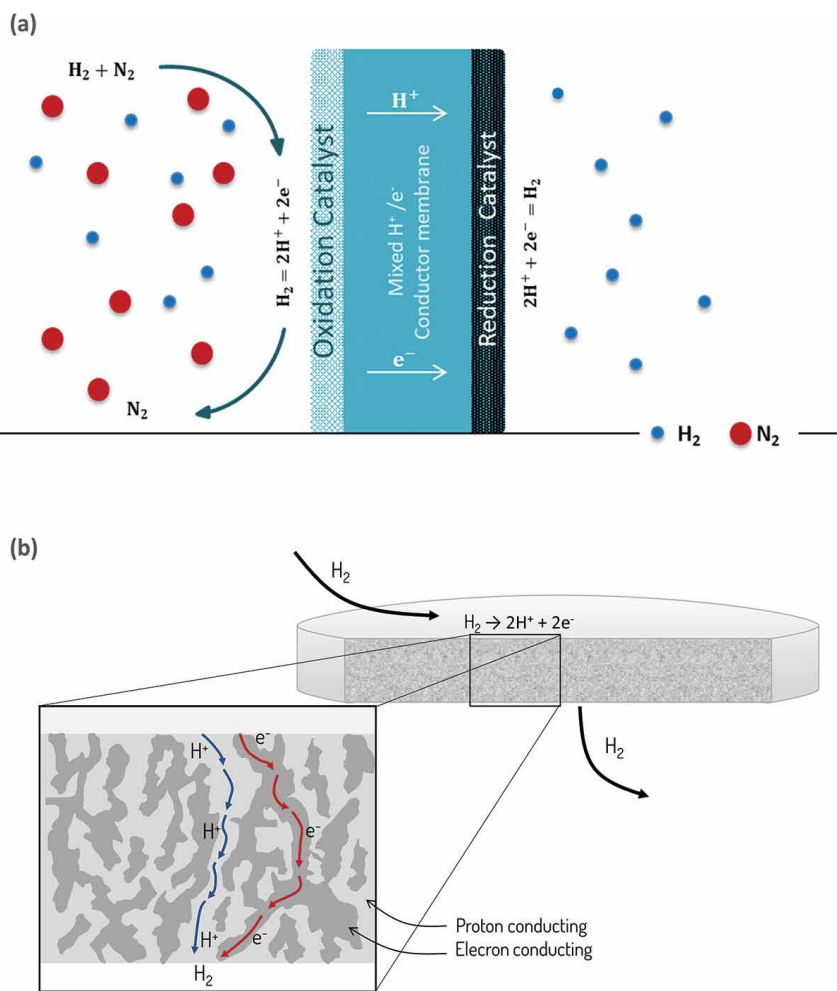


Figure 5: Influence of temperature on proton conductivities of various perovskite-type oxides. The results were calculated from proton concentration and mobility data gathered by Norby (100), with $p_{\text{H}_2\text{O}} = 0.03 \text{ atm}$ and 10 mol.% acceptor level except for BCN17 ($\text{Ba}_{2.17}\text{Nb}_{1.83}\text{O}_{8.745}$) and $\text{Ba}_2\text{YSnO}_{5.5}$, which were calculated with the acceptor level of each formula.

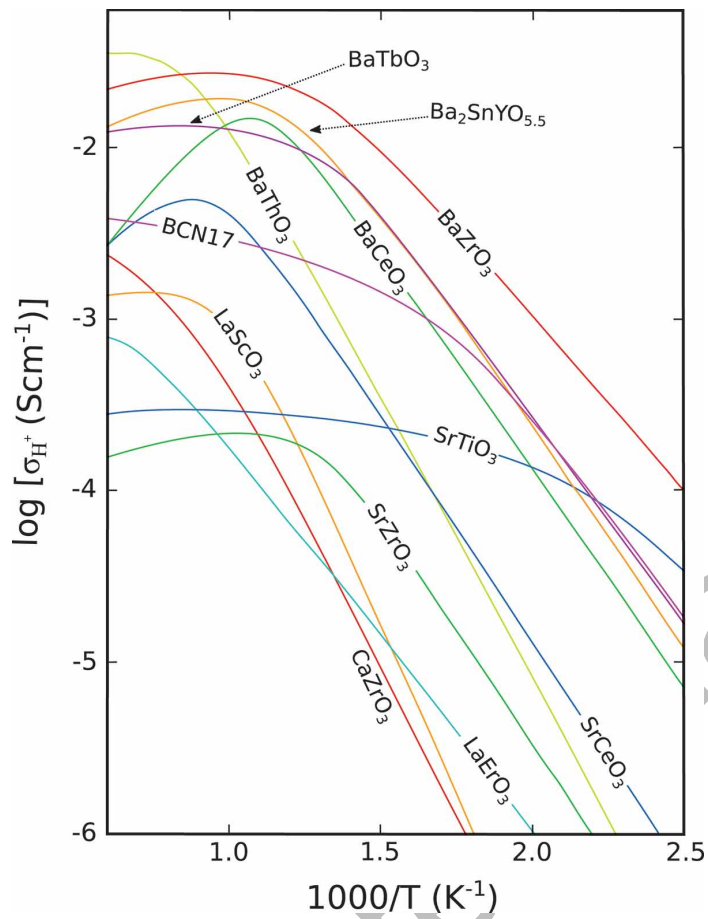


Figure 6: Schematic structure of an asymmetric layered composite membrane.

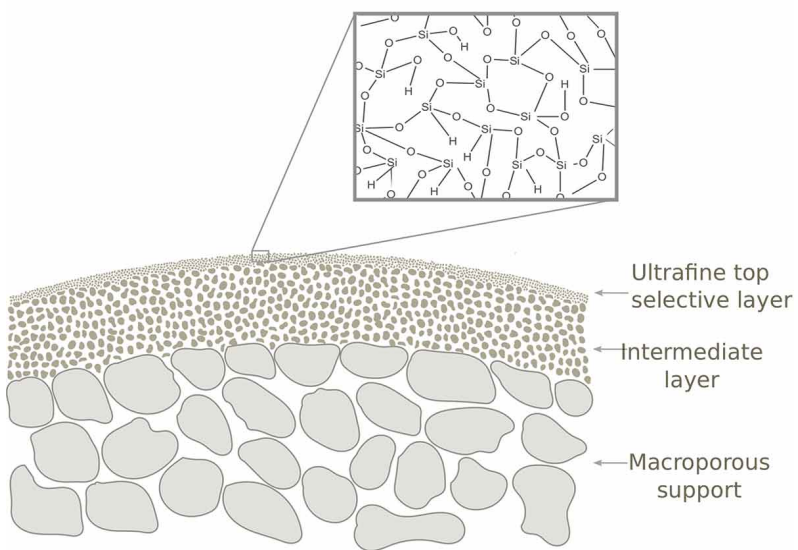


Figure 7: Distint mass transfer mechanisms involved in gas transport in porous media. Taken from (188, 189).

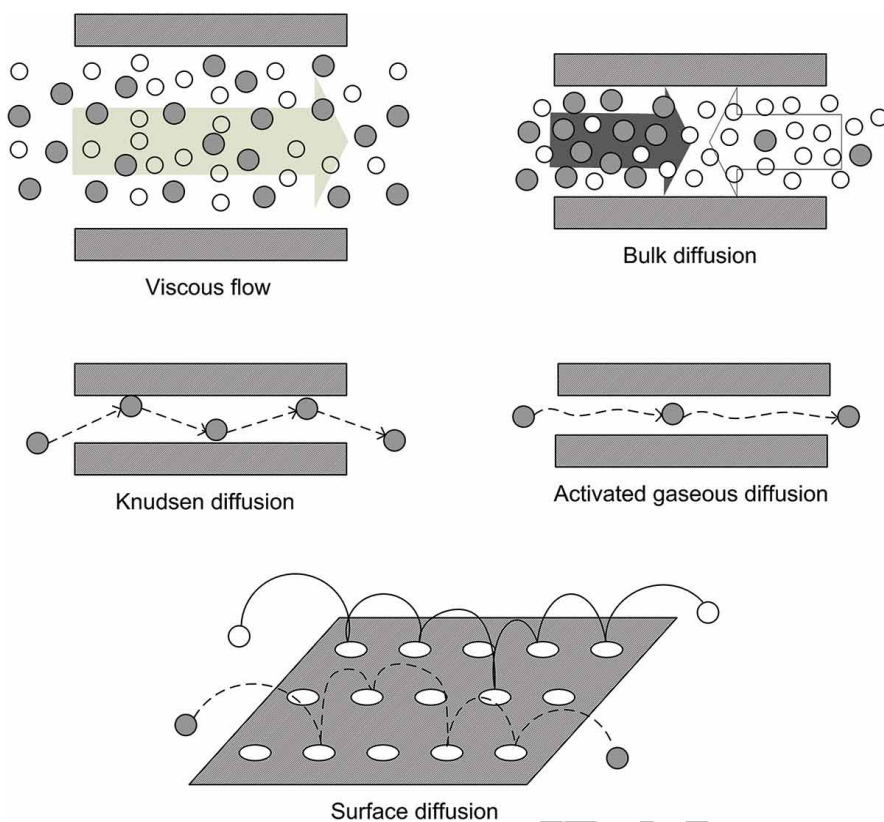


Figure 8: Helium, hydrogen and nitrogen gas permeances over (a) time and (b) temperature, after hydrothermal treatment (773 K, 300 kPa), using a silica membrane (open symbols) and a Co-doped (33 mol.% Co) silica membrane (filled symbols). Adapted from (222).

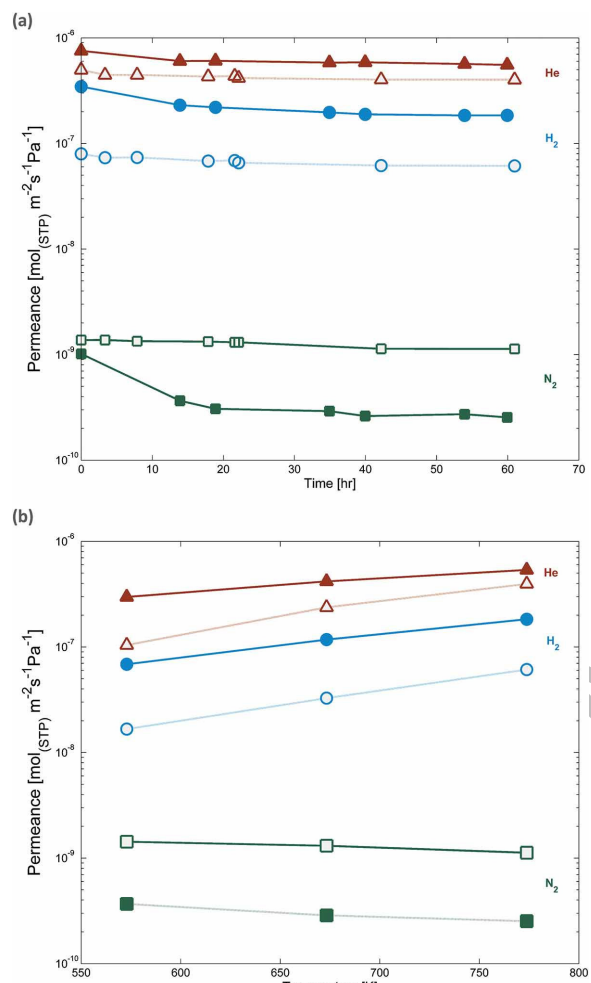


Figure 9: Topology of (a) FAU, (b) MFI, and (c) CHA zeolites (237).

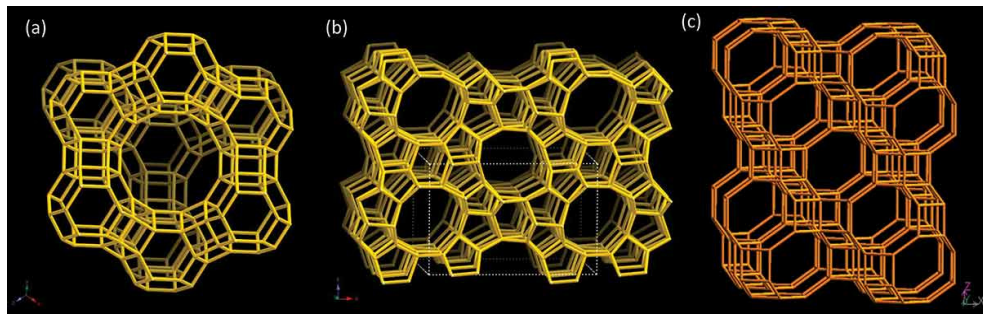


Figure 10: Revised Robeson's upper bound for H₂/CO₂ separation (line) (247) and H₂/CO₂ selectivity against H₂ permeance data for zeolite membranes. The list of membranes is presented in Table SM4 (Supplemental Material); the selectivities were compiled or calculated from literature.

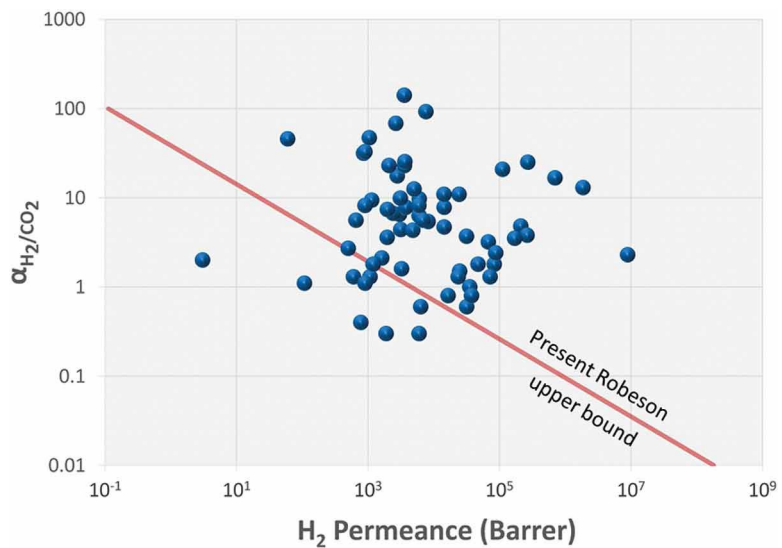


Figure 11: Permeance and ideal selectivity for H₂ and CO₂ in MFI membranes, at 723 K, as function of time on-stream CVD modification. The insert schemes illustrate permeation through unmodified (left) and CVD modified (right) MFI membranes. Adapted from (283).

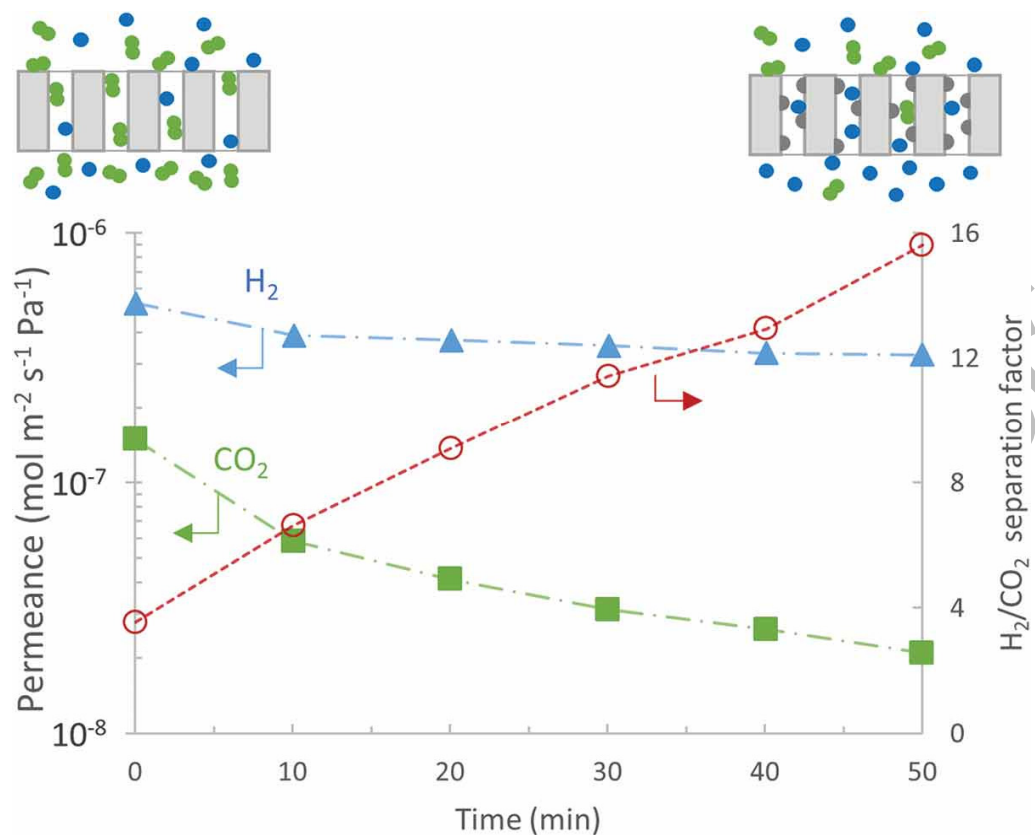


Figure 12: Permeance and H₂/CO₂ selectivity as function of time on-stream, for (a) MFI and (b) HMFI membranes modified by CCD of MDES at 773 K. Adapted from (288).

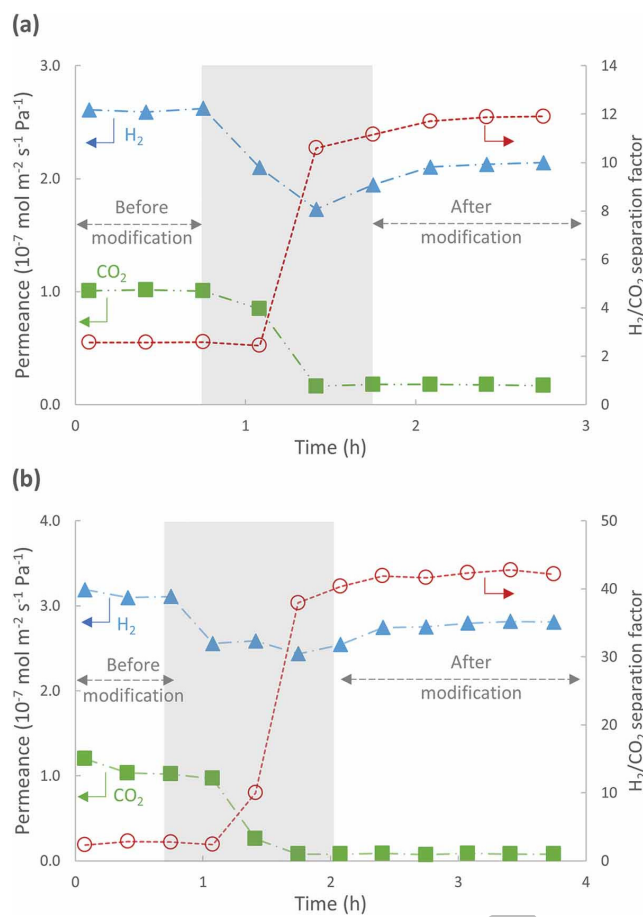


Figure 13: (a) H₂/CO₂ selectivity of clinoptilolite with different cations exchanged at 573 K and 773 K (291). (b) Selectivity for equimolar mixtures H₂/CH₄, H₂/N₂, H₂/O₂, and H₂/CO₂ in LTA membrane prepared with APTES covalent linker and without APTES. Adapted from (296).

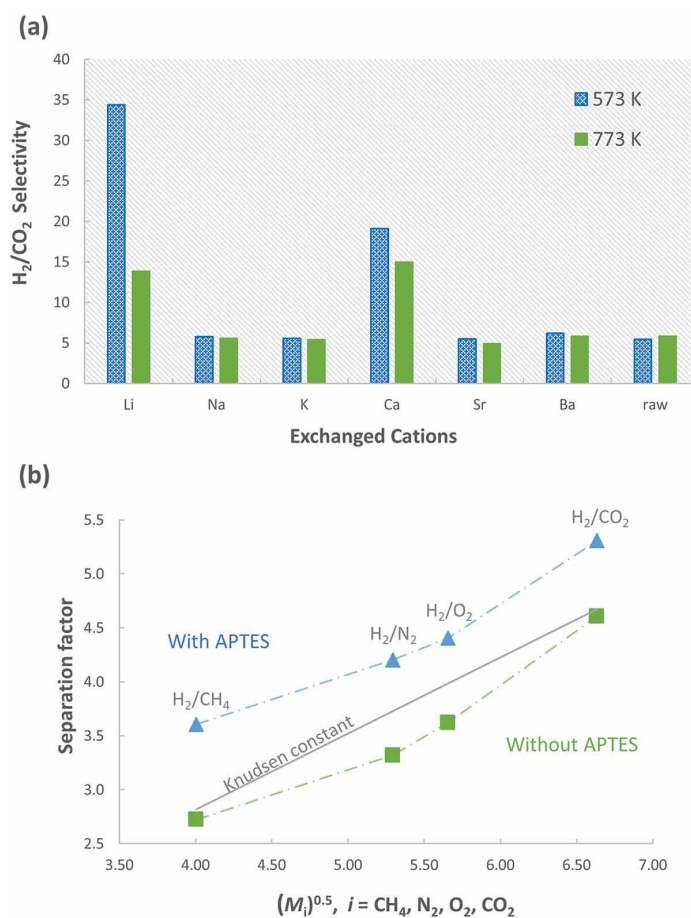


Figure 14: Separation performance of different CMSMs for H₂/CO₂ and H₂/N₂ pairs, illustrated by the Robeson trade-off curves and permeability-selectivity data. The list of CMSMs is presented in Table SM (Supplemental Material); the selectivities were compiled or calculated from literature.

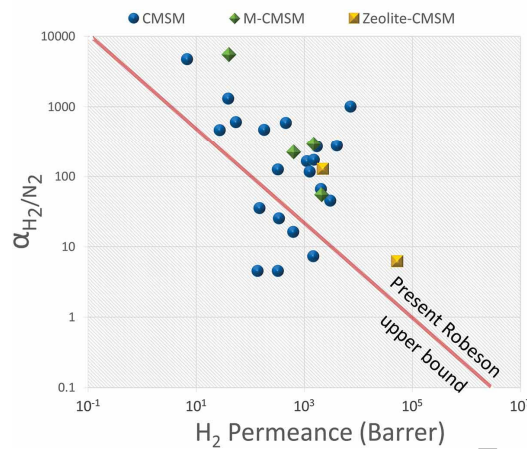
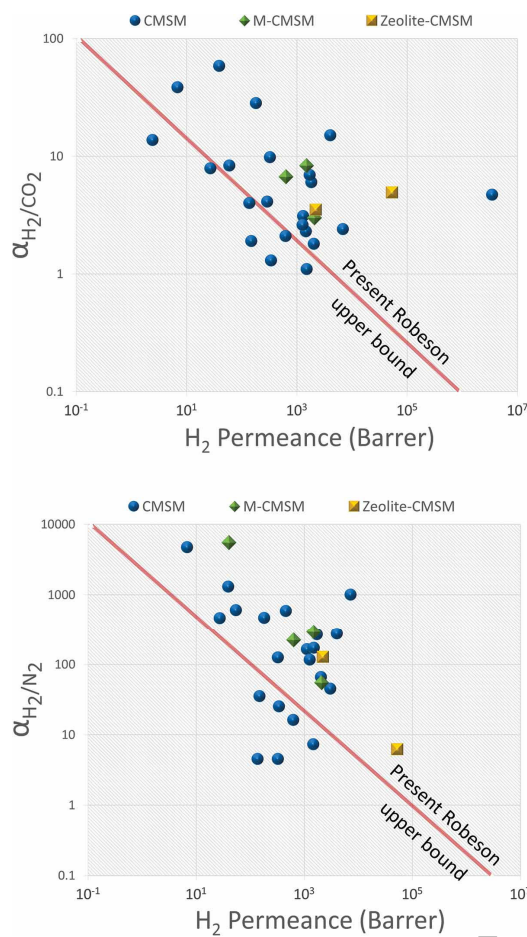


Figure 15: Influence of palladium content in H₂/N₂ selectivity for Pd-CMSM. Data from Suda *et al.* (347).

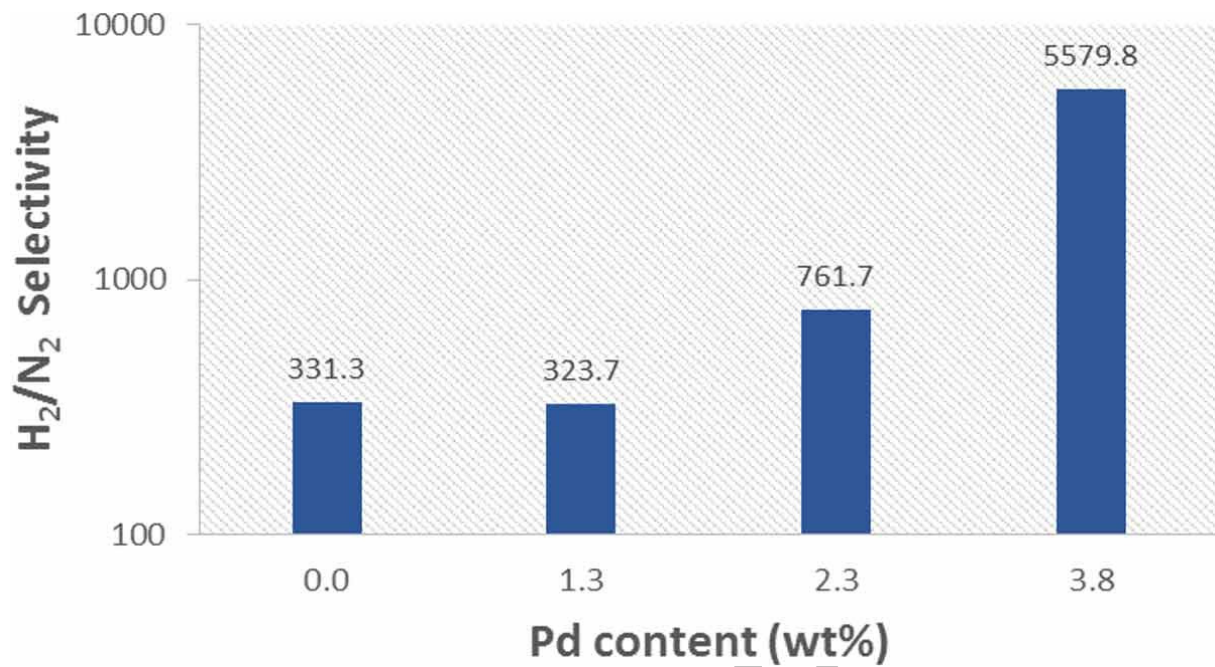


Table 1: Comparison between the different types of inorganic membranes for hydrogen separation.

Features	Dense membranes		Porous membranes		
	Metallic	Proton Conducting (ceramic)	Silica	Zeolite	Carbon Molecular Sieve
Transport mechanism	Solution–diffusion	Vehicle mechanism/ Grotthuss mechanism	Visc, Kn, D _{surf} D _{act,g} , D _{bulk}	Visc, Kn, D _{surf} D _{act,g} , D _{bulk}	Visc, Kn, D _{surf} D _{act,g} , D _{bulk}
Studied temperature (K)	523-823	923-1273	473-873	298-723	298-423
Typical H ₂ selectivity	10 ³ - ∞	Similar to metallic	>100	<50	<100
Typical H ₂ permeance (mol m ⁻² s ⁻¹ Pa ⁻¹)	10 ⁻⁶	10 ⁻⁹	10 ⁻⁸	10 ⁻⁸	10 ⁻⁸
Stability issues	α→β phase transition	-	Presence of H ₂ O	-	Moisture; brittle; mechanical stability
Main poisoning compounds	H ₂ S, HCl, CO ₂ , CO	Hydrocarbons	-	-	Organic vapors
Other limitations	-	Low proton and electron conductivity	-	-	Low reproducibility
Cost	Expensive	Moderate	Low	Moderate	Moderate

Visc - Viscous flow; Kn - Knudsen; D_{surf} - Surface diffusion; D_{act,g} - Activated gaseous diffusion; D_{bulk} - Bulk or molecular diffusion